Mechanical Design for the Tactile Exploration of Constrained Internal Geometries

by

Daniel Terrance Kettler

Bachelor of Science in Mechanical Engineering
Harvard University (2007)

Submitted to the Department of Aeronautics and Astronautics
in partial fulfillment of the requirements for the degree of

Master of Science in Aeronautical and Astronautical Engineering

at the

MASSACHUSETTS INSTITUTE OF TECHNOLOGY

June 2009

Author .....
Department of Aeronautics and Astronautics
May 22, 2009

Certified by .....
Steven Dubowsky
Professor
Thesis Supervisor

Accepted by .....
Prof. David L. Darmofal
Associate Department Head Chair
Committee on Graduate Students

Mechanical Design for the Tactile Exploration of Constrained Internal Geometries

by

Daniel Terrance Kettler

Submitted to the Department of Aeronautics and Astronautics
on May 22, 2009, in partial fulfillment of the
requirements for the degree of
Master of Science in Aeronautical and Astronautical Engineering

Abstract

Rising world oil prices and advanced oil recovery techniques have made it economically attractive to rehabilitate abandoned oil wells. This requires guiding tools through well junctions where divergent branches leave the main wellbore. The unknown locations and shapes of these junctions must be determined. Harsh down-well conditions prevent the use of ranged sensors. However, robotic tactile exploration using a manipulator is well suited to this problem. This tactile characterization must be done quickly because of the high costs of working on oil wells. Consequently, intelligent tactile exploration algorithms that can characterize a shape using sparse data sets must be developed.

This thesis explores the design and system architecture of robotic manipulators for down-well tactile exploration. A design approach minimizing sensing is adopted to produce a system that is mechanically robust and suited to the harsh down-well environment.

A feasibility study on down-well tactile exploration manipulators is conducted. This study focuses on the mature robotic technology of link and joint manipulators with zero or low kinematic redundancy. This study produces a field system architecture that specifies a unified combination of control, sensing, kinematic solutions for down-well applications.

An experimental system is built to demonstrate the proposed field system architecture and test control and intelligent tactile exploration algorithms. Experimental results to date have indicated acceptability of the proposed field system architecture and have demonstrated the ability to characterize geometry with sparse tactile data.

Serpentine manipulators implemented using digital mechatronic actuation are also considered. Digital mechatronic devices use actuators with discrete output states and the potential to be mechanically robust and inexpensive. The design of digital mechatronic devices is challenging. Design parameter optimization methods are developed and applied to a design case study of a manipulator in a constrained workspace.

This research demonstrates that down-well tactile exploration with a manipulator is feasible. Experimental results show that the proposed field system architecture, a 4 degree-of-freedom anthropomorphic manipulator, can obtain accurate tactile data without using any sensor feedback besides manipulator joint angles.

Thesis Supervisor: Steven Dubowsky
Title: Professor

Acknowledgments

My time at MIT has been challenging and rewarding in equal parts. At the core of my experience has been the help, advice, and guidance of a number of people to whom I am very thankful:

- Professor Steven Dubowsky for guiding me through the twists and turns of research and for trusting in my abilities.
- Julio Guerrero and Schlumberger Doll Research for funding and guiding my research and education.
- Mark Belanger, Todd Billings and all of the other machine shop staff I have harassed for their assistance and patience.
- My colleagues in the Field and Space Robotics Lab for their assistance, camaraderie, and good humor. I wish to specifically thank Peggy Boning for her patience and wisdom.
- My research partner Francesco Mazzini for your invincible good spirit. Never change.
- My friends at Riverside Boat Club for keeping me sane. *Mens sana in corpore sano.*

Most importantly, I would like to thank my family and my parents for their wisdom, advice, and support.

Contents

List of Figures

List of Tables

Chapter 1

Introduction

1.1 Motivation

The ability to map the unknown geometry of junctions within an oil well is an essential capability not currently provided by existing oil industry tools. Rising world oil prices and advanced oil recovery techniques have made it economically attractive to rehabilitate previously abandoned oil wells. This requires lowering instruments and tools into the wells. These wells often have a number of junctions where divergent branches leave the main well at unrecorded depths, see Figure 1-1. Most junctions are not designed to be re-entered after their construction. To rehabilitate a divergent branch, the location and shape of its junction must be determined. This information may then be used to guide tools into the desired well branches. The data acquisition to map a junction must be done quickly given the very high cost of working on a well.

Well mapping is challenging because the opaque fluids, that fill the well to avoid its collapse, prevent the use of visual sensors to measure the junction. Ultrasonic sensors have been suggested for this application. However, studies have yet to show that ultrasonic sensors possess the desired performance in down-hole conditions [57]. Also a layer of *mud cake* often obscures the wellbore surface. This mud cake is a thick paste of particulate that settles out of the well fluid and collects on well surfaces. Consequently, robotic tactile exploration using a manipulator is appealing; see Figure 1-1 [36].

Junction mapping is just one example of a general oil industry need for new down-well tools that offer both greater adaptability and new capabilities relative to existing tools. World oil demand is rising. At the same time, available reserves are becoming more difficult

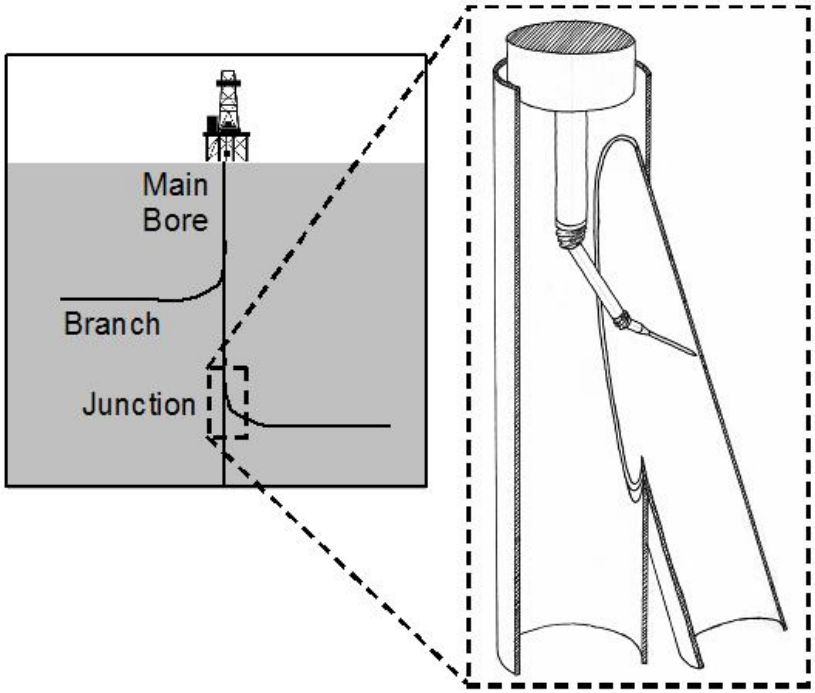

Figure 1-1: Typical oil well branching structure with cutaway junction detail showing deployed tactile inspection manipulator.

to extract. These factors are driving the need for new tools and methods. With the exception of modern directional drilling and sensing equipment, the oil industry is traditionally very conservative in the design and deployment of tools for down-well applications. One of the considerations underlying all decisions is the need to minimize the risk of damaging or blocking a wellbore and thereby losing a huge investment. As a result, tools for down-well applications are historically both very simple and highly specialized to a specific task in order to be mechanically robust [55]. While this approach minimizes risk to the well, it often does so by sacrificing efficiency and ability.

Another illustrative example is the technology used to recover lost or broken objects from a well. If a cable holding tools breaks and blocks a wellbore, it must be removed through a process called *fishing*. A large barbed hook (Figure 1-2)[1] is lowered into the well and repeatedly stabbed at the object in the hope that it might be snagged and pulled to surface. This approach is highly stochastic and has no guarantee of success [55]. It is also very expensive because it costs tens of thousands of dollars per hour in labor, capital, and lost profit to work on the well. If recovery attempts are eventually abandoned, the wellbore,

[1]Image Credit: Charles A. Templeton Inc.

representing a large investment, is lost [55].

Robotics has the potential to answer the needs of the oil industry for more capable and adaptable tools. A robotic manipulator can tactilely map an unknown well junction. Similarly, in fishing operations a manipulator can deterministically search out and grasp or attach to a lost object. Furthermore, a robotic manipulator-based tool suitable for these two problems and a number of others can be envisioned. This introduces the possibility of reducing cost and operational complexity by having fewer, more generally capable robotic tools.

Figure 1-2: Tool for snagging broken cables.

Exploration and measurement using tactile data presents unique challenges compared to using visual or other range sensors. Tactile data acquisition is expensive in terms of time. One visual image can very quickly provide thousands of data points for an object surface. In comparison, the time required for moving a manipulator to acquire a tactile data point outweighs its associated computation and processing costs. Hence, the key to efficient tactile characterization is the intelligent selection of where to search for new touch points. This search should maximize the amount of new information provided by each data point and thereby minimize the number of data points needed to generate the map of a given geometry.

At the same time, the design of the robotic system itself must be developed. To the best of our knowledge, robotic manipulators have never been used within the challenging environment of an oil well. Considerations including sensing schemes, actuation, and kinematic structure must be tailored to the harsh temperatures, high pressures, and constrained workspaces found inside an oil well.

Research on the tactile oil well exploration problem has correspondingly been into two areas: control and search algorithms and system design. Francesco Mazzini is investigating control and search algorithms. His work has focused on developing and testing control and search algorithms in simulation and experiment. This thesis focuses on system design and development. The system architecture for down-well tactile exploration is investigated.

An experimental robotic manipulator is developed as a proof of concept for the system architecture as well as for testing control and search algorithms.

1.2 Tactile Exploration Background Literature

Past research on tactile characterization of geometries has developed a number of approaches and representation techniques. Different search approaches and surface representation methods have been applied to known and unknown geometries [10, 56, 2]. Some methods try to exploit the data already obtained to guide further data acquisition and minimize the amount of data, and consequently time, needed to characterize an object [56, 52, 65]. Other methods use a more brute-force, dense sampling approach with no consideration for exploration time [10, 12].

In an early study, a tactile exploration technique for locating and identifying a 2D object from a library of known objects is developed [56]. In this work, a tree of object identity hypotheses is made and the search for the next data point is selected to maximize the potential of pruning this tree. The method has been extended to 3D polygonal objects [52]. While this method produces efficient searches for known objects, it cannot handle unknown geometries because it relies on a library of specific objects.

A common approach for representing general unknown surfaces is with a mesh [10, 12]. Either a single mesh or two bounding meshes may be used [10]. This second bounding approach can also be used with a tree search for object recognition [4]. While a mesh is an effective representation of a general surface, it requires dense data and it is therefore not applicable for sparse and efficient tactile characterization approaches.

An alternative approach for general unknown objects represents surface geometry as a composition of primitives, such as planes, cylinders, and spheres. These primitives are often determined with curve and surface fitting methods [2, 48]. Alternatively, they can be determined using differential invariants [27]. All of these methods use an evenly spaced grid to collect data points. The importance of intelligently selecting where to collect data points for an efficient tactile exploration has been recognized [65]. In this prior work, when a series of grid points are found to belong to the same fitted curve or surface, the spacing between subsequent data points is increased. While adaptive, this method is still tied to the grid sampling concept and therefore inherently uses dense data.

In conclusion, while important methods have been developed for both intelligent exploration and the characterization of general unknown geometries, the integration of these concepts to achieve fast general geometry characterization with sparse data remains unsolved.

The approach assumed in this work is based on the use of surface fitting to characterize geometries, subject to the assumption of sparse data collection [36]. The environment to be mapped is assumed to be composed of the intersection, in the mathematical sense, of a set of basic primitives. The approach builds this model as the data is acquired. The search for additional data points is directed based on the information obtained at that point in the process. Basically, the algorithm searches for new data in directions where little information has been previously gathered. The intent is to minimize the time, and similarly the distance traveled by the manipulator end-point, to reconstruct an unknown surface to a given accuracy.

1.3 Robotic Mechanisms for Oil Well Applications

The design of robotic manipulators for down-well applications is a challenging problem. The workspace requirements of tactile junction exploration and the spatial constraints of a wellbore force a highly specialized kinematic structure. At the same time the harsh conditions the system will experience both inside the well and in the field during deployment constrain the hardware options for implementing the system.

The robotic manipulator needs to access a challenging workspace. Branching wellbores diverge with a typical angle of approximately $\alpha = 5^\circ$. With representative main and lateral bore diameters of 9 in (22.9 cm) and 7 in (17.8 cm), a junction is 80.3 in (204.0 cm) long. See Figure 1-3. This very long and narrow workspace prevents the use of common manipulator architectures that have been designed for an open workspace.

There is significant research on the development of highly articulated serpentine manipulators for use in challenging constrained workspaces [22]. The hyper-redundant nature of these manipulators enables them to reach around obstacles and follow end effector trajectories through tight spaces. While serpentine designs have significant workspace and obstacle avoidance advantages, there are a number of control and implementation challenges. Motion planning for these hyper-redundant manipulators requires the specification

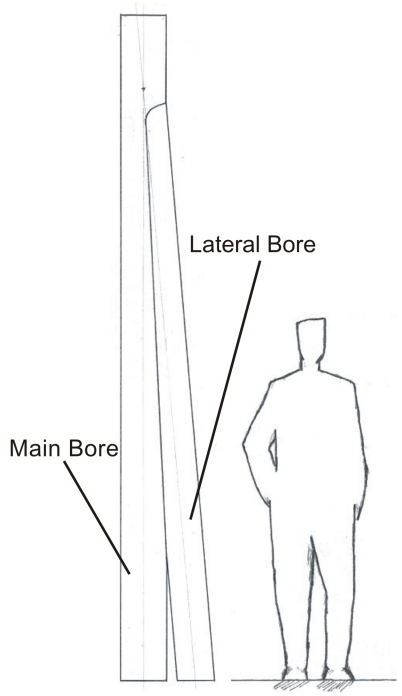

Figure 1-3: A scale comparison of an oil well junction and an average man.

of an arm curve shape and its evolution over time. In comparison, only the position of the end effector must be specified for traditional non-redundant manipulators. The much more computationally challenging control of hyper-redundant manipulators is the cost of their collision-avoidance abilities in constrained workspaces. The physical implementation of hyper-redundant serpentine manipulators is also much less mature than the implementation of traditional non-redundant, or low-redundancy manipulators. Most notably, there is an on going search for actuators that are compact, light, and sufficiently powerful [22]. Consequently, there is also research on new mechanism structures and actuation approaches [22, 24, 61]. For these reasons, the feasibility study and development of system architecture do not consider serpentine manipulators, instead focusing on more mature non-redundant and low-redundancy robotic technology. Hyper-redundant serpentine manipulators still have considerable potential for oil well applications. Consequently, this thesis considers an appropriate mechanism implementation and related design methods.

The system architecture study considers the application of traditional non- or low-redundancy manipulators to the constrained workspace inside an oil well junction. Previous research has developed ways of reconstructing and evaluating manipulator workspaces [15, 58]. Similarly, there are a number of metrics for characterizing the dexterity of a given

manipulator design [20, 28]. These metrics and tools can be used to guide a human designer through an iterative design process. This approach is used in the design architecture study. Alternatively, there are efforts to automate this design process using numerical optimization techniques [11, 20, 21]. While not used directly, these studies of numerical optimization techniques provide insight about design objectives and metrics.

Considering the harsh conditions that the robotic system will be operated in, its design must be mechanically robust. Down-well, the robot will be subjected to temperatures and pressures as high as $250°C$ and 70 MPa. Uncased wellbores can have bumpy irregular faces and there is significant potential for the manipulator to experience collisions and shocks as it is moved through the well. The system may also experience challenging conditions above ground during transport, set-up, and routine handling. It will be transported over rough terrain and through environmental extremes by work crews that likely will not have the specialized training and tools needed to maintain and repair the system on site. The system must be mechanically resilient enough to withstand the harsh conditions both in and above the well. Oil services companies have significant background gained through experience in designing and building these types of hardened systems. The final design of a down-well robotic system should logically be handled by those with the proper experience. However, to insure success, the design of the overall system architecture must properly recognize these considerations. In particular, the selection of control and sensing approaches can be used to minimize the reliance on delicate sensors that are temperature and shock sensitive. The development of an inherently physically robust system is a major design concern. This concern will be addressed in the development of the system architecture.

1.4 Digital Mechatronics

While traditional link and joint manipulators with non-redundancy or low-redundancy in their degrees-of-freedom can be effective within an oil well, they are not an ideal kinematic design. The low number of joints increases the likelihood of undesirable contact between projecting joints and the environment. As an alternative, hyper-redundant serpentine manipulators are well suited for working in the constrained environments found inside oil well junctions. By virtue of their extra degrees-of-freedom, arms of this type can position and orient their end effector while avoiding obstacles [14, 22]. Their highly articulated nature

also allows them to maneuver and follow trajectories in constrained spaces that would inhibit the motion or configuration change of traditional, less articulated robotic manipulators [22]. While serpentine manipulators are promising, the mechanical implementation and associated design methods of these manipulators are not mature. Research on mechanism design and implementation is necessary to make hyper-redundant manipulators viable options for down-well robotic systems.

One promising implementation for serpentine manipulators is the use of digital mechatronics. Digital mechatronic devices use a large number of actuators with discrete bistable states to approximate continuous actuation [3, 43, 53]. This actuation concept is the physical analog of the digital representation of real numbers. Digital mechatronic devices replicate the continuous workspace volume of traditional mechanism designs with a distribution of discrete output states. Typically, digital mechatronic devices must be hyper-redundant in order to effectively approximate the workspace of continuous designs. Examples of digital mechatronic mechanisms include snake-like serial manipulators (Figure 1-4(a))[2], walking robots, and positioning mechanisms for surgical probes (Figure 1-4(b))[3] [34, 59, 16]. Two types of digital actuation have been demonstrated: fully constrained actuation, and elastically-averaged over-constrained actuation. In the fully constrained case, the inputs of individual actuators do not overlap. In the elastically-averaged over-constrained case, conflicting actuator inputs are accommodated by elasticity in the mechanism structure [16, 44, 45, 62]. Previous digital mechatronic serpentine manipulator implementations use fully constrained actuation, although elastically-averaged actuation could be used as well.

Digital mechatronics offers a number of advantages over traditional continuously actuated designs. It can greatly reduce the number and complexity of sensors required for a given mechanism, and can be operated open loop since actuators have only two stable states [13, 43, 59, 62]. If actuator states must be verified, only simple limit sensors are required. Such sensors can be much more rugged and less expensive than continuous joint position sensors. Digital mechatronic devices are also much less prone to complete loss of functionality by virtue of the hyper-redundancy that is typical in their design. In continuous, non-redundant designs, the loss of an actuator decreases the dimensionality of the workspace. In digital mechatronic devices, if one actuator fails, the mechanism will lose

[2]Image Credit: V. Sujan [59]
[3]Image Credit: L. DeVita [16]

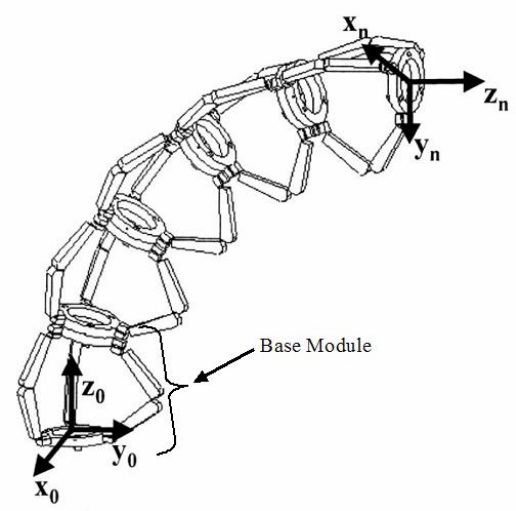

(a) A serial digital mechatronic manipulator composed of 5 modules with 2^{15} discrete states.

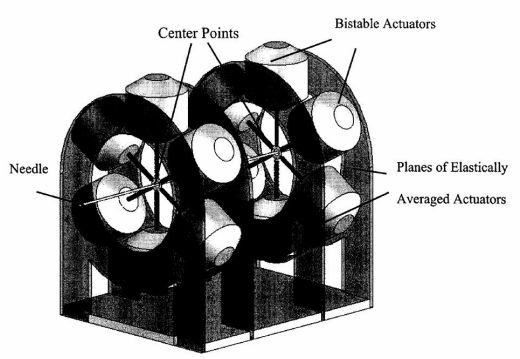

(b) A MRI compliant mechanism for prostate biopsy with 2^{12} discrete states.

Figure 1-4: Examples of previously developed digital mechatronic mechanisms.

half of its output states. However, it will still be able to operate within most of the original workspace due to hyper-redundancy. Digital mechatronic actuation also presents the potential for significant cost and implementation advantages [59, 13]. Digital mechatronic devices use simple, low cost actuators and sensors in conjunction with bistable joints to achieve precise actuation rather than expensive continuous sensors, motors, and control hardware [43, 62]. Consequently, digital mechatronic devices have the potential to be inexpensive and even disposable [67]. The use of standardized actuators or modules could further reduce cost and enable easy repair. These are essential characteristics for an oil industry tool which would be deployed in rough and remote areas where it could easily be damaged and must be quickly repaired.

The design of digital mechatronic devices offers significant and unique challenges because this design process requires shaping a cloud of discrete output states rather than a continuous workspace volume. These discrete output states must be *well distributed* within the desired workspace of the device. Proper distribution prevents redundant output states from collecting and overlapping in certain areas of the workspace while other areas contain no output states and are unreachable. The definition of well distributed must be determined with reference to the device's purpose. Output states may need to be evenly distributed within some desired space, concentrated at regions where greater accuracy is required, or located exactly at specific places. This is a challenging optimization problem because digi-

tal mechatronic devices have large numbers of output states. The number of output states increases exponentially with the number of actuators n as 2^n. To further complicate issues, high degrees of symmetry or modular repetition tend to produce mechanisms with redundant states. Consequently, intuitive designs are typically suboptimal.

Several approaches to digital mechatronic device parameter optimization have been developed in the past. Given a mechanism architecture, the challenge is to find linkage and actuator parameters that most evenly distribute output states within the desired workspace.

The earliest consideration of this design problem considers the design of a serpentine arm for repetitive pick-and-place operations [13]. The design approach developed uses inverse kinematics methods to alter an existing manipulator design so that a set of states comprising the desired pick-and-place trajectory are included in the optimized workspace. These changes are achieved by making minimal modifications to the existing actuator output states. This design technique was originally demonstrated on planar manipulators. Subsequent research has adapted the approach to larger manipulators, with 3 dimensional workspaces, included the consideration of orientation and not just position [40]. This method is analytical and fast. However, this method is not helpful for developing a mechanism with a general, non-task-specific workspace.

One method for optimizing the density of reachable points in a general manipulator workspace has been demonstrated for high numbers of actuators [30]. This approach assumes that the arm is composed of a series of identical modules cascaded together. This assumption along with the use of Fourier methods, enables an efficient approximation of the workspace point density distributions through the convolution of module workspace density distributions [18, 31]. To optimize a manipulator, the desired workspace density distribution is modeled with a representative function. This desired density distribution is then decomposed into the required distribution of the repeated module. Numerical optimization of module parameters is used to match this required module workspace density distribution [30]. The use of decomposition during optimization makes the process efficient for manipulators with a high number of degrees-of-freedom. While this approach has demonstrated good results, it is partially limited by methods used to make the problem more computationally tractable. The assumption of identical, repeating modules restricts the form of the manipulator. Qualitative experiences have also shown that such repetition or symmetry can lead to overlapping and wasted output states. Finally, the method of approximating

the workspace density distribution does not allow for the addition of constraints on the manipulator workspace imposed by the environment.

Direct numerical optimization of a manipulator would allow for general manipulator forms and could include environmental constraints. However, this direct numerical approach is computationally expensive. A direct numerical method for optimizing a general workspace has been demonstrated [34]. This method uses genetic algorithms to minimize the variance in a measure of output state density over a desired workspace. This algorithm is demonstrated on a planar manipulator test case. Trials show good results indicating that the conceptual approach is correct. However, the method scales poorly to higher dimensional workspaces and more complex mechanisms with a greater number of design parameters to optimize.

This thesis develops effective numerical optimization techniques for handling digital mechatronic device optimization. An efficient and representative cost function is first developed. The focus then switches to the evaluation and development of effective numerical optimization routines. Notably, while mechanism output states are discrete, the optimization problem is continuous and nonlinear. The size of links and the discrete states of actuators may be specified continuously and, as a result, effect the position of each discrete mechanism output state continuously. The development of optimization algorithms therefore focuses on continuous methods. The performance of a number of continuous optimization algorithms is compared, including trust region methods and the Nelder-Mead Simplex method. Subsequently, the most successful algorithm, the Nelder-Mead Simplex, is further modified and tuned to the problem. Finally, the abilities of the optimization approach are demonstrated with a test case.

1.5 Overview

As robotic manipulation has not been previously applied to down-well tools, initial investigations of field system feasibility are discussed in Chapter 2. The tactile junction mapping task is used to develop a set of requirements for a down-well robotic manipulator. The overall system approach including sensing, control, and actuation methods are considered. Workspace, force, and dexterity requirements guide the development of acceptable kinematic structures. Environmental and tool resource constraints are considered in suggesting

components for actual implementation. The mechanical design of a manipulator hardened to function in the down-hole environment with its extreme temperatures is a difficult challenge and beyond the scope of this thesis. This problem is left in the capable hands of oil industry engineers with applied experience in these issues.

The design and construction of a scaled-down experimental manipulator and test environment is discussed in Chapter 3. This experimental system is intended to aid in the ongoing development, testing, and demonstration of control and intelligent search algorithms for efficient, autonomous tactile exploration. The experimental arm is derived from the proposed field system architecture developed in the feasibility study. The environment tank replicates the geometry of an oil well junction and can be filled with fluids to test the performance of control approaches in high viscosity fluids.

This experimental system is evaluated and initial test results reviewed in Chapter 4. These results guide improvements to the experimental mechanism. They also reveal the need for several changes to the proposed field system architecture. Initial trials of intelligent, data-efficient tactile search algorithms demonstrate the feasibility of geometry characterization with small data sets.

Finally in Chapter 5, design optimization methods are developed for manipulators with hyper-redundant kinematic structures based upon binary actuation. Numerical optimization methods and objective functions suited for this problem are developed and demonstrated for the design of a manipulator within a constrained, well-like workspace.

1.6 Results

Analysis shows that a field system is feasible. Given the narrow and constrained nature of workspaces inside an oil well, redundant manipulator designs will be necessary in order to reach the desired workspace. For the case of mapping the geometry of an unknown junction, a 4 degree-of-freedom arm is proposed. This manipulator consists of a 3 degree-of-freedom anthropomorphic arm mounted on a fourth prismatic joint aligned with the main bore axis. In order to produce a mechanically rugged field system, a system architecture utilizing a minimal number of sensors is suggested.

The experimental system has provided considerable information about the proposed tactile exploration approach during system tuning and initial trials. Notably, it has re-

vealed the important trade-offs between the mechanical design of the robot joints and their resulting friction coefficients, and the control of the manipulator. These findings have produced refinements of both the experimental system's mechanical design and the proposed manipulator control approach. Initial tactile exploration experiments have demonstrated that accurate, efficient, and autonomous tactile exploration is possible. Future work should focus on developing intelligent search and exploration algorithms. Additional tests on control problems caused by the influence of environmental effects, including viscous fluids and surfaces coated with mud cake, are also needed.

The application of digital mechatronic serpentine manipulators to down-well robotics is considered. A parameter optimization method for digital mechatronic mechanisms with a moderately large number of actuators is demonstrated. The approach is computationally tractable for meaningfully large numbers of actuators. This design optimization approach is demonstrated in a design study optimizing a serpentine manipulator for a well-like workspace. While developed and demonstrated for the optimization of serpentine manipulators, the design optimization algorithm is applicable to digital mechatronic mechanisms in general. This includes both mechanisms with fully constrained actuation as well as devices with elastically-averaged, over-constrained actuation.

1.7 Summary

Robotics offers great promise for a new class of down-hole tools that offer increased flexibility and new capabilities. This thesis shows the feasibility of designing a traditional link and joint manipulator tailored for the narrow cylindrical workspace typical of an oil well. Initial tests with a purpose-built experimental system have demonstrated the viability of autonomous, data-efficient tactile mapping as well as the proposed minimal-sensor field system architecture. Promising non-traditional serpentine manipulators developed using optimized digital mechatronics offer alternative implementations attractive both for their capabilities in constrained environments and their robustness in harsh environments.

Chapter 2

Field System Feasibility and System Architecture Study

2.1 Introduction

The proposed design for a tactile junction exploration robot consists of a 4 degree-of-freedom manipulator mounted on an industry standard wireline tool module, an 8 ft cylinder that is lowered into wells on a cable (Figure 2-1). The redundant 4^{th} degree-of-freedom allows the arm to reach the entirety of the long and constrained workspace within a well junction. Impedance control is used to govern the manipulator allowing it to easily transition between operating in free space and in contact with surfaces in the environment. This control approach also minimizes the number of delicate sensors that the system requires. No force/torque or tactile sensors are used. The only necessary feedback is provided by joint angle encoders.

2.2 System Requirements

2.2.1 System Integration and Deployment

The robotic manipulator will be deployed from the end of a wireline tool module. These cylindrical modules are designed to carry sensors and tools into a well. They are connected in a serial fashion to create a *tool string* which is lowered into the well mounted on a cable. This cable contains wires which provide power and communication links with the surface. These

Figure 2-1: Proposed field system in a cutaway junction.

connections will power the manipulator and allow computationally expensive code to be run at the surface under less harsh conditions. Tool modules come in standard sizes dictated by the diameter of the well and the length of the trucks used to transport the tools to the well site. For a 9 in (22.9 cm) diameter well, a standard 4 in (10.2 cm) diameter tool module that is 8 ft (243.8 cm) long is assumed. These standard dimensions determine the envelope in which the manipulator mechanism must fit. Additional tool modules can be used to carry other components such as motor amplifiers and control computers.

When measurements are being made, the tool module containing the manipulator is mounted to the wellbore in order to provide a stable, fixed base from which to make measurements. This will be achieved using expanding rubber rings on the exterior of the tool module (see Figure 2-1). The tool will be initially positioned in the well near the junction to be explored using records or data from initial sensor sweeps. From this initial position the manipulator will have to search for the junction and then map it. If the tool module base is too far from the junction, it may need to be repositioned.

2.2.2 Mapping Requirements

The shapes of well junctions need to be characterized with millimeter scale resolution. Nominally, the junction is the intersection of two

cylinders. See Figure 2-2. The important information describing this idealized junction shape can be represented by a small number of parameters: the diameters of the main and lateral bores, the angle of divergence α between the main and lateral bores, and the azimuthal angle θ in which the divergent branch heads. The actual junction will differ from this ideal model, especially in the region of edges where the two bores come together. The shape of this lip must be accurately characterized in order to provide a useful map of the junction.

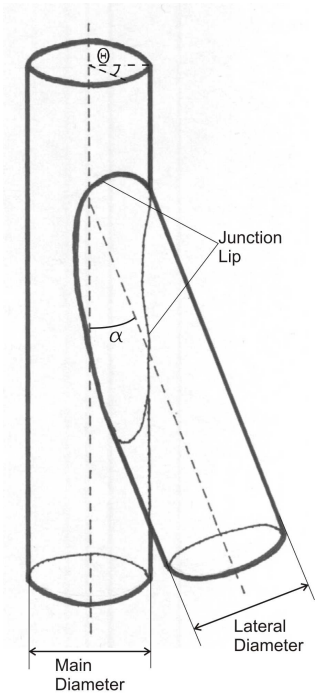

Figure 2-2: Schematic junction diagram showing key characteristics.

2.2.3 Environment Constraints and Requirements

The system must be able to survive the harsh conditions inside an oil well and the surface environments in which oil wells are located. The system will likely experience collisions and mechanical shocks. Additionally, the manipulator will endure extremely high temperatures and pressures as well as large fluctuations in temperature and pressure as it is lowered into the well. The sensors and actuators used must be insensitive to these conditions or capable of being rendered so reliably through compensation. It is also important to recognize that the thermal expansion produced by such large temperature changes will introduce significant backlash into the mechanism. This backlash must be compensated

for mechanically or algorithmically in order to generate accurate measurements of surface geometry. The effects of backlash and angular error on the accuracy of tactile data may be evaluated for a specific manipulator design using:

$$\Delta\vec{x} = J(\vec{q})\Delta\vec{q} \tag{2.1}$$

where $\Delta\vec{q}$ is a vector of small joint angle errors, $J(\vec{q})$ is the state dependent manipulator Jacobian, and $\Delta\vec{x}$ is the resulting error in the Cartesian coordinates of the manipulator end effector.

2.2.4 Workspace Requirements

The junction mapping task imposes demanding requirements on the manipulator workspace. For the purposes of the design and feasibility study, the nominal case of a 9 in (22.86 cm) main bore and 7 in (17.78 cm) lateral bore meeting at a 5° divergence angle is assumed. Modeling the junction as two intersecting cylinders, the junction length L_{junc} may be approximated as:

$$L_{junc} = \frac{D_{lat}}{\sin(\alpha)} \tag{2.2}$$

where D_{lat} is the diameter of the lateral bore. The desired workspace then consists of the junction which is approximately 80 in (204 cm) long and has a narrow cross section defined by converging bores. The manipulator must be able to operate, preferably without having to reposition the arm's fixed base, in this long, narrow, and constrained workspace in order to fully map the junction.

2.3 Design Approach

In response to the harsh operating conditions and the stringent reliability requirements that the system must meet, a design approach promoting mechanical robustness through simplicity is pursued. Sensing and control approaches are evaluated in part based on the number and inherent durability of the sensors each approach requires. Consequently, tactile sensing pads are not considered. Instead the use of a single, fine-pointed, passive probe mounted at the end of the manipulator is assumed. Design trades on sensing and control methods determine whether or not a force/torque sensor is necessary.

Motivated by the same desire to minimize complexity and thereby promote reliability, kinematic evaluations in the feasibility and field system design study focus on traditional link and joint manipulator architectures with minimal degrees-of-freedom. Robots with a low number of degrees-of-freedom and continuous revolute and prismatic joints are a mature technology. These designs therefore provide a good baseline model for evaluating the feasibility of the proposed field system. The use of a minimal number of degrees-of-freedom both limits design complexity and cost and minimizes the number of components that can fail. The resulting manipulator designs are also relatively easy to control.

While traditional low degree-of-freedom manipulators serve well to evaluate system feasibility, hyper-redundant kinematic designs may be better suited to constrained down-well workspaces. This class of manipulators is considered in Chapter 5. Such hyper-redundant manipulators have many more joints that must be monitored for potential undesirable contact with the environment. However, when properly controlled, the continuously curved shapes and serpentine trajectories that these manipulators achieve provide greater capability to work around obstacles [22]. This potential must be harnessed through intelligent control, arm shaping, and trajectory planning techniques that are beyond the scope of this work.

2.4 Control and Sensing Architecture

Two different control and associated sensing schemes were reviewed during the development of the system design. These approaches were impedance control and hybrid force/velocity control. These approaches were evaluated using both mechanism design and control performance criteria. Control performance was evaluated through a series of simulations developed by Francesco Mazzini. The results and conclusions from these simulations are covered in greater detail and with a control-centered focus in his PhD thesis [37]. These were supplemented with data additional bench top experiments using an existing planar manipulator. The impact of control method selection on mechanism design was developed through design trade studies using representative sensor data from commercially available sensors.

For either control architecture, DC electric motors are the best source of actuation. A source of DC power will be available via the wireline to power these actuators. DC electric motor technology also meets the maturity and reliability requirements of down-well

applications.

2.4.1 Hybrid Force/Velocity Control

Hybrid force/velocity control decomposes the control space into subspaces in which force or velocity control are applied [49]. When in contact with a surface, force control is applied to subspace components normal to the surface while velocity control is applied to components tangential to a surface. While in free space, velocity control is used in all components. See Figure 2-3. A full review of this control algorithm may be found in [9, 49].

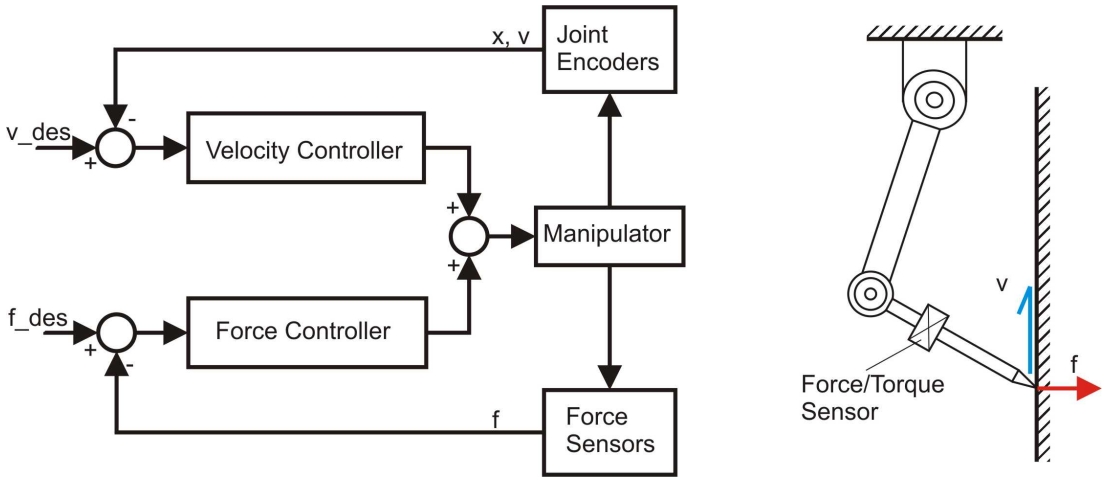

Figure 2-3: Block diagram of a hybrid force/velocity controller with a manipulator showing the force and velocity components of control. Note the required force/torque sensor.

This control approach requires accurate knowledge of surface normals and therefore necessitates the use of force/torque sensors. The inclusion of force/torque sensors greatly increases the complexity of the manipulator and reduces its inherent reliability. Force/torque sensors are very sensitive to the thermal expansion induced by temperature changes. Consequently, compensation will be required in order to handle the large temperature changes the manipulator will experience as it is lowered into and out of the well. These sensors will also make the manipulator sensitive to collisions and mechanical shocks. Loads high enough to damage a force/torque sensor could be created by collisions of the heavy tool string while moving through the well or during surface transport of the tool. Consequently, the inclusion of force/torque sensors required by hybrid force/velocity control makes the system far more fragile than a simpler, less expensive system that does not include force/torque sensors.

In simulations, hybrid force/velocity control also demonstrated previously-known issues

with transitioning between operating in free space and operating in contact with a surface. During this transition the controller must switch from using pure velocity control to a combination of force and velocity control. In order to avoid oscillations, a special touch-down procedure using high forces is used. These difficulties increase the amount of time required to transition from free space to contact as well as the likelihood of damaging the manipulator during this process. Consequently, hybrid force/velocity control promotes the use of a continuous tracing strategy that minimizes the number of transitions. However, this tracing approach suffers from accidental loss of contact with the environment and related oscillations and transition events. This is especially true when the surface being traced is rough, irregular, and unknown as in the case of an oil well junction.

2.4.2 Impedance Control

Impedance control uses a virtual impedance between a command point and the manipulator end effector to generate the forces commanded for the end effector [23]. See Figure 2-4. In free space, as the command point moves away from the end effector, forces increase causing the end effector to track the command point. If the command point moves through a surface, the end effector will be held to the surface by the force commands generated by the virtual impedance. See Figure 2-4.

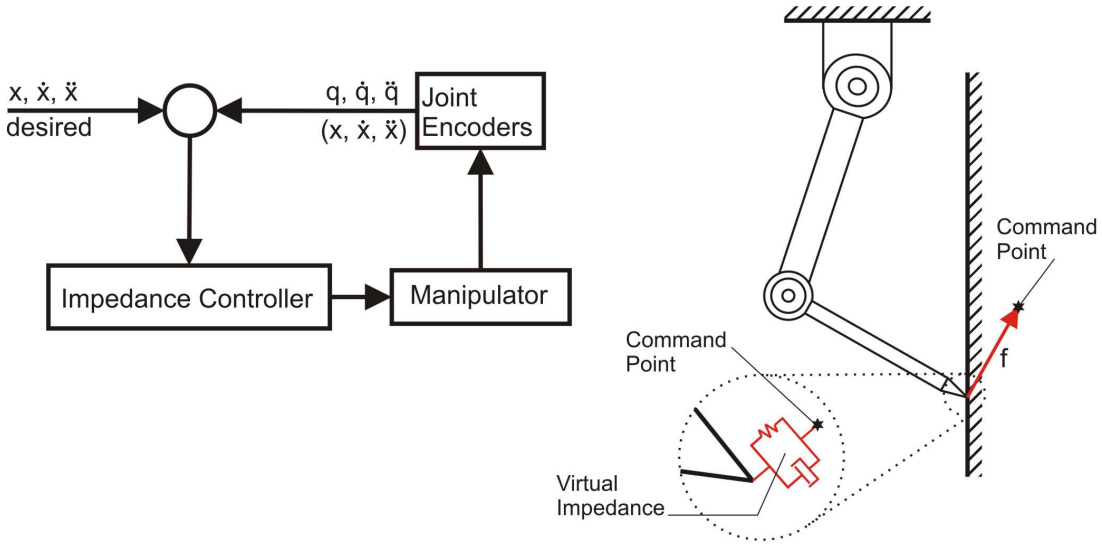

Figure 2-4: Block diagram of an impedance controller with a manipulator showing the virtual impedance and the force pulling the manipulator towards the command point.

Typically, impedance control is implemented using force/torque sensors in order to create

closed motor torque control loops and exactly achieve the forces specified by the combination of commanded impedance and trajectory. This enables impedance control to accomplish delicate tasks that require specific force levels. However, for the tactile exploration task, specified force levels are not important while maintaining contact with the surface is. Consequently, motor torques may be commanded open loop if the drive train is well-characterized, and problematic force/torque sensors are no longer required.

In contact with the environment, the manipulator dynamics in joint space are described by:

$$H(q)\ddot{q} + C(q,\dot{q})\dot{q} + g(q) = u + J^T(q)f \tag{2.3}$$

In this equation, $H(q)$, $C(q,\dot{q})$, and $g(q)$ are the manipulator inertia matrix, Coriolis matrix, and gravitational loading all described in joint space. $J(q)$ is the geometric Jacobian. The contact forces applied to the manipulator by the environment are represented by f and u is the control input. Using feedback linearization, the dynamics (equation 2.3) may be simplified to $\ddot{x} = \bar{u}$ where u is given by:

$$u = H(q)J_a^{-1}(q)(\bar{u} - \dot{J}_a(q)\dot{q}) + C(q,\dot{q})\dot{q} + g(q) - J_a^T(q)f_a \tag{2.4}$$

where $J_a(q)$ is the analytical Jacobian and the representations of environment forces are related by: $J^T(q)f = J_a^T(q)f_a$. The desired impedance behavior is then achieved by selecting $\bar{u}$:

$$\bar{u} = \ddot{x}_d + J_a(q)H^{-1}(q)\Big(D_m(\dot{x}_d - \dot{x}) + K_m(x_d - x) + f_a\Big) \tag{2.5}$$

where x_d specifies the reference trajectory of the command point and x indicates the state of the manipulator. The damping and stiffness matrices D_m and K_m represent the desired impedance characteristics of the manipulator in the second order model:

$$J_a^{-T}(q)H(q)J_a^{-T}(q)(\ddot{x} - \ddot{x_d}) + D_m(\dot{x} - \dot{x_d}) + K_m(x - x_d) = f_a \tag{2.6}$$

The resulting control law:

$$u = H(q)J_a^{-1}(q)\Big(\ddot{x}_d - \dot{J}_a(q)\dot{q}\Big) + C(q,\dot{q})\dot{q} + g(q) + J_a^T(q)\Big(D_m(\dot{x} - \dot{x_d}) + K_m(x - x_d)\Big) \tag{2.7}$$

does not require force feedback. Therefore, the mechanism does not need force/toque sen-

sors. Further details on impedance control are provided in [9, 23].

In simulations, impedance control performs well. It does not demonstrate transition problems when switching from operation in free space to operation in contact with a surface. Consequently, this control strategy may be used for continuous surface tracing or discrete point sampling. This makes the algorithm applicable to the interior surfaces of well junctions which are unknown and may be irregularly cut and corroded.

Impedance control is selected as the best control strategy for tactile oil well exploration systems. With an open torque loop implementation, impedance control allows sensing requirements to be reduced to the minimal level of joint angles alone. The strategy's reliable performance through transition events also allows data to be easily sampled at discrete points that are very dispersed.

2.5 Kinematic Design

Initial exploration of manipulator configurations focused on kinematic configurations with 3 degrees-of-freedom. These designs can position the probe tip with minimal kinematic complexity. After reviewing possible designs, three were selected for further consideration: the cylindrical, spherical, and anthropomorphic or elbow manipulators (See Figure 2-5). The workspace and operation of these different designs were considered within the nominal and off-nominal junctions. These workspaces were calculated numerically using for 3D junction models. Reachable workspace volumes were calculated by searching through the manipulator's forward kinematics for states where the manipulator does not collide with the environmental constraints. Reachable points on the junction surface were discovered by using the manipulator's inverse kinematics. For clarity, when workspaces are depicted below, 2D cross-sections are shown.

2.5.1 Anthropomorphic Configuration

The anthropomorphic configuration proved to be the most suitable of these three designs. The elbow manipulator has the greatest possible workspace within the constrained down-well environment of the three options considered. The elbow configuration is also very adaptable to off-nominal well environments. Its greater reach allows the manipulator to operate in wells with a main bore diameter larger than the nominal case. At the same time,

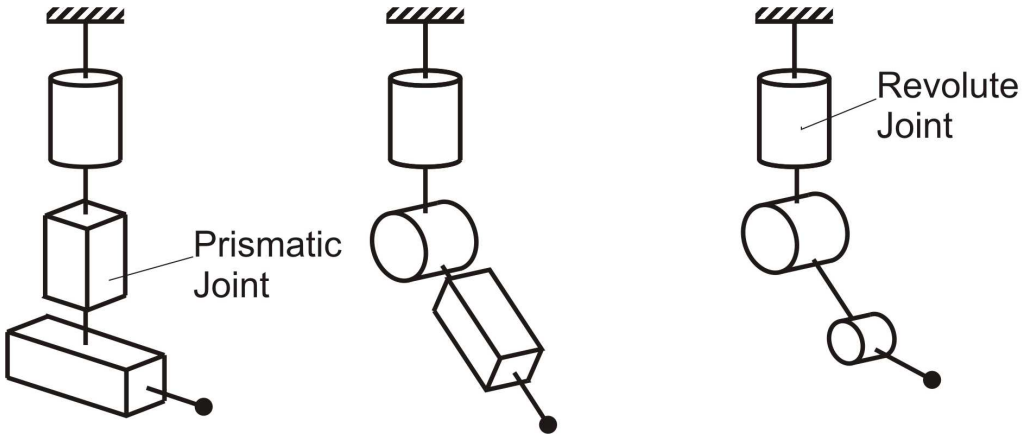

Figure 2-5: The 3 degree-of-freedom kinematic structures that were considered: *Cylindrical*, *Spherical*, *Anthropomorphic*.

the way in which the manipulator's links move allows it to continue operating within wells of smaller diameters with a relatively graceful reduction in workspace. Within a closed cylindrical section of casing, a narrower main bore diameter will prevent the manipulator from translating its links across the diameter of the bore. Consequently, the links will have to remain in roughly the arrangement in which they enter the well, allowing the manipulator to access only a portion of its typical workspace. However, in many cases the extra maneuvering space provided by a junction will allow an elbow manipulator to pass through these limitations and access most of its workspace. A 2D plot of the anthropomorphic manipulator's workspace within a nominal junction may be seen in Figure 2-6. The junction geometry in this figure corresponds to the nominal case with 9 in main diameter, 7 in lateral diameter, and 5° divergence angle. Note that this manipulator can reach all parts of the junction including the lower side of the lateral bore. However, the limited length of the workspace along the well axis prevents the manipulator from exploring the entire junction without moving the wireline tool base.

2.5.2 Spherical Configuration

The spherical configuration is inferior to the anthropomorphic design primarily because of its limited reach and limited adaptability to off-nominal well environments. The length of the manipulator's extendible prismatic link is limited by the diameter of the main bore. In the fully retracted position, this link must be able to rotate inside the main bore. A 2D plot of the spherical manipulator's workspace within a nominal junction may be seen

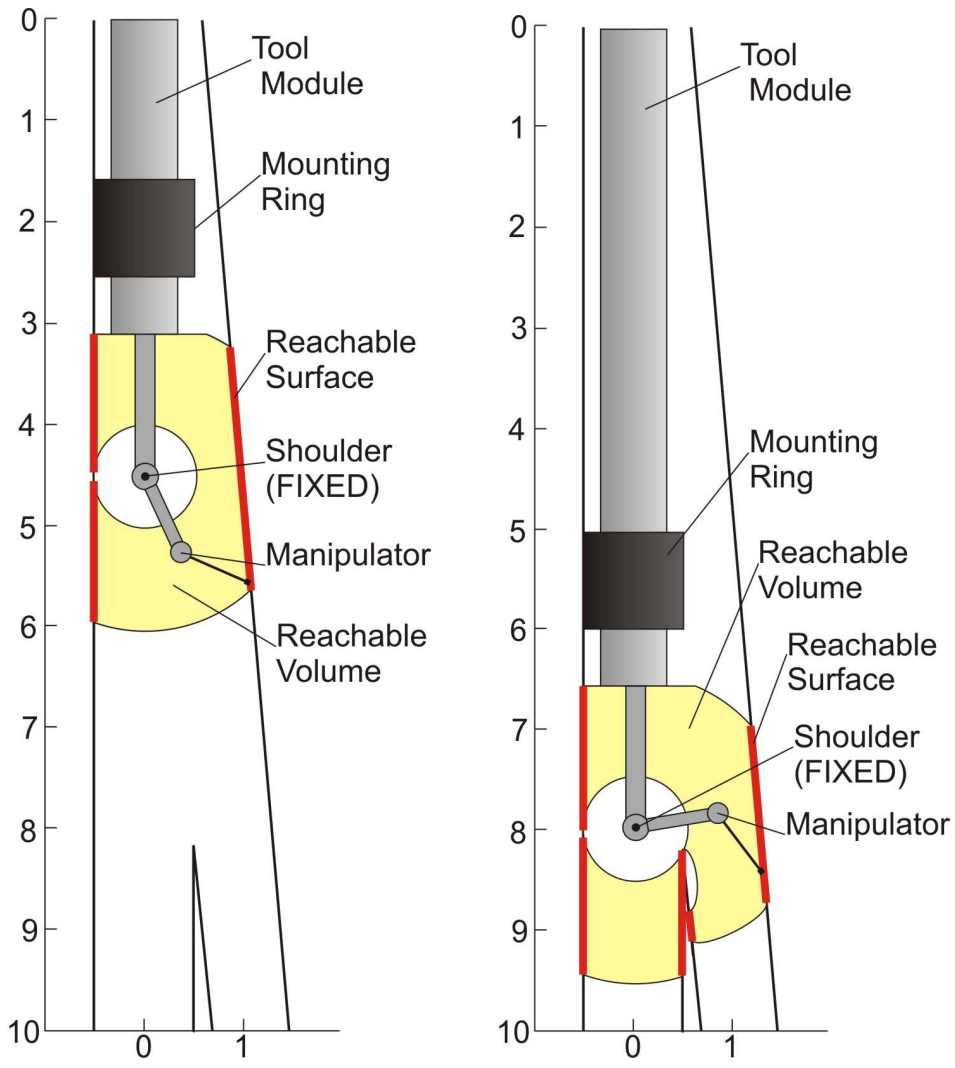

(a) Workspace with manipulator base located in the center of a junction.

(b) Workspace with manipulator base located near the bottom of a junction.

Figure 2-6: The workspace of an anthropomorphic manipulator within a junction. Dimensions are listed in units of main bore diameter.

in Figure 2-8. The junction geometry in this figure corresponds to the nominal case with 9 in main diameter, 7 in lateral diameter, and 5° divergence angle. Note that even with the manipulator located near the bottom of the junction, it cannot reach the lower side of the lateral bore. Longer extensions could be achieved using telescoping prismatic links. However this mechanism would be very complex. It could also potentially introduce high levels of backlash and elasticity due to the action of thermal effects on so many hard to adjust prismatic joint bearings.

The spherical kinematic design is also less adaptable to well environments with off-nominal characteristics. Its shorter reach would reduce performance in larger diameter wells. More importantly, its bulkier prismatic joint would be impossible to fully to rotate through the diameter of smaller than nominal main bores, creating a very limited set of orientations in which the manipulator could reach. Figure 2-7 shows how a smaller-than-nominal main bore diameter limits the range of motion of the revolute joint and the volume of the reachable workspace.

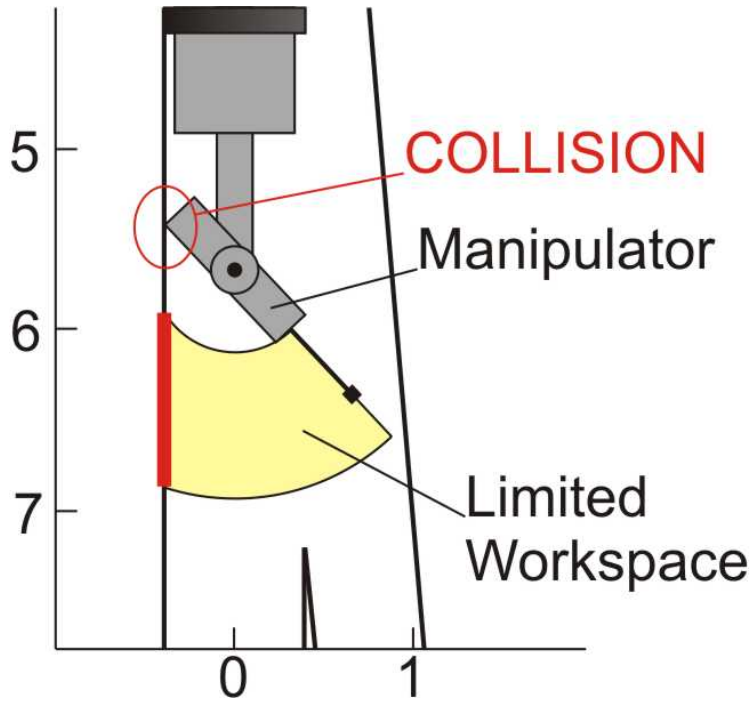

Figure 2-7: Limited adaptability of spherical manipulator to smaller-than-nominal bore diameters.

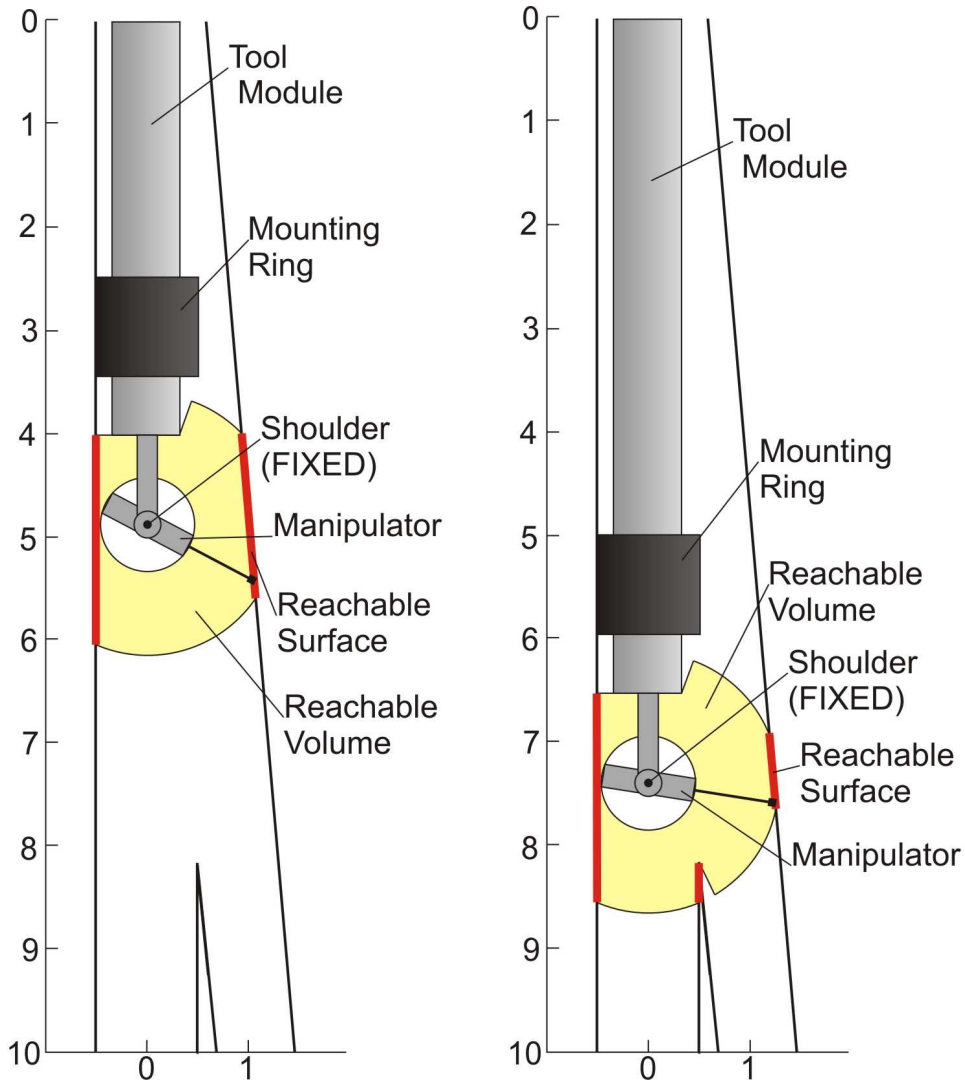

(a) Workspace with manipulator base located in the center of a junction.

(b) Workspace with manipulator base located near the bottom of a junction.

Figure 2-8: The workspace of an spherical manipulator within a junction. Dimensions are listed in units of main bore diameter.

2.5.3 Cylindrical Configuration

The cylindrical manipulator suffers from limitations similar in kind, but greater in magnitude, than the spherical configuration. The cylindrical configuration's one advantage is that one of its prismatic joints is aligned with main well axis and the long axis of the desired workspace. Consequently, cylindrical manipulator designs can potentially reach down the whole length of the desired junction. However, the cylindrical configuration is inherently incapable of reaching the bottom wall in lateral branches. More specifically, it is incapable of reaching around lips or obstacles like the elbow configuration can. A 2D plot of the spherical manipulator's workspace within a nominal junction may be seen in Figure 2-9(a). The junction geometry in this figure corresponds to the nominal case with 9 in main diameter, 7 in lateral diameter, and 5° divergence angle. Note that the manipulator cannot reach the lower edge of the lateral bore. It also loses contact with the far side of the lateral bore as the lateral bore diverges. This occurs because the reach of the manipulator's horizontal link is limited by the main bore diameter.

The cylindrical configuration also suffers from radial reach restrictions similar to those on a spherical configuration. In a cylindrical configuration, the distal prismatic link length is limited by the diameter of the main well bore. Consequently, the cylindrical configuration has limited adaptability to off-nominal well environments. It will be unable to reach junction surfaces in wells with larger diameters. This indicated by the way the manipulator cannot reach the far wall of the lateral bore as it diverges in Figure 2-9(a) It will be impossible to lower into wells with smaller diameters because the length of the retracted distal prismatic link and this link base would be larger than the bore diameter. See Figure 2-9(b)

2.5.4 4 Degree-of-Freedom Configurations

The comparison of 3 degree-of-freedom designs clearly indicates that from among the group reviewed, the anthropomorphic configuration is the best. This configuration has the largest workspace in well junctions with nominal dimensions and the best adaptability to off nominal cases. It also has the ability to reach around obstacles and lips by changing the configuration of its elbow. However, the anthropomorphic configuration has one major deficiency; it cannot reach the full length of the junction. It lacks the extended reach that a prismatic link aligned with axis of the main wellbore provides the cylindrical configuration. A re-

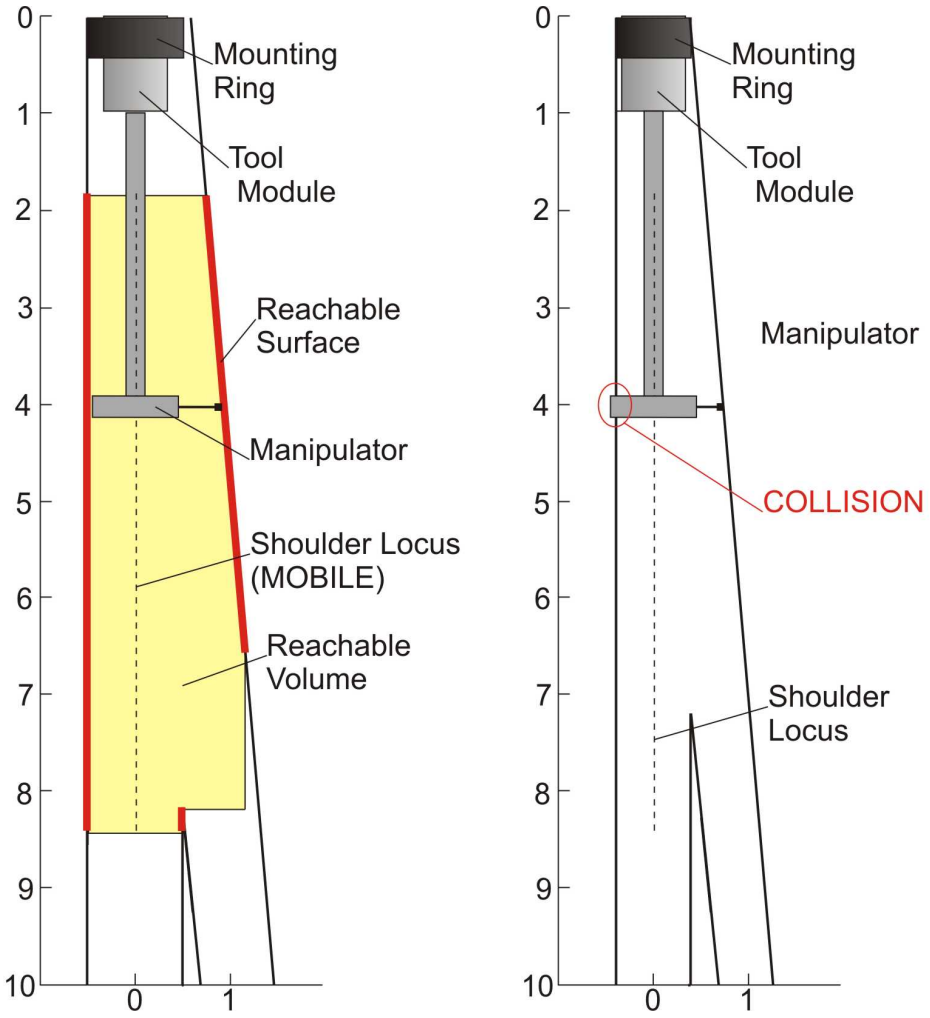

(a) Workspace in a nominal junction.

(b) Collision preventing deployment in smaller junctions.

Figure 2-9: The operation of a cylindrical manipulator within a junction. Dimensions are listed in units of main bore diameter.

dundant 4^{th} degree-of-freedom is required to be able to reach the entire desired workspace within the constrained wellbores.

A number of options were considered for implementing the 4^{th} degree-of-freedom and extending the manipulator's reach. Investigations focused on the spherical and anthropomorphic manipulator types which performed best in earlier analysis. In both cases, the best solution for increasing the number of degrees-of-freedom is a prismatic link aligned with the axis of the main wellbore at the base of the manipulator's kinematic chain. The workspaces of anthropomorphic and spherical manipulators augmented in this way can be seen in Figure 2-10(a) and Figure 2-10(b) respectively. This aligns the long axis of the desired workspace inside the junction with the long travel that can be achieved with a prismatic joint mounted in the tool base. This kinematic configuration is also the best in terms of implementation. The long travel required of the joint is aligned with the long axis of the standard 8 ft (243.84 cm)long wireline tool module. Assuming that a telescoping prismatic link is not used and that $\frac{1}{3}$ of the prismatic link's length must remain retracted for support and alignment, a joint extension of 64 in (162.56 cm)or 80% of the total junction length can be achieved. More complex telescoping prismatic joints would be able to reach the entire junction. The remaining links and joints of the manipulator should be in the antropomorphic configuration as suggested by earlier analysis. This will allow the manipulator to adapt to off-nominal well dimensions and give it some ability to reach around obstacles inside the junction.

Besides allowing the manipulator to explore the full length of a junction, a 4^{th} degree-of-freedom provides a number of other positive characteristics. The manipulator's longer reach will allow it to explore larger areas without needing to release and remount the robot's base inside the wellbore. This will allow the manipulator to do initial searches for branch locations faster. The redundant degree-of-freedom also enables the use of another constraint in determining how the manipulator end effector reaches a target position. Consequently, issues such as torque and power requirements, obstacle avoidance, and orientation may also be considered in choosing how the manipulator reaches certain positions.

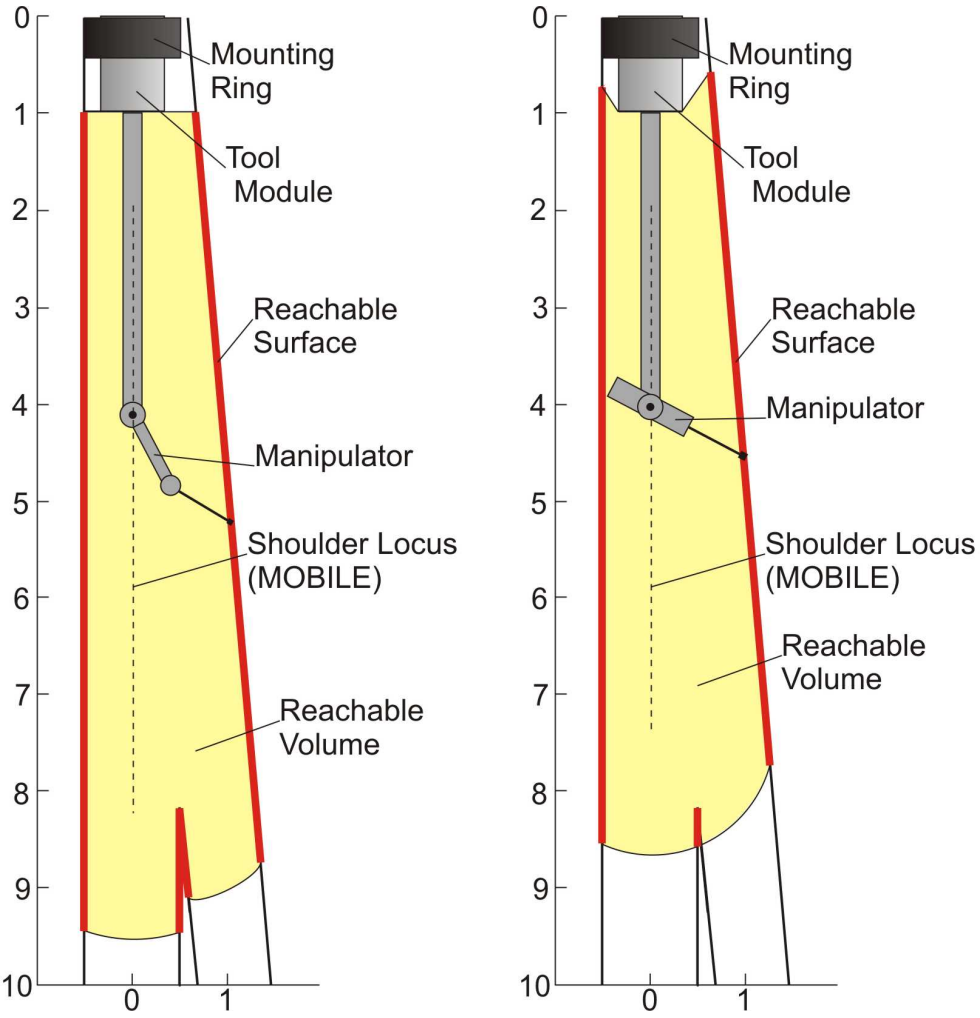

(a) 4 DOF anthropomorphic manipulator workspace.

(b) 4 DOF spherical manipulator workspace.

Figure 2-10: The workspace of 4 degree-of-freedom manipulators within a junction. Dimensions are listed in units of main bore diameter.

2.6 Conclusion: Field System Concept

The results of field system feasibility and design study indicate that a down-well tactile exploration system may be implemented using mature and reliable technologies. The tactile exploration manipulator has 4 degrees-of-freedom comprised of a 3 degree-of-freedom anthropomorphic arm mounted on a fourth prismatic joint. Joints are actuated by DC electric motors. Power and data processing are provided by wireline connections to the surface. The use of impedance control enables a minimal sensor approach requiring only joint angle measurements. The resulting system design is inherently very reliable.

Implementation and mechanical design issues are not addressed in the field system feasibility study. Link length and stiffness analysis are required to insure adequate manipulator dexterity and minimize flexibility that could produce tactile measurement errors. Similarly, joints and drive trains must be designed. These issues are considered within the bounds of developing an experimental system in Chapter 3.

Chapter 3

Experimental System Design

3.1 Introduction

An experimental system was designed and built in order to test and guide the development of control and intelligent search algorithms for efficient tactile characterization. Additionally, this experimental system acts as a proof of concept for the for the kinematics and control aspects of the field system architecture developed in Chapter 2. The experimental system consists of an environment tank and a purpose-built tactile probing manipulator, Figure 3-1. The environment tank represents an oil well junction and is capable of being filled with fluids to replicate down-well junctions filled with viscous fluids. The manipulator follows the design architecture developed during the field system feasibility and design study described in Chapter 2.

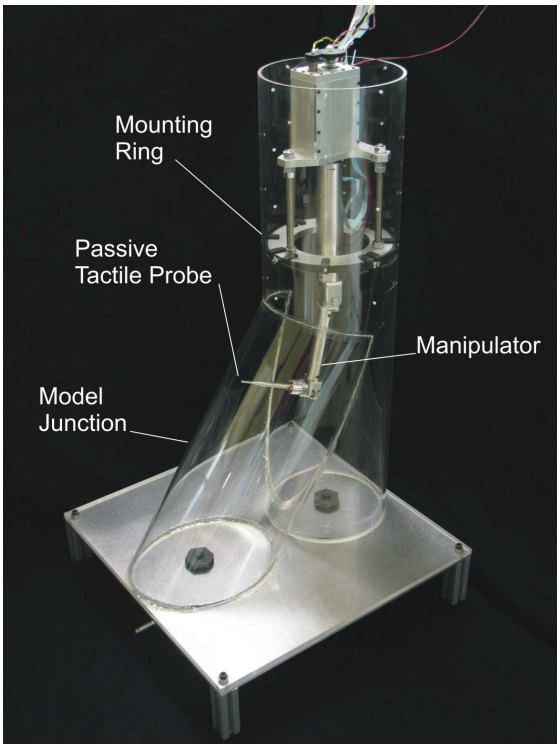

Figure 3-1: Experimental system.

3.2 Laboratory Scaling and Simplifications

In order to adequately test the complex interactions between proposed field system hardware, control, and search algorithms with the down-well environment, the experimental system must replicate the important characteristics of the actual field situation. At the same time the experimental system must be adequately scaled to meet budgetary, time, and laboratory space constraints.

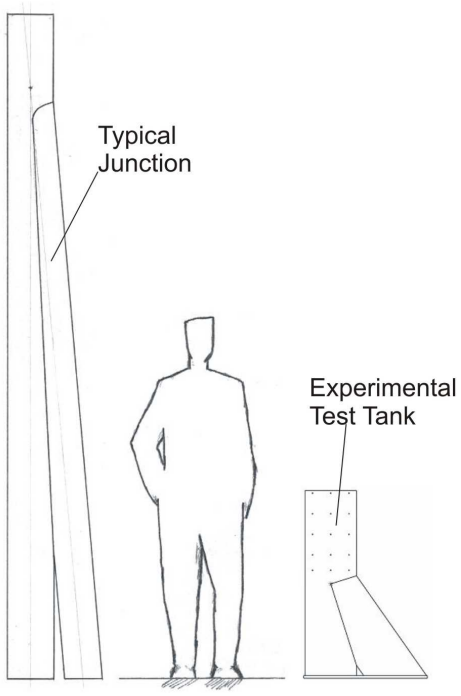

Figure 3-2: A comparison of an actual well junction, an average man, and the experimental test tank showing relative scaling.

Many of the necessary simplifications are related to the experimental representation of the down-well environment. While it is important to test effects of representative viscous fluids on the performance of control algorithms and the proposed tactile probing scheme, extreme down-well temperature and pressure will not be replicated by the experimental system. Fluid interactions with the manipulator and control algorithms are complex, difficult to simulate, and could have a potentially large impact on the system performance. It is both important and feasible to represent these fluid related conditions in the experimental system. Extreme down-well temperatures and pressures however, will have negligible influence on manipulator and control algorithm performance as long as the manipulator is properly temperature hardened and pressure compensated. These are field system implementation

issues that do not need to be addressed in an experimental proof of concept. Similarly, the size of a typical oil well junction (with an assumed length of 80 in) (203.2 cm)is too large to be manageable in a laboratory setting. The experimental test tank therefore represents a junction reduced in length by increasing its divergence angle to $\alpha = 30^\circ$. See Figure 3-2

The experimental manipulator is simplified by removing the redundant 4^{th} degree-of-freedom. This greatly reduces the cost and complexity of the mechanism as well as the control of the manipulator. The challenges of controlling redundant manipulators are well known and not the focus of this research. The simpler non-redundant manipulator still enables the exploration of the important challenges raised by this tactile exploration research. Namely, in the controls area, the manipulator may still be used to test control algorithms for tactile exploration with minimal sensing (joint angles measurements and no force/torque information). In the intelligence area, the simplified non-redundant arm can still be used to test new algorithms for efficient tactile characterization with minimal data.

3.3 Experimental Test Tank

The experimental test tank (Figure 3-3) represents a scaled oil well junction and is capable of holding simulated well fluids. The tank is made out two 9.5 in (24 cm) inside diameter, 0.25 in (0.6 cm) thick acrylic tubes joined at a 30° divergence angle. The clear acrylic enables easy observation of manipulator performance. The decision to use tubes with identical diameters allowed for easier cutting and joining operations than the use of different diameters. The combination of 9.5 in tubes and a 30° divergence angle results in a junction 19 in (48.3 cm) long. This is still too long for a non-redundant, 3 degree-of-freedom manipulator to reach. To enable this manipulator to reach all areas of the junction, a series of mounting holes is provided along the axis of the tube representing the main bore. This series of mounting positions enables gross positioning of the manipulator relative to the junction. Figure 3-3(b) shows a drawing of the test tank assembly listing reference numbers for the primary parts. Detailed design drawings for these referenced parts are provided in Appendix A.2.

(a) Test tank with manipulator mounting supports affixed at top of main bore.

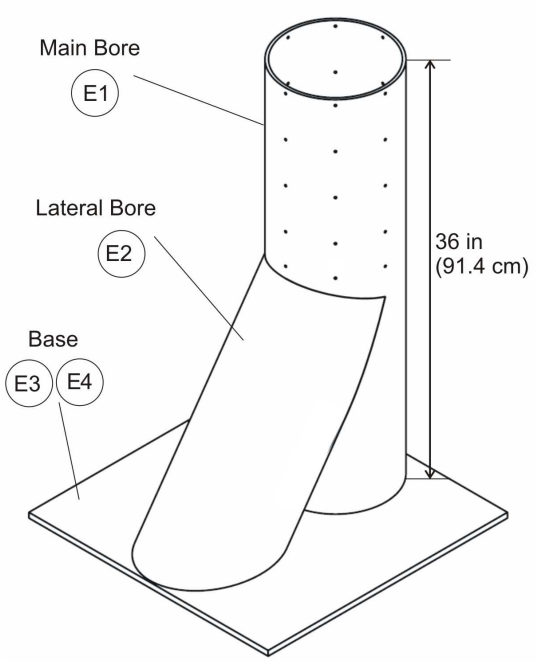

(b) Drawing of the test tank assembly listing part numbers.

Figure 3-3: The experimental test tank. Note the series of mounting holes along the axis of the vertical tube enabling the gross adjustment of the manipulator base position.

3.4 Experimental Manipulator Design Process

The experimental manipulator is a 3 degree-of-freedom anthropomorphic arm designed according to the system architecture developed in Chapter 2. See Figure 3-4. Most notably, the mechanism design assumes the use of impedance control with minimal sensing. To demonstrate the use of minimal sensing, the only sensors the arm incorporates are joint angle encoders. The final mechanical design of the manipulator was developed through an iterative design sizing process. Specific details including link length, link structural design, as well as drive train and joint design were determined while conducting design trades between these individual elements.

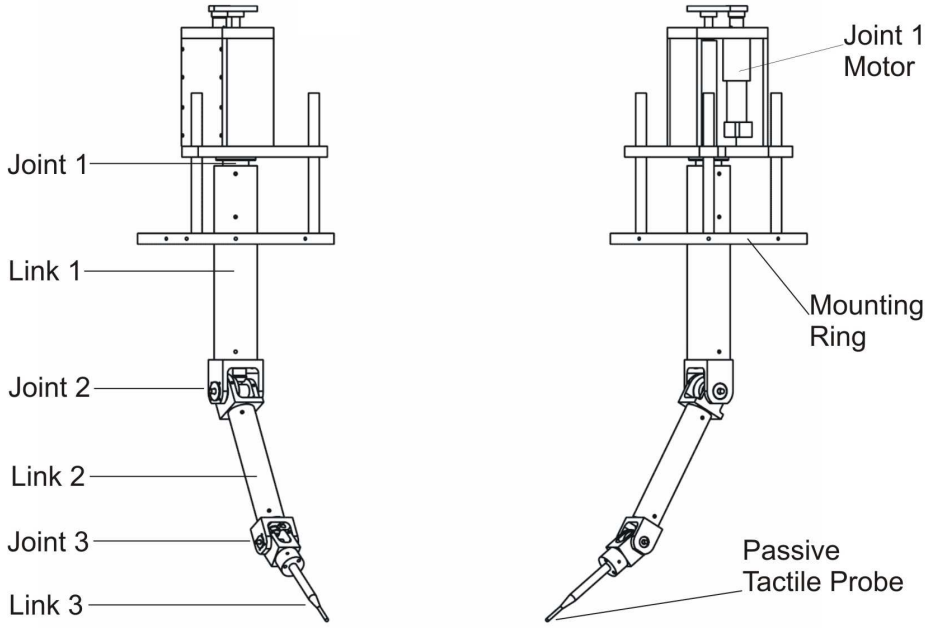

Figure 3-4: Essential elements of the tactile probing manipulator.

3.4.1 Kinematic Structure: Link Lengths

Link lengths were selected based on evaluations of manipulator workspace inside the experimental test tank as well as the manipulator's dexterity within this workspace. The effects of link lengths on the workspace of the manipulator were numerically evaluated as in Chapter 2. The dexterous quality of the manipulator workspace was evaluated using the

measure of isotropy Δ [28]:

$$\Delta = \frac{M}{\Psi} \qquad \text{where} \qquad (3.1)$$
$$M = \sqrt[m]{\det\left(JJ^T\right)}$$
$$\Psi = \frac{\text{trace}(JJ^T)}{m}$$

In these equations J is the analytic Jacobian of the manipulator and m is the number of degrees-of-freedom.The measure of isotropy provides a quantitative evaluation of dexterity that is scale-independent of link lengths [28]. As a result, this metric can be used to compare the dexterity of manipulators with differently sized links. The measure of isotropy has a maximum value of 1. Higher Δ values indicate increased isotropy in the Jacobian matrix eigenvalues and consequently increased isotropy in the forces and velocities the manipulator is able to produce at its end effector. In order to evaluate the overall dexterity of the manipulator within the constrained workspace of the experimental test tank, a global volumetric average of the measure of isotropy was considered [20]. This global metric is given by:

$$\Delta_{global} = \frac{A}{B} \qquad \text{where} \qquad (3.2)$$
$$A = \int_V \Delta dV$$
$$B = \int_V dV$$

where V is the volume of the workspace.

Link lengths were subjectively chosen using the guidance of workspace size and dexterity analysis. Additionally, as the manipulator design developed, the space requirements for joint and drive train components were considered in selecting link lengths. This design trade process ultimately resulting in link lengths of 8 in (20.32 cm) and 6 in (15.24 cm) for links 2 and 3 respectively. Link 1 is 10.5 in (26.67 cm) long. This length was determined by joint 2 drive train requirements as well as manipulator reach and sealing considerations for when the test tank is filled with fluid.

3.4.2 Link Structural Analysis and Design

The structural design of the manipulator links was guided by a stiffness analysis of the manipulator. The links were designed such that link deflections under maximum nominal operating loads introduce negligible error into measurements of the position of the manipulator end effector. Linear elastic solid mechanics theory was used to analyze manipulator deflections. The effects of both bending and torsional deflection were considered. In the analysis of each deflection component, the manipulator was assumed to be in the configuration for maximum deflection and under a maximum expected load. Nominal manipulator force loadings were obtained from simulation results. These results indicated maximum nominal forces at the end effector of 10 N. Allowing for a factor of safety, an end effector loading of 20 N was used in the stiffness analysis. A a maximum allowable deflection of 0.1 mm in the position of the end effector was used.

To analyze the bending stiffness of the manipulator, it was considered in a fully extended state under perpendicular loading. See Figure 3-5. The manipulator is modeled by an equivalent cantilevered beam. In the general case, the displacement of the elastic curve of the beam is described by:

$$y = \int_0^x \Big(\int_0^x \frac{M(x)}{E(x)I(x)} dx + C_1 \Big) dx + C_2 \qquad \text{with boundary conditions} \qquad (3.3)$$

$$y(x = 0) = 0$$

$$\frac{dy}{dx}(x = 0) = 0$$

where $M(x) = F(L - x)$ is the bending moment, $E(x)$ is the Young's Modulus of the beam at x, and $I(x)$ is the moment of inertia of the beam's cross-section at x. In this form, the equation can handle variable modulus of elasticity and moment of inertia along the length of the beam.

However, it is reasonable to assume that both E and I are constant. The excellent stiffness, machining, and corrosion characteristics of aluminum make it ideal for all 3 links of the manipulator. The simple concentrated end loading of the manipulator does not motivate the use of variable moment of inertia among its links. With these simplifying

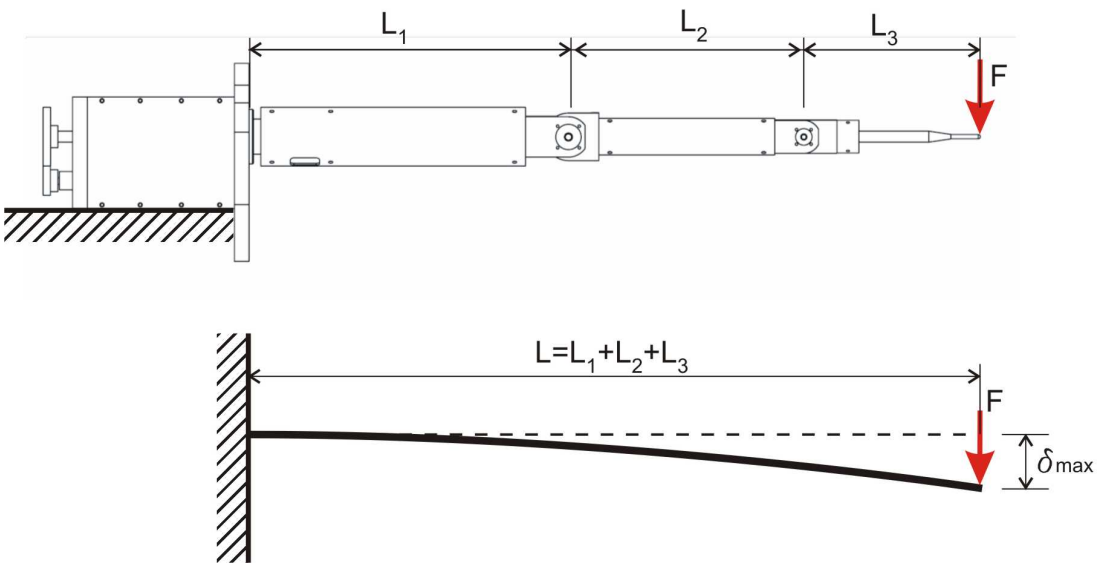

Figure 3-5: Beam bending model of worst case manipulator tip deflections.

assumptions, the elastic curve equation reduces to:

$$y = \frac{F}{6EI}(x^3 - 3Lx^2) \tag{3.4}$$

where F is the force acting on the end of the beam. The maximum deflection δ_{max} occurring at the end of the beam, the end effector of the manipulator is:

$$\delta_{max} = -\frac{FL^3}{3EI} \tag{3.5}$$

This equation may be reworked in order to solve for a required moment of inertia I in terms of known manipulator and loading parameters and the specified allowable deflection $\delta_{spec} = 0.1$ mm:

$$I = \frac{FL^3}{3E\delta_{spec}} \tag{3.6}$$

The torsional stiffness of the manipulator was similarly analyzed by considering configurations that create worst-case torque loadings. See Figure 3-6. Two configurations were considered: one maximizing the axial torque on link 1 and a second maximizing the axial torque on link 2. Assuming constant material properties and constant polar moment of inertia J for all manipulator links, the angular deflection of the links is described by:

$$\phi = \frac{TL}{JG} \tag{3.7}$$

where T is the applied torque, L is the length of the link or links undergoing torsion, J is the polar moment of inertia, and G is the shear modulus. This equation may be solved for J in terms of the specified allowable deflection:

$$J = \frac{TL}{G \arcsin(L_{distal})} \tag{3.8}$$

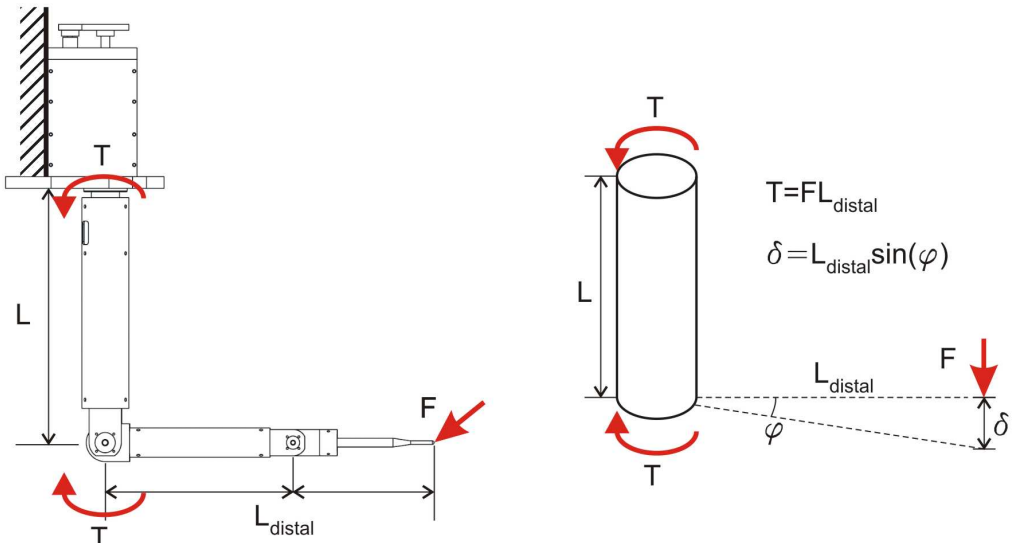

Figure 3-6: Torsional model of worst case manipulator tip deflections.

The structural design of the links was determined by the results of the stiffness analysis, the space requirements of the joint drive trains, and the need for compact links. Link 1 and 2 have hollow circular cross sections with outside diameters of 1.87 in (4.75 cm) and 1.25 in (3.18 cm) respectively. These provide isotropic stiffness properties and the required space for motors and drive trains. Link 3 has a solid circular cross section of 0.375 in (0.9525 cm). This provides the required stiffness with a narrow link that is less likely to accidentally contact the environment at a point other than the tip. This third link acts as the passive tactile probe end effector.

3.4.3 Joint and Drive Train Design

In designing the joint mechanisms, issues of stiffness, compactness, ease of assembly and adjustment were balanced. To minimize the risk of undesired contact between protruding joints and the environment, compact joint designs were pursued. At the same time, concessions were made for ease of assembly and adjustment. Given the experimental nature of the

Table 3.1: Joint Torques: Specified and Achieved

Joint Number	Specified Torque (Nm)	Continuous Torque (Nm)	Stall Torque (Nm)
Joint 1	5.3	8.0	9.4
Joint 2	6.1	8.0	9.4
Joint 3	2.4	3.1	4.4

system, it is likely to be rebuilt and adjusted often. Drive trains were designed to meet joint torque and velocity requirements derived from simulations. These simulations found that in order to reliably maintain contact with the environment and collect tactile data points, the manipulator needs to be able to apply a force on the order of 10 N to the surface. This end effector force requirement, padded by a factor of safety of 1.5, was converted into the joint torque requirements listed in Table 3.1. The continuous and stall joint torques achieved by the final design are also listed in Table 3.1. The essential components of these drive trains are listed in Appendix A.1.

Each joint assembly consists of a motor, gear train, encoder, and associated support bearings. See Figure 3-7. Brushed DC motors are used. Each drive train has a large gear ratio in order to provide the necessary torque to meet the design force requirements. The drive train transmissions consist of a planetary gear drive and a final open gear mesh. In Joint 1 this final mesh is made of spur gears. In Joint 2 and Joint 3, spiral and straight bevel gears respectively produce the change in torque direction required in these joints. See Figure 3-8. Joint angle sensing is provided by encoders mounted on the motor output shafts. High gear ratios between the encoder and joint increase the angular resolution of the joint angle measurements. The joints are designed to be sealed by encasing them within rubber bellows. The sealed manipulator can be used to test the system and control approach within fluids simulating down-well conditions. An exploded view of the entire arm assembly may be seen in Figure 3-9. Detailed design drawings for all manipulator parts are provided in Appendix A.1. These drawings are organized by the part numbers listed in Figure 3-9.

3.4.4 Manipulator Mounting

To replicate tool mounting conditions within an oil well, the manipulator is attached to the experimental test tank via a mounting ring. As mentioned in Section 3.3, a series of axially located mounting holes provide a number of positions for this mounting ring to be attached.

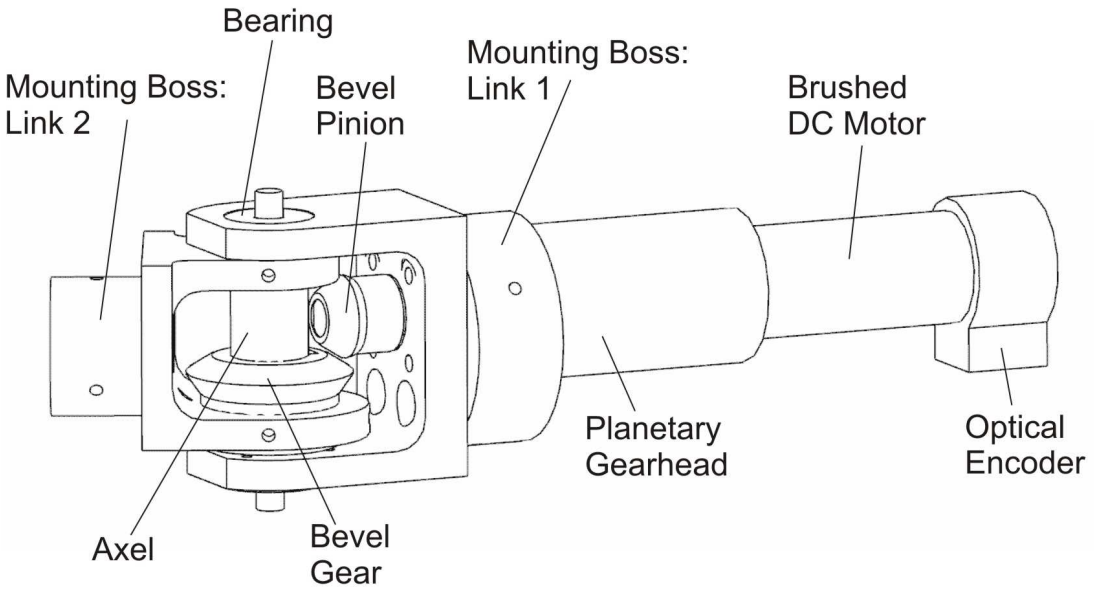

Figure 3-7: Primary components of joints 2 and 3. Joint 2 shown.

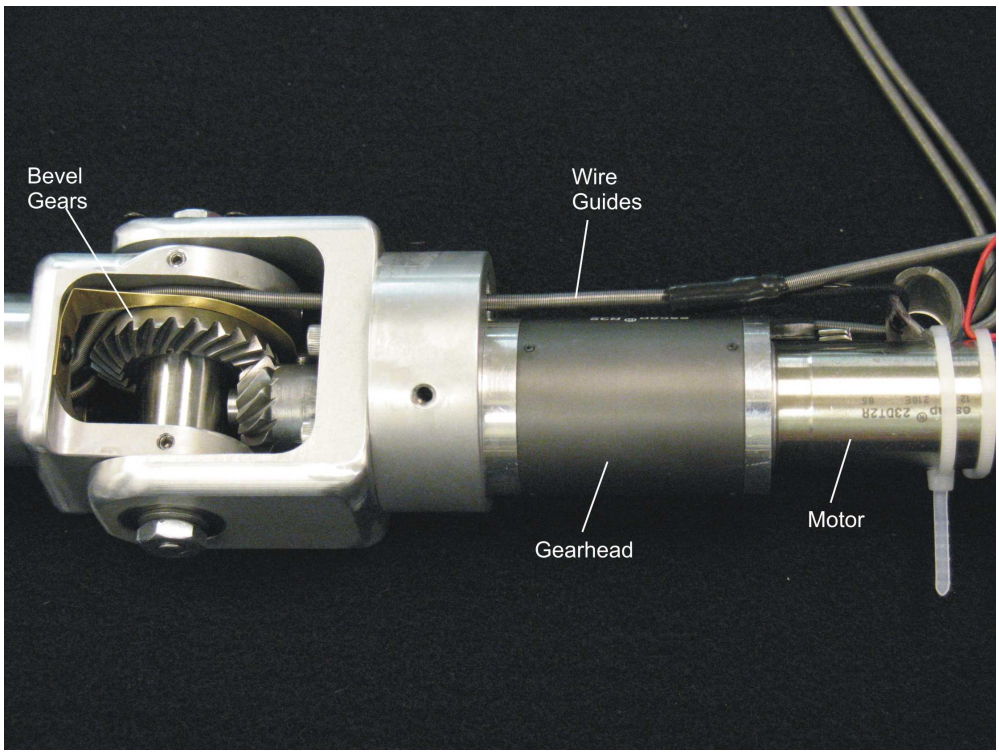

Figure 3-8: Joint 2 assembly showing motor, planetary drive train, bevel gears, and wire guides.

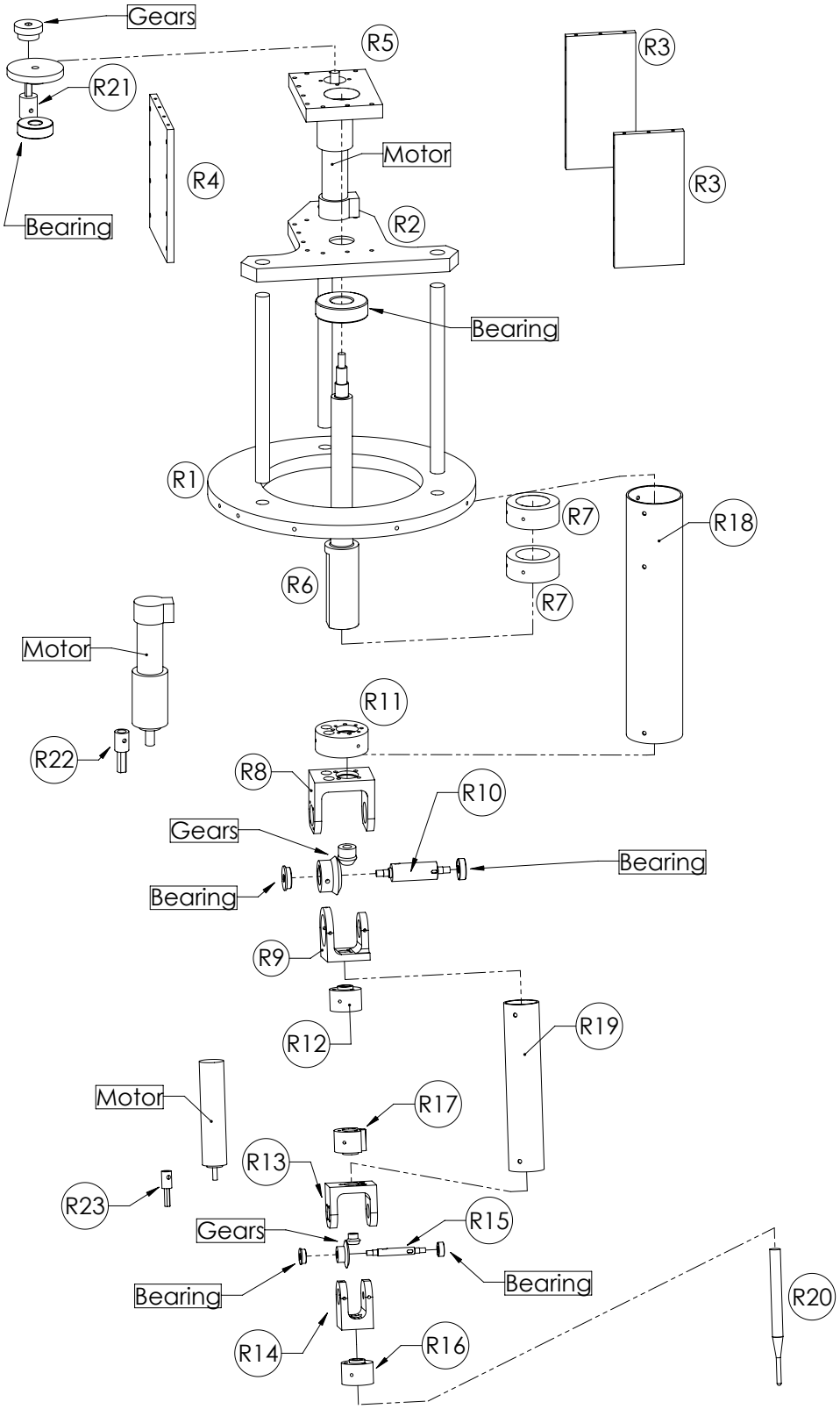

Figure 3-9: Exploded-view of the manipulator mechanism.

This facilitates the gross adjustment of the position of the manipulator relative to the model junction. A set of three threaded rods attaching the base of the manipulator to the mounting ring provides for fine position adjustment and the alignment of the manipulator's axis with the model wellbore axis. See Figure 3-10.

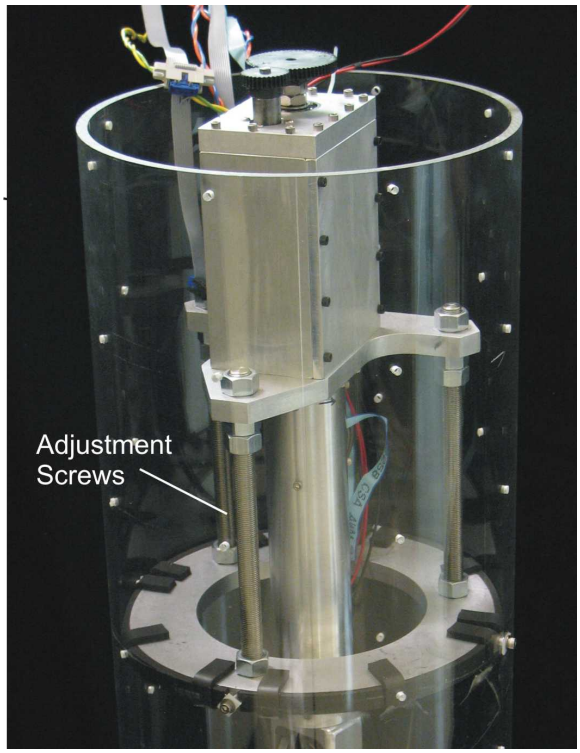

Figure 3-10: Manipulator mounting detail showing the mounting ring and three threaded rods for fine position adjustment. Note the series of ring mounting holes for coarse adjustment.

3.4.5 Computation and Control

Control for the manipulator is implemented in *Matlab xPC* on a PC computer dedicated to real-time control. A *ServoToGo* 8 axis servo I/O card provides joint encoder and motor command interfaces. The collected tactile data is processed incrementally as it is measured in a second data-analysis computer networked to the real-time control computer. This data-analysis computer attempts to fit geometric models to the collected data and chooses where to search next. Manipulator command trajectories are returned to the real-time control computer where they are executed. Torque commands are sent to the motors using current controlled amplifiers. See Figure 3-11.

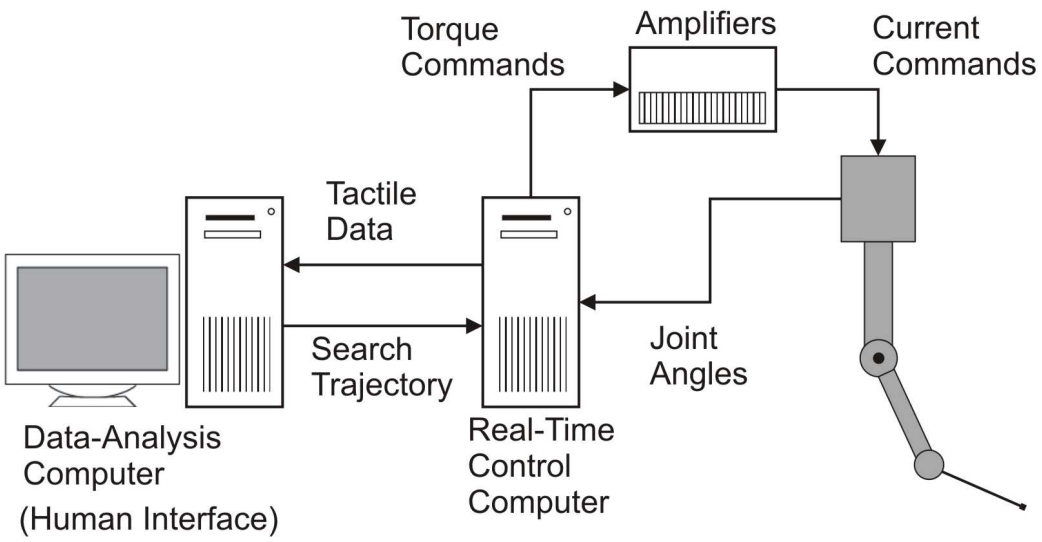

Figure 3-11: System architecture diagram showing command and data flows.

3.5 Conclusion

The completed experimental hardware may be seen in Figure 3-12. It consists of tactile probing manipulator and test environment that replicates the shape of an oil well junction. Additional shapes and objects may be placed inside this environment to create richer tactile exploration tasks. In addition to this hardware, the complete system includes computers and control electronics for planning and controlling tactile searches. This system provides a means of testing control and tactile search algorithms. It also serves as a proof a concept and testbed for the field system architecture developed in the feasibility study conducted in Chapter 2.

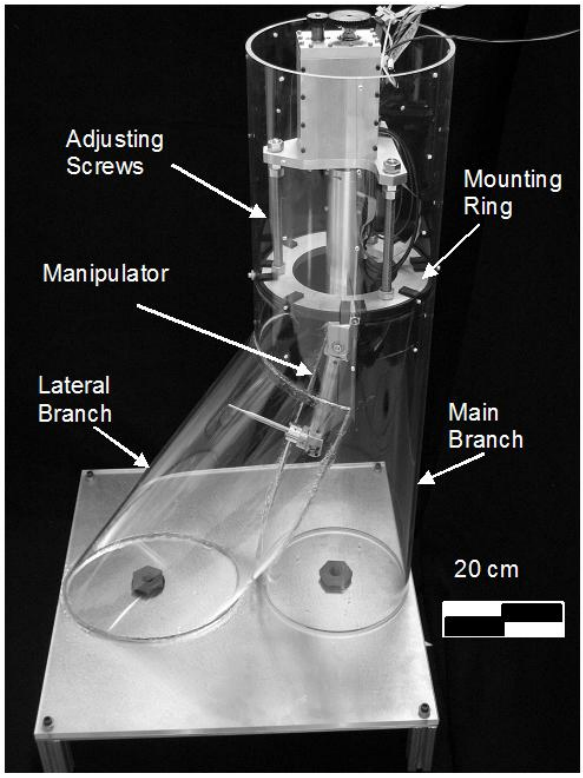

(a)

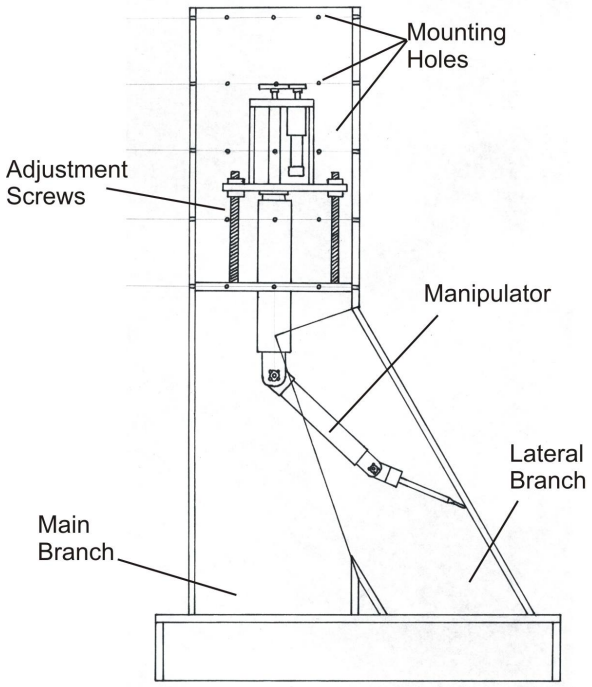

(b)

Figure 3-12: The fully assembled experimental system.

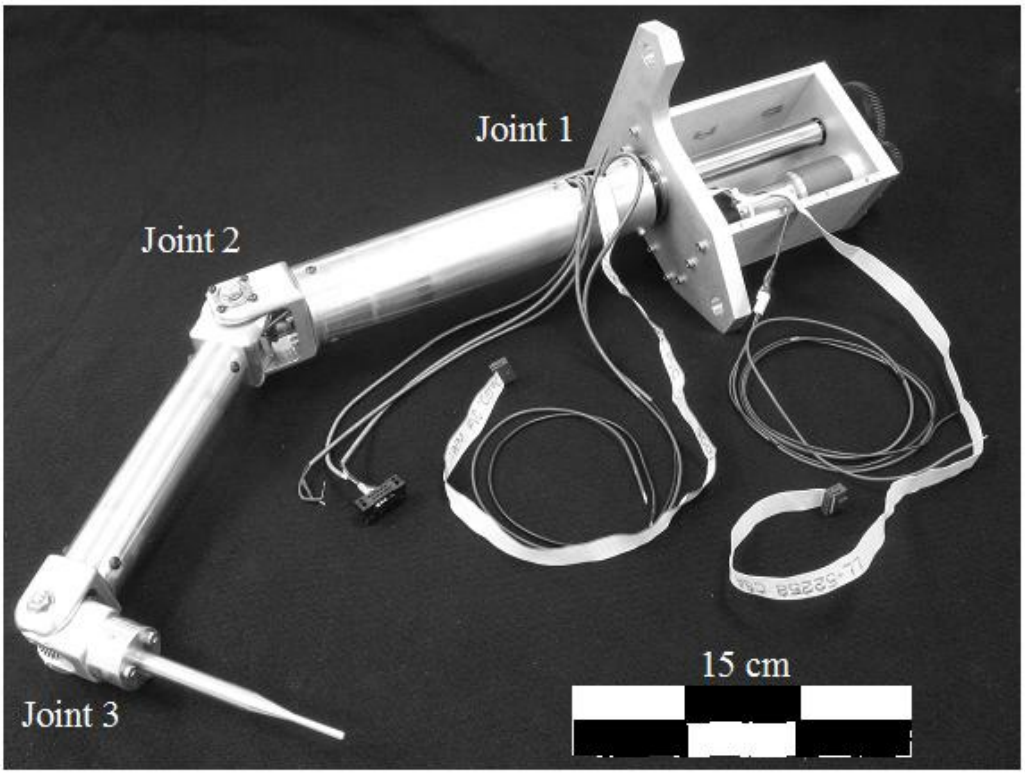

Figure 3-13: Tactile probing manipulator showing passive tactile probe.

Chapter 4

Experimental System Evaluation

4.1 Introduction

The experimental system has been used in a number of tests providing valuable evaluations of the proposed field system architecture, and the prospects of intelligent tactile exploration, as well as the experimental system itself. Characterizations of the experimental manipulator during assembly and initial motion trials revealed several defects and operating regions where the manipulator's performance did not meet requirements. Some of these problems were related to the specific design implementation used in the experimental manipulator and were remedied with design changes. Other shortcomings indicate problems with the original proposed field system design. Further experimentation and adjustment have produced refinements on the proposed field system architecture. In some cases small changes to this architecture were made. In other cases, critical features that will require careful design and system tuning were identified. Finally, the experimental system has been used to perform preliminary trials on intelligent tactile exploration algorithms that minimize the amount of data and time needed to characterize an unknown geometry. These initial trials demonstrate the feasibility of intelligent, data-efficient tactile exploration approaches using mechanisms with a minimal number of sensors.

4.2 Experimental Mechanism: Evaluation and Modifications

Initial testing revealed several design flaws in the experimental system that needed to be corrected.

An angular dependency in joint backlash was detected in Joint 2 and Joint 3. This was traced to concentricity and axis alignment errors in the mounting of the bevel gears in each joint. These gears were fixed to their shafts using set screws resulting in the observed eccentricity and misalignment between shaft and gear axes. This mounting method was chosen based on the selection of commercially available gears and the desire for spatially compact joints. A better, more concentric mounting option would be the use of gears with split, compression mounted hubs [38]. The use of commercially available compression collars would produce less compact joints, but the compression collar function could be built into the body of the joint with little or no loss of compactness. In the existing experimental system, these changes could not be made. However, during assembly careful adjustment and setting of the gears removed the loss of parallel alignment between gear and shaft axes reducing the final error levels.

The bevel gear meshes in Joint 2 and Joint 3 of the experimental system were also inadequately supported in the original design. These joints demonstrated backlash and elasticity far greater than predicted during the design process from component specifications. Furthermore, this behavior was nonlinear in both joints with especially pronounced nonlinear behavior and directional dependence in Joint 2. Because of the scale and nonlinearity of the errors, it was difficult to accurately predict and compensate these errors in the control algorithms. Careful observation and testing revealed that, in each joint mesh, forces between the bevel gear and pinion were causing the pinion to deflect. In both joints, the pinion was mounted on a cantilevered shaft supported by a bearing in an enclosed planetary gear drive. In order to stiffen both pinion shafts in the axial and transverse directions, a second ball bearing and retaining plate was attached to each shaft closer to the bevel gear mesh. See Figure 4-1. This greatly improved the stiffness of both joints. Of the residual joint elasticity, some may still be attributable to the deflection of the bevel gear pinion shaft. Ideally, the pinion shaft would be simply supported with bearings on each side of the pinion gear. However, within the space constraints of the current joint designs, this change is not possible. This problem reveals a case where joint compactness considerations took improper precedent over joint stiffness in the design process.

Following the completion of drive train improvements, the backlash of the experimental system was characterized again. The backlash of each joint was measured externally by manually moving the joint through its range of backlash and recording changes in the

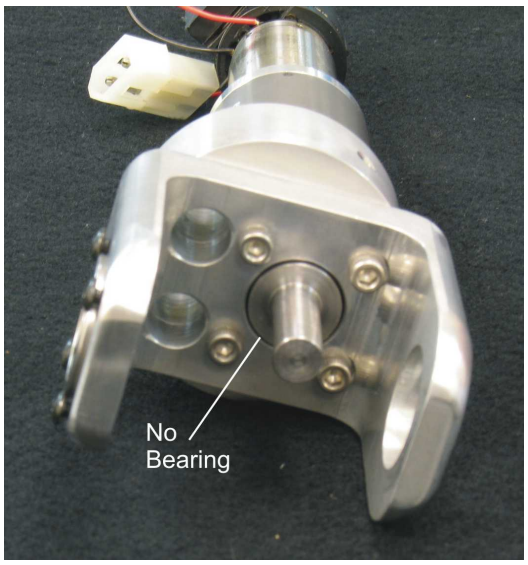

(a) Pinion shaft support prior to improvement.

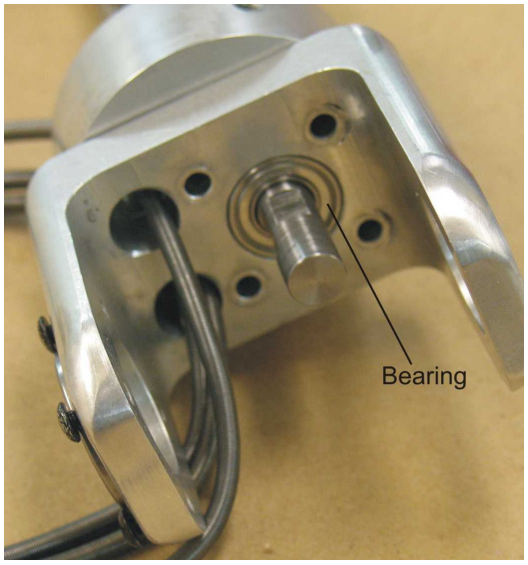

(b) Pinion shaft support after design improvement showing an additional bearing.

Figure 4-1: The support of the bevel gear pinion shafts in Joints 2 and 3 was improved by adding additional bearings close to the bevel gear meshes.

Table 4.1: Predicted and Measured Joint Backlash

	Joint 1	Joint 2	Joint3
Predicted Backlash	0.67°	0.75°	0.98°
Measured Backlash	1.23°	0.85°	1.26°

position of the corresponding link with a dial indicator. These measured backlash values closely match those predicted using component specifications; see Table 4.1. This indicates that with design improvements, the experimental system meets design expectations. When used to correct joint angles for the effects of backlash, these measured backlash values improve the accuracy of tactile data points taken from a test surface.

4.3 Findings on the Proposed Field System Architecture

A series of motion and tactile probing trials have provided an important evaluation of the field system architecture developed in Chapter 2. This information has guided a number of small changes to the proposed system architecture and revealed sensitive parts of the system that must be carefully implemented. Most importantly, these trials have shown

that the interaction of control methods and joint design have a critical impact on both motion performance and the accuracy of retrieved tactile data.

Motion trials revealed that under the control methods specified in the original system architecture, the manipulator's movements neither meet requirements nor match simulation results. While in free space, the manipulator would occasionally stop with non-zero errors between its probe tip and the command point referenced by the impedance controller. Consequently, this point was erroneously treated like a real tactile data point on a surface. This behavior resulted from stiction and binding in the manipulator drive trains, primarily in the bevel gears in Joints 2 and 3, that caused the manipulator to stop prematurely under the torque commands created by the impedance controller. This behavior appeared at much higher levels in the experimental system than in simulations because the complex friction that occurs in the bevel gear sets was not fully modeled in these simulations. The interaction of unexpected stiction and binding with the proposed minimal-sensor system architecture produces a high likelihood of erroneously identifying points in free space as data points on the surface of an unknown geometry.

This issue was solved by adding a integral term to the standard proportional-differential formulation of the impedance between the manipulator's probe tip and the command point:

$$\begin{aligned} u = H(q)J_a^{-1}(q)\Big(\ddot{x}_d - \dot{J}_a(q)\dot{q}\Big) + C(q,\dot{q})\dot{q} + g(q) \\ + J_a^T(q)\Big(D_m(\dot{x} - \dot{x_d}) + K_m(x - x_d) + \underbrace{L_m \int (x - x_d)}_{\text{new integral term}}\Big) \end{aligned} \tag{4.1}$$

where L_m is a matrix of gains for the integral error. See Section 2.4.2 for a more detailed review of impedance control. This additional term causes the command forces applied to the probe tip to wind-up to specified integration limits whenever a position error persists between the probe tip and command point. The integrator is reset whenever the sign of error changes. When in contact with the environment, this causes the contact force to ramp until the specified limit. In free space, this extra term causes the torques commanded at the joints to ramp and overcome binding and stiction whenever these unmodeled forces momentarily stop the manipulator. See [37] for a more detailed review of these control algorithms.

Tests of tactile data acquisition similarly revealed resolution significantly lower than ex-

pected. Depending on the configuration of the manipulator, errors as large as ±10 mm were observed in measurements of a test surface. The errors are an order of magnitude larger than the millimeter scale resolution specified in the design requirements. These measurements were made with compensation intended to remove the effects of joint backlash and elasticity. Here again, the performance issues are traced to the bevel gears. The elasticity introduced by the bevel gear meshes is not well represented by the simple linear model used in the compensation algorithms. The elastic behavior of these gear meshes appears to be directionally dependent and nonlinear. Consequently large elastic deformations are not properly corrected with the linear model used. This problem was corrected by decreasing the force applied by the tactile probe to the environment. This resulted in lower elastic deformations and correspondingly lower errors on tactile data points.

Both deficiencies discovered in field system architecture proposed in Chapter 2 were corrected by making small changes to the proposed control approach. Contact forces were lowered to decrease joint deflection and an integral term was inserted to overcome stiction problems. The choice to revise control methods makes sense for the experimental system given the relative ease of making these changes versus changing the hardware. Alternatively, these deficiencies may be viewed as mechanically related and hardware solutions may be pursued. The tests indicate that manipulator performance is very sensitive to the design of the joint drive trains and especially the arrangement and support of the bevel gear meshes. Future mechanical implementations could solve these problems by very carefully testing and vetting the designs of these bevel meshes or by removing them completely. The test results reveal the trade-offs between control and mechanical design in the proposed field system architecture.

4.4 Preliminary Tactile Exploration Algorithms Trials

A set of preliminary exploration algorithm experiments has also been completed on the experimental system. These trials tested algorithms developed by Francesco Mazzini for the intelligent tactile exploration of unknown surfaces with minimal data sets [36, 37]. At the time these trials were completed, tuning of the manipulator and control algorithms had reduced sensing errors to a range of ±10 mm. Despite this measurement inaccuracy, initial experimental results are still quite promising.

Table 4.2: Preliminary Experimental Results

Method	Cylinder 1 Radius (119 mm)	Cylinder 2 Radius (119 mm)	Number of Points	Distance Traveled by Manipulator	Time
Uniform Surface Density	122 mm	119 mm	76	8.16 m	556 s
Best Cone	122 mm	118 mm	26	4.52 m	169 s

Figure 4-3[1] shows the pattern of experimental touch points produced by a *Uniform Surface Density search*. This search algorithm attempts to cover the unknown surface with a even density of tactile data points. This search serves as a baseline for the comparison of other intelligent search algorithms that try to minimize the amount of data required to identify unknown geometry. The primitives fit to these touch points are also shown. The results of the surface modeling are given in Table 4.2. The algorithm was able to successfully map the two well elements as cylinders with about 3% accuracy. It took 76 points in this case to achieve this accuracy, see Figure 4-3. Here the manipulator needed to travel 8.16 m to make these measurements over a period of 556 s.

Figure 4-4[2] shows the touch points for a *Best Cone search*. This algorithm locally samples points until it fits a primitive. It then identifies the cone of largest angle from the current probe position that does not contain sample points. The axis of this cone serves as the new search direction; see Figure 4-2[3]. By searching regions where the least data has exists, this algorithm attempts to minimize the number of points that are required to identify a geometry. In this case, the search was stopped when the accuracy of the fitted cylinders' radii matched that achieved by the Uniform Surface Density search. As shown in Table 4.2, the number of points for the Best Cone method was reduced to 26 and the total distance traveled was reduced by half. Similarly, the required time was reduced greatly to 169 s or 30% of time required by the Uniform Surface Density search. It should be noted that the modeled cylinder intersection with respect to ground for the Best Cone search was not as good. This is attributed to the very small number of points required by the Best Cone strategy to match the radii accuracy. The conclusion is that different parameters in the environment geometry will converge at different rates.

[1]Image Credit: F. Mazzini [36]
[2]Image Credit: F. Mazzini [36]
[3]Image Credit: F. Mazzini [36]

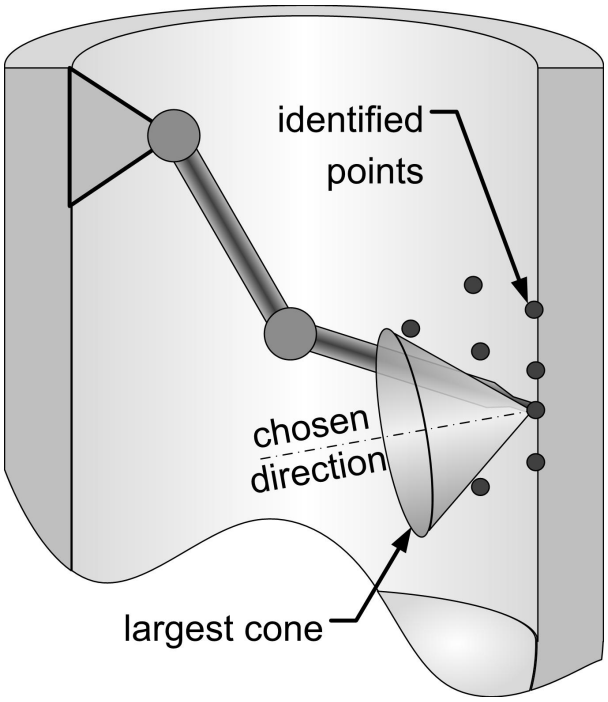

Figure 4-2: Depiction of the Best Cone search algorithm.

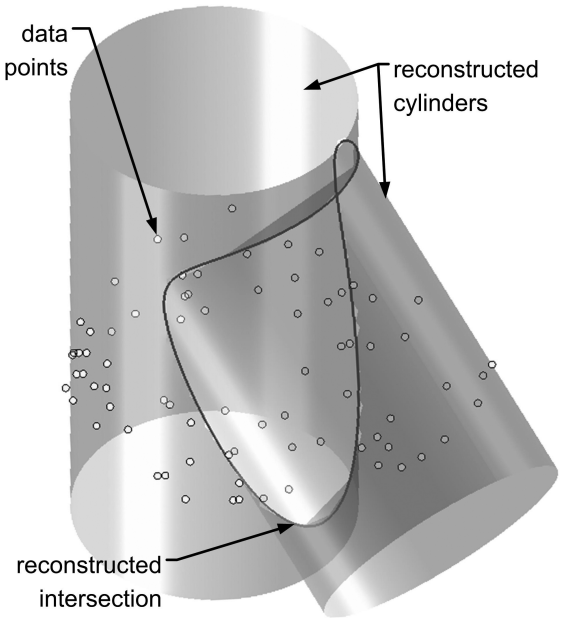

Figure 4-3: Search points for a Uniform Surface Density search.

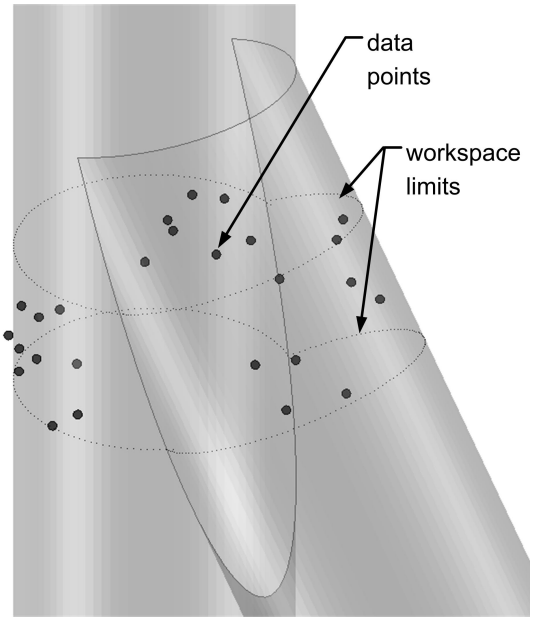

Figure 4-4: Search points for a Best Cone search.

The preliminary experimental results obtained to date suggest that the proposed algorithms for the tactile exploration of unknown environments are feasible, even under conditions where the manipulator precision does not meet expectations.

4.5 Conclusion

Evaluations of the experimental system have produced improvements of both the experimental system itself as well as the proposed field system architecture. For proper motion performance and accurate tactile measurements it is essential to achieve the proper balance of good joint mechanism design and effective control and compensation. Testing of the system design and control algorithms operating in a fluid-filled environment remains to be completed.

Preliminary experimental trials of intelligent search algorithms demonstrate that intelligent tactile characterization using sparse data is feasible. The Best Cone algorithm demonstrates a significant reduction in the required number of data points and characterization time in comparison with other search algorithms. This algorithm is able to identify the well geometry with an impressively small number of data points.

Chapter 5

Digital Mechatronic Design Optimization

5.1 Introduction

In Chapter 2, the field system feasibility and design study considers a traditional, continuously actuated manipulator with a low number of degrees-of-freedom. This approach is motivated by the desire to minimize mechanism complexity. Such simplification offers the potential of a more reliable mechanism, easier control, and fewer opportunities for undesirable collisions between projecting joints and the environment. Alternatively, hyper-redundant manipulator designs can be pursued. Although more difficult to control, hyper-redundant serpentine manipulators can be conformed to arbitrary curves and commanded to trace continuous trajectories. Consequently, they can avoid obstacles that would block traditional, low degree-of-freedom manipulators [22]. If implemented using digital mechatronics, these types of manipulators can still be robust and inexpensive despite the large number of actuators.

While digital mechatronic serpentine manipulators have great potential for applications in constrained environments like tactile oil well junction exploration, these manipulators are difficult to design. Intuitive designs tend to have many overlapping output states and unreachable regions in the desired workspace. This chapter develops techniques for optimizing manipulator designs through numerical parameter optimization and considers their application to constrained, junction-like workspaces in a case study.

5.2 Serpentine Manipulator Kinematics

To facilitate the study of optimization techniques, a class of serpentine digital mechatronic manipulators previously developed in design literature is considered [34, 59]. These manipulators have a hybrid parallel/serial structure composed of serially connected modules of parallel actuators. This design results in a stiff, serpentine manipulator. An example manipulator may be seen in Figure 5-1[1]. In this manipulator, each module as has three legs actuated at the knee by shape-memory alloy [59]. With 5 modules, this arm has with 2^{15} discrete states, or reachable points. Note that in this example arm, all modules are identical and axisymmetric.

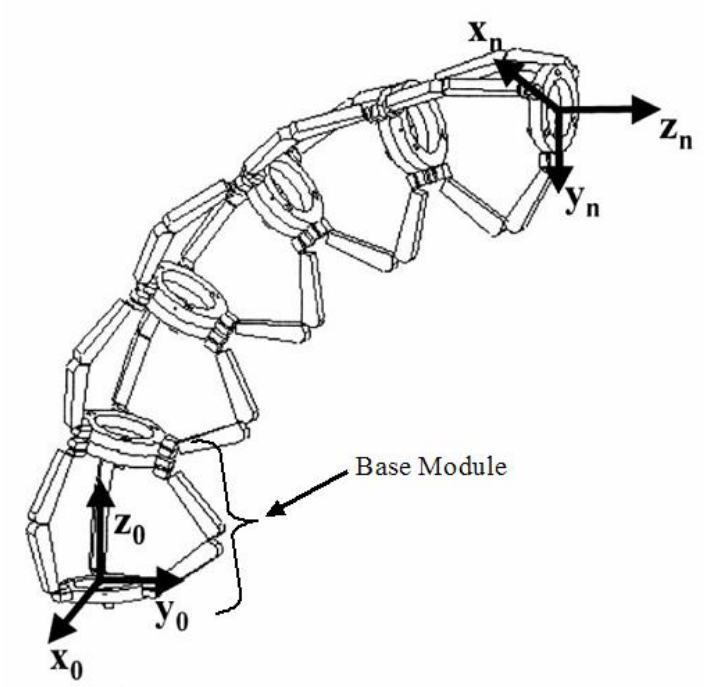

Figure 5-1: A hybrid serial-parallel digital mechatronic manipulator.

This study of digital mechatronic serpentine manipulators uses a generalization of the previously demonstrated kinematic model [59]. The assumptions that modules are identical and axisymmetric are removed. The kinematics of the manipulator are still best approached by decomposing the overall manipulator kinematic transformation into the module transformations. Each module consists of two "proximal" and "distal" circular base rings connected by three struts. Each module may be completely described by 10 parameters

[1]Image Credit: V. Sujan [59]

listed in Figure 5-2. The connection between each strut and the proximal base has one rotational degree-of-freedom, while the connection with the distal base has two rotational degrees-of-freedom. Each strut is a digital linear actuator with two discrete length states. Consequently, each module has $2^3 = 8$ discrete states. Each state may be represented by a transformation matrix relating the position and orientation of the proximal and distal base rings. With the assumption of axial symmetry, these transformation matrices may be solved for analytically. Asymmetry complicates these solutions. These asymmetric kinematic equations and their solution are described in Appendix B.

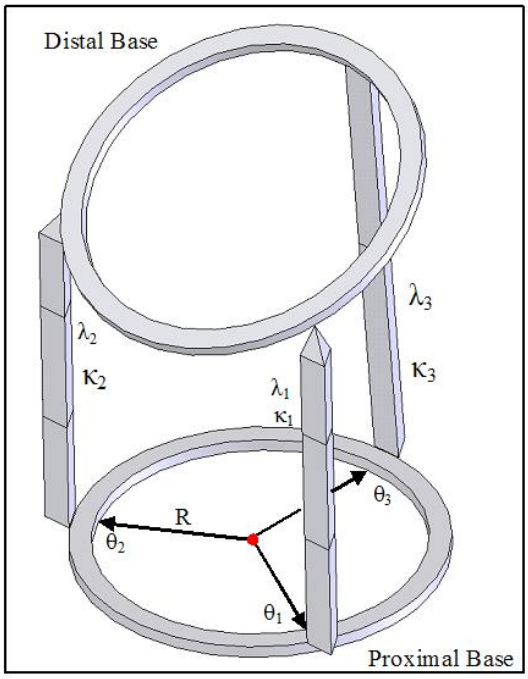

Figure 5-2: Kinematic structure of one module in a serpentine digital mechatronic manipulator.

5.3 Objective Function

In order to optimize a digital mechatronic device, the density and distribution of its discrete output states within a desired workspace must be characterized. A number of potential methods exist. As a metric for developing inverse kinematic solutions, [17] evaluates a workspace point's reachability using a discretized mechanism state density distribution. This distribution is calculated by dividing the desired workspace into uniform volume elements and counting the number of mechanism output states within the each element.

Similarly, [34] uses another form of the state density distribution in order optimize a planar digital mechatronic manipulator. In this work, a smoothed density distribution is developed by convolving the reachable states with a Gaussian distribution. The standard deviation of the resulting distribution is used to represent how uniformly a mechanism's states are arranged. Alternatively, the mechanism state distribution may be characterized by the minimum distance from discrete test points within the desired workspace to the nearest mechanism output state. The average of the minimum distances represents how well distributed the mechanism states are.

The average minimum distance objective function is used in this study. This option was chosen both for the quality of its evaluation and its computational efficiency (O(n) in mechanism states). The use of standard deviation as an objective value is avoided because in some cases optimization leads to tightly clustered rather than evenly distributed points. While it was not tested, a metric based on [17]'s density concept also has potential as an efficient objective function.

The objective value is calculated by discretizing the desired workspace into a multi-dimensional matrix of test points. For manipulator optimization, this matrix has three dimensions corresponding to the position of the end of the manipulator. End effector orientation is not considered here. However, orientation could be added to optimization problem by adding the necessary three extra dimensions to the desired workspace. The elements of this matrix are all initialized to a large value M. For each discrete state of the mechanism, the distances to neighboring elements in the discretized workspace matrix are calculated using the 2-norm (Figure 5-3). If this value is less than the value currently stored in this element of the matrix, this distance value is substituted in the matrix. As matrix values are updated, the sum of matrix elements is maintained and the average minimum distance is calculated.

The objective value may be viewed as an approximation of the average distance from any arbitrary point in the desired workspace to the closest discrete mechanism state. This approximation varies from the actual minimum distance for two reasons. First, the discretization of the desired workspace introduces small errors. More importantly, the algorithm trades computational efficiency for accuracy. Some test points may not be in the neighborhood of any mechanism output state. As a result, these elements will retain their initial value M, and don't contribute a true minimum distance to the metric. The mag-

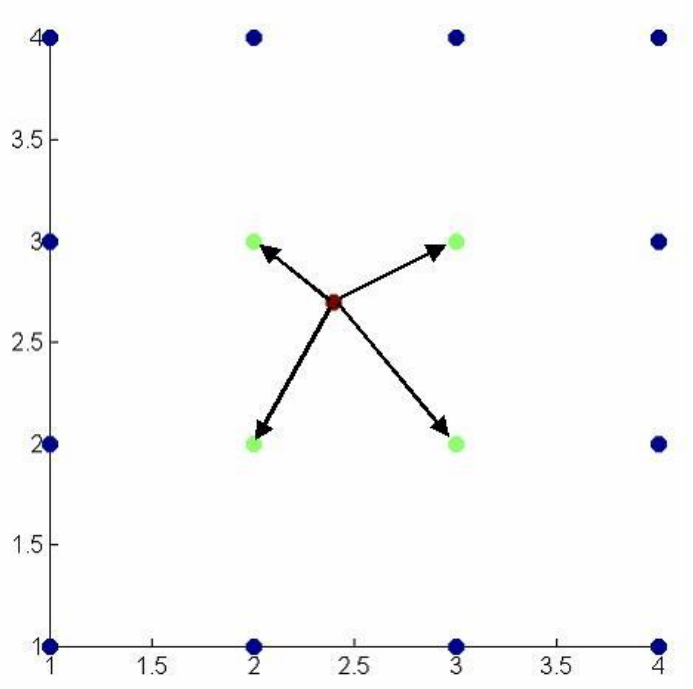

Figure 5-3: Discretized 2D workspace. The distances to workspace elements within a 1-unit neighborhood of a mechanism state are calculated. Elements outside this neighborhood are ignored.

nitude of this initial value M may be used as an optimization tuning factor. Increasing this initialization factor places a larger penalty on not having any mechanism state in the neighborhood of a given workspace element.

5.4 Optimization Methods for Digital Mechatronic Design

Numerical optimization algorithms demonstrate problem dependent performance. Consequently, potential methods must be compared in order find the most efficient approach. Four different optimization methods are considered. Two of these methods, the Nelder-Mead Simplex method and genetic algorithms, are heuristic. The remaining algorithms, COBYLA and NEWUOA, are both trust region methods. For the purposes of comparison, an arm composed of 4 modules (2^{12} states) is considered.

In these comparison trials, nonlinear kinematic constraints related to parallel linkages are handled using a multiplicative penalty on the objective value. This solution allows the easy comparison of a wide range of algorithms using available implementations.

5.4.1 Nelder-Mead Simplex Method

Nelder-Mead minimizes a nonlinear continuous function by heuristically adapting a simplex ($n+1$ linearly independent points) in the parameter space R^n. It is described in [41]. The algorithm consists of three basic steps: reflection, expansion, and contraction.

The reflection operation reflects the point with the worst objective value through the centroid of the simplex according to:

$$P^* = (1+\alpha)\bar{P} - \alpha P_h \tag{5.1}$$

where P^* is the new simplex point, P_h the point in the original simplex with the highest objective value, and $\bar{P}$ is the centroid of the n points in the original simplex except P_h. The reflection coefficient α determines proportionally how far the new point reflects past the centroid P_h. Typically a value of $\alpha = 1$ is used. Given an initial simplex of points, the algorithm selects the simplex point with the highest objective value. This point is reflected across the centroid of the simplex with the expectation of finding a new point with a lower objective value. If the objective value of P^* lies between the lowest and highest objective values in the simplex, P^* replaces P_h.

If the objective value of P^* is lower than any other objective value in the simplex, it makes sense to search or expand further in this same direction. The expansion step is governed by:

$$P^{**} = \gamma P^* + (1-\gamma)\bar{P} \tag{5.2}$$

where P^{**} is the newest simplex point that lies further in the direction of the previous objective value decrease. The expansion coefficient γ determines proportionally how far the new point reflects past the centroid $\bar{P}$. Typically a value of $\gamma = 2$ is used. If the objective value of P^{**} is less than P^* then P^{**} is inserted into the simplex for P_h. Otherwise P^* is placed in the simplex.

However, if the objective value of P^* is greater than the objective value of all points in the simplex except P_h, this point is instead contracted in towards the simplex of the centroid. This contraction is given by:

$$P^{**} = \beta P_h + (1-\beta)\bar{P} \tag{5.3}$$

The contraction coefficient β determines what fraction of the previous distance from the centroid $\bar{P}$ the new point is. Typically a value of $\beta = 0.5$ is used. The new point P^{**} is accepted into the simplex unless it does not improve on the objective value of P_h. In this case all points are contracted about the simplex point P_l with the lowest objective value according to the equation:

$$P_i^* = \frac{(P_i + P_l)}{2} \tag{5.4}$$

During each iteration, the simplex point with the worst objective value is replaced by a new point with a much lower objective value. By repeating these steps, the simplex shifts towards and contracts around regions with lower objective values. Except for the simplest of low-dimensional linear problems, Nelder-Mead is not guaranteed to find an absolute minimum [32]. However, experience shows that it still effectively minimizes complex problems [32].

For this analysis, the Nelder-Mead *Matlab* implementation supplied in the NLopt optimization package is used [26].

5.4.2 COBYLA and NEWUOA

The trust region algorithms COBYLA and NEWUOA share the same basic optimization structure [46, 47]. These functions generate a linear or quadratic approximation G of the objective function F about a parameter estimate x_0 using only the objective value and no gradient information. This approximation G is only assumed valid in a local trust region about the generating estimate x_0. The approximation G may be optimized easily. As this optimization occurs, the validity of the approximation G is constantly checked, and G is updated as necessary. The difficult objective function F is optimized by working with a series of tractable local approximations G.

COBYLA (Constrained Optimization BY Linear Approximations) uses a linear local approximation of the objective function [46]. NEWUOA (NEW Unconstrained Optimization Algorithm)uses a quadratic local approximation of the objective function [47]. In this analysis, the COBYLA and NEWUOA *Matlab* implementations supplied in the NLopt optimization interface are used [26].

Table 5.1: Optimization Progress after 250 Function Evaluations

	No Optimization	Nelder-Mead Simplex	Genetic Algorithm	COBYLA	NEWUOA
Objective Value	0.982	0.736	0.965	0.792	0.776

5.4.3 Genetic Algorithm

A genetic algorithm attempts to minimize a function through a process analogous to evolution in nature [19]. A population of designs is "evolved" through a series of generations using a stochastic process of "mating" and "mutation." In each generation, the most fit individuals, those with the best objective value, are most likely to contribute to the next generation of individual designs.

Initial research made very strong claims about the abilities of genetic algorithms [19]. However, further research and experience has shown that some assumptions fundamental to previous proofs and claims concerning genetic algorithm convergence and performance do not always hold [50]. Genetic algorithms tend to work well on discrete problems. However, they generally do not perform as well on problems with continuous parameters. Despite these issues, genetic algorithms are common in manipulator optimization literature. This approach is used by [34] to optimize a planar digital mechatronic manipulator.

For this evaluation, the *Matlab* genetic algorithm package is used. Algorithm methods and parameters were tuned to the current application through a number of test runs.

5.4.4 Evaluation Method

The algorithms are compared by determining the objective value that each algorithm can achieve in 250 function evaluations. In all cases, the algorithms are initialized using the same initial parameter values. For the genetic algorithm, an initial population was selected in the region about this initialization value.

5.4.5 Results

The minimization progress made by each algorithm after 250 objective function evaluations is listed in Table 5.1 and plotted in Figure 5-4.

The results clearly indicate that the continuous methods are far superior to genetic

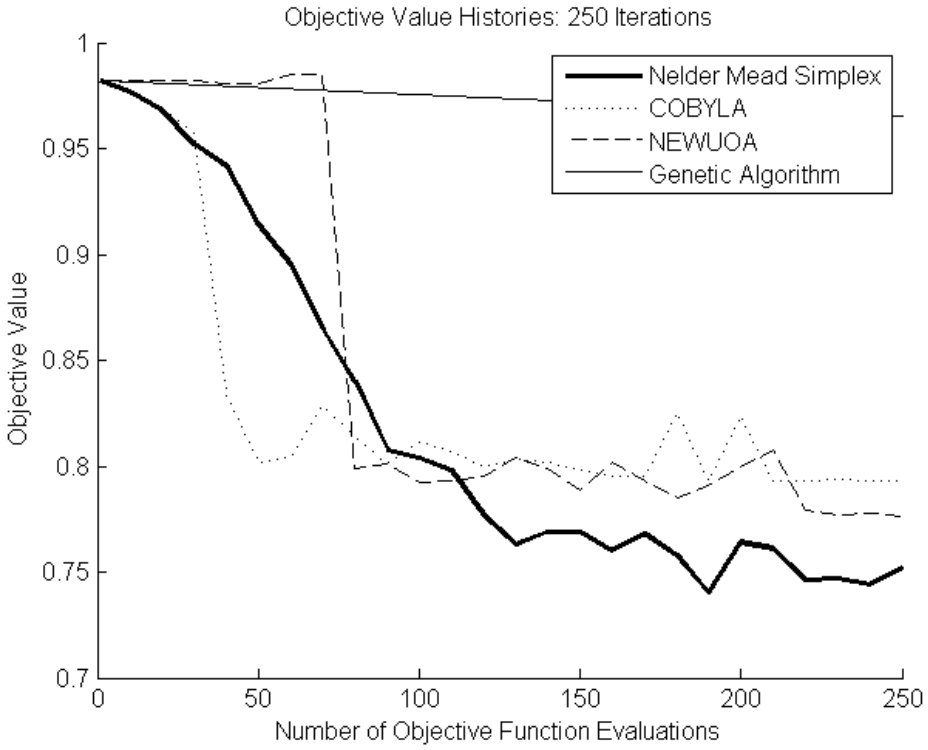

Figure 5-4: An objective value history over 250 function evaluations for different optimization algorithms.

algorithms for this application. Among the three leading algorithms, results are less definite, but suggest that the Nelder-Mead simplex method has the best characteristics. COBYLA and NEWUOA produce large initial reductions in objective value. However, Nelder-Mead quickly surpasses these algorithms with a more gradual but consistent trend resulting in better performance. More importantly, Nelder-Mead acts evenly on all parameters while doing so, a trait neither COBYLA nor NEWUOA demonstrate. COBYLA and NEWUOA tend to focus on the actuator extended and contracted length parameters, ignoring the angular distribution of these actuators about each module. These algorithms maximize the length change that the manipulator can achieve and in this way the spread of the reachable workspace. However, by ignoring the actuator angular placement parameters, these algorithms miss an opportunity to adjust how the mechanism bends and therefore how its states are distributed laterally in the workspace. In contrast, Nelder-Mead adapts angle and length parameters equally. The benefits of this are demonstrated in Table 5.1 and Figure 5-4 where the Nelder-Mead method achieves lower objective values.

5.5 Nelder-Mead Simplex Improvements

While the Nelder-Mead Simplex method performed well in comparison tests, it requires improvements and tuning to best address the digital mechatronic design optimization problem. Most importantly, the algorithm must be able to handle constraints on the design parameters in order to ensure the development of feasible designs. In order to operate efficiently, the optimization algorithm must also be tuned to the problem. Adjustment mechanisms include the factors of reflection, expansion, and contraction.

5.5.1 Constraint Handling

The Nelder-Mead Simplex method was re-implemented to address the wide range of constraint types introduced by the digital mechatronic design problem. Bound constraints limit the allowable range of parameters. Implicit linear inequality constraints express relations between different parameters, e.g. the maximum achievable extension of linear actuators. Grashof conditions on the closed parallel kinematic structures of the modules introduce nonlinear constraints. Parameter solutions must be found for which all of the components of each module may still be connected.

An effective method of handling bound and implicit linear constraints in convex regions is developed in [8]. Parameters that violate a bound constraint are set equal to that constraint limit. If implicit constraints are violated, this work suggests that the new simplex point be stepped half way back to the simplex centroid until a valid simplex point is achieved. These methods were adopted with a slight variation. For implicit constraints, rather than taking a series of half steps back towards the centroid, the invalid point is stepped back using a fixed step length, towards the previous valid simplex point.

$$P^{\dagger} = \min_{\delta}(\tilde{P} + (P - \tilde{P})\delta) \qquad \text{such that} \tag{5.5}$$

$$f(P^{\dagger}) = 0$$

$$\delta \in \{0, \quad \frac{1}{n}, \quad \frac{2}{n}, \quad \ldots 1\}$$

$$\text{for some constant } n$$

Where $\tilde{P}$ is the new simplex point that does not satisfy constraints, P is the existing simplex point that does satisfy constraints, $f(P^{\dagger}) = 0$ is the set of constraints that must be satisfied, and $P^{\dagger}$ is a new simplex point that does satisfy constraints. Depending on whether $\tilde{P}$ is created through reflection, expansion, or contraction, P is selected as $\bar{P}$, P^{*}, or P_h. These choices for P prevent the premature contraction of the simplex. Similarly, the use of small incremental steps prevents the simplex from contracting quickly and becoming dependent, a problem with the original constraint handling implementation. These same methods were adapted to handle the nonlinear kinematic constraints introduced into the problem. As for implicit constraints, when nonlinear constraints are violated, the new simplex point is again incrementally stepped backwards to the previous valid simplex point. These methods of handling the constraints are efficient and do not increase the dimensionality of the already large problem.

5.5.2 Performance Tuning

The parameters controlling the algorithm's operation must also be adjusted. Tests indicate that standard expansion and contraction coefficient values of 2 and 0.5 respectively work well. However, as noted by [8], the constraint handling methods tend to induce early simplex contraction. This may be counteracted by increasing the reflection coefficient from

the standard value of 1. Trials indicate that a value in the range of 1.2 to 1.5 is best. These results are shown in Figure 5-5. Higher reflection coefficients of 1.4 to 1.5 produce larger reductions in objective value early in an optimization run, but are not as effective as values of 1.2 and 1.3 at higher iterations. As the simplex approaches a local minimum, higher reflection coefficients produce over-reflection to higher valued points. This results in slower advances towards the local minimum. A reflection coefficient of 1.2 is selected as best for approximately 1000 optimization iterations.

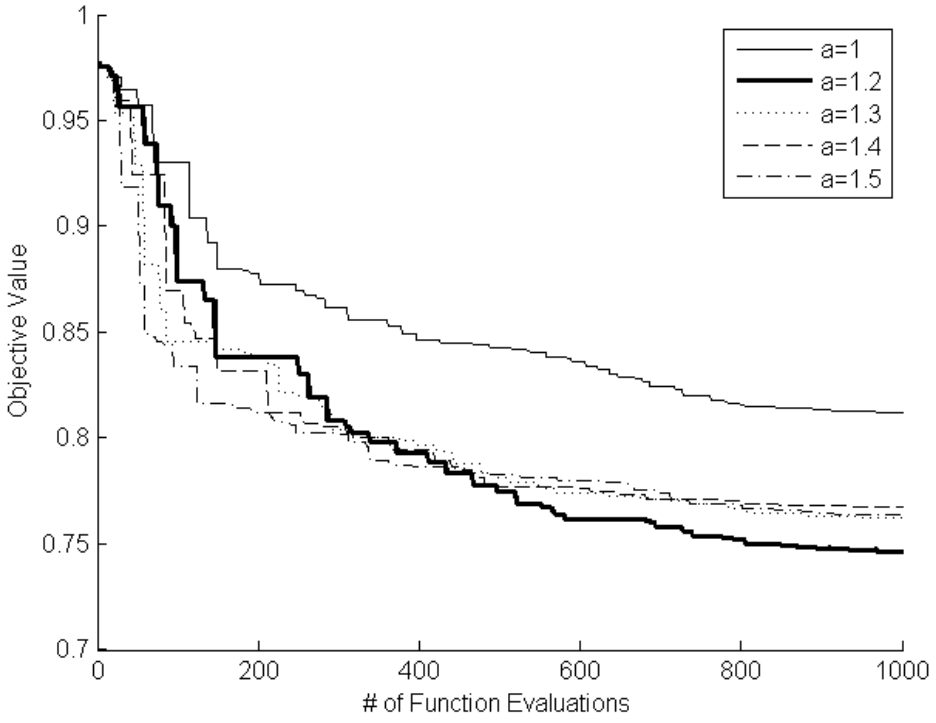

Figure 5-5: Nelder-Mead Simplex performance for different reflection coefficients.

5.6 Design Case Study

In order to demonstrate the workspace optimization methods developed above, a test case is considered. A workspace with dimensions of 5x5x15 units is specified. This workspace is similar in quality to an oil well junction workspace but less challenging because it is less elongated. The manipulator base is placed at the center of one of the square faces of the workspace. The lengths of the module actuator states are able to vary between .5 and 5 units with maximum ratio of 3 setting a limit to achievable actuation extension. Designs are

optimized using 1000 iterations of the constraint-handling Nelder-Mead Simplex algorithm.

As an initial solution, a 4 module serpentine arm is considered. This manipulator has $2^{12} = 4096$ discrete states. The optimization process achieves an objective value of 2.907, and the resulting workspace is shown in Figure 5-6(a). This optimization required 8.85 hours using one core of a 2.40 GHz Intel Core 2 Duo with 2.00 GB of Ram. Clearly, an arm with this topology performs poorly in covering the entire workspace. While the arm effectively covers the width of the workspace, it is incapable of reaching the entire length of the slender space. This occurs because the kinematic module is not well suited for providing large extensions. The Grashof conditions on each module's closed kinematic chain prevent extended and contracted module states that are widely separated so that there are not kinematic conflicts when a mixture of extended and contracted actuator states is commanded. Consequently, this version of the serpentine manipulator has the same limited ability to reach down the length of the narrow workspace that a 3 degree-of-freedom continuously-actuated anthropomorphic manipulator has.

By adding modules intended specifically for linear extension, this workspace deficiency may be corrected. Two discrete linear actuators are placed in series at the base of the serpentine manipulator before the 4 serpentine modules. These actuators are aligned with the long axis of the workspace. This manipulator has $2^{14} = 16384$ discrete states. This solution is analogous to the proposed addition of a redundant prismatic joint to augment the length of a continuously actuated robot discussed in Chapter 2. The design optimization process adjusted not only the parameters of the 4 serpentine modules, but also of the 2 discrete linear extension stages. This process took 19.35 hours on the same platform and achieved an objective value of 0.526. A plot of the manipulator's discrete workspace may be seen in Figure 5-6(b). The 4 serpentine modules of the manipulator produce an even coverage across the workspace similar to the previous design. The discrete linear extension stages replicate this pattern evenly throughout the length of the workspace, providing much better access to the entire desired workspace. The manipulator is shown in several different views in Figure 5-7 with varying extension and serpentine states.

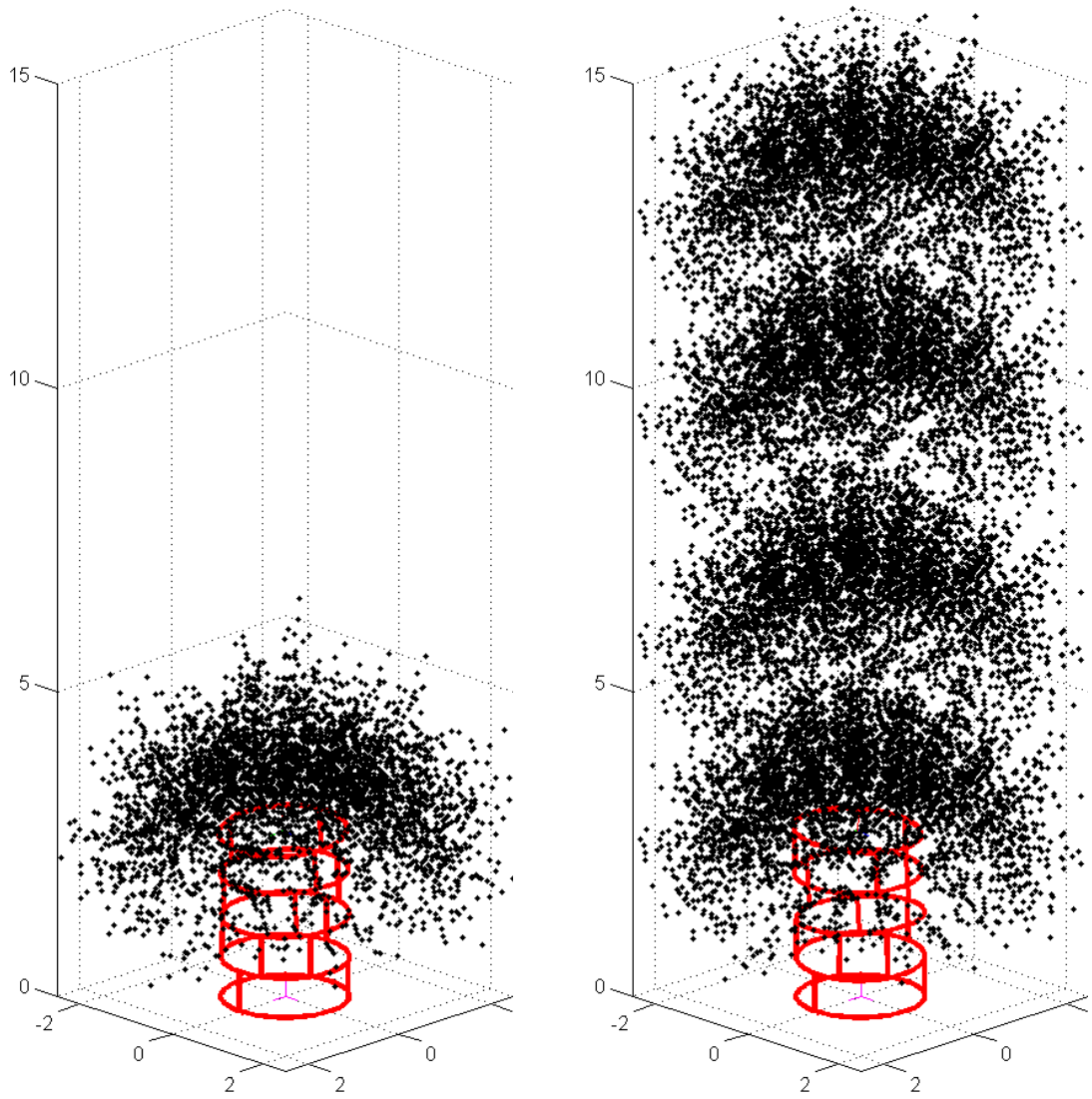

(a) Workspace and fully retracted manipulator of a design without linear extension modules.

(b) Workspace and fully retracted manipulator of a design with 2 linear extension modules.

Figure 5-6: A comparison of optimized workspaces for manipulators with and without linear extension modules.

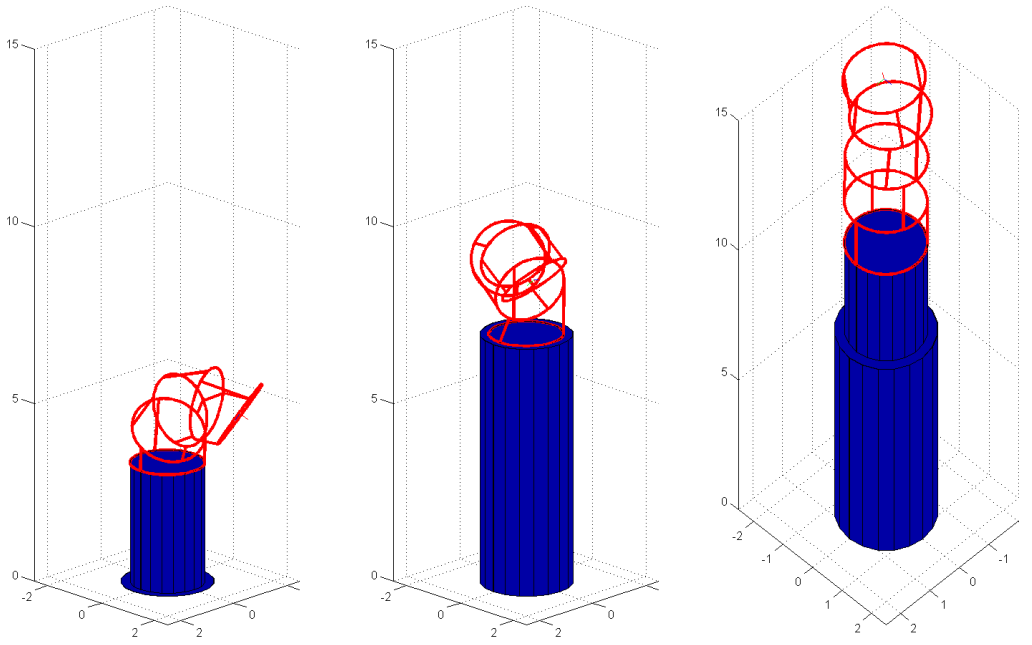

(a) Arm partially extended: one actuator extended in each module.

(b) Arm partially extended: two actuators extended in each module.

(c) Arm fully extended: all 3 actuators extended in each module.

Figure 5-7: Digital mechatronic manipulator in a series of states approaching full extension.

5.7 Conclusions

The case study demonstrates the value of this method for the optimization of a digital mechatronic device. Given a mechanism topology, the tool provides an effective means of design parameter optimization. Through trial and error, the tool can also be used to guide the development of better mechanism topologies. The optimization approach developed here is demonstrated for a serpentine manipulator with fully-constrained actuation, it is applicable to diverse digital mechatronic mechanism optimization problems. The range of cases in which it may be used include other mechanisms with fully-constrained actuation as well as mechanisms that use elastic-averaging and over-constrained actuation. In these cases the fundamental problem state of distributing discrete output states in a desired workspace by varying continuous parameters remains constant.

While the optimization methods developed here are effective, they do have shortcomings. By its nature, the process is very computationally expensive and time intensive. Parallelization is the best way to further speed the process. One option would be to add

the adaptations applied here to the Subplex algorithm [54]. The Subplex algorithm breaks the parameter space into subspaces and pursues the simplex method individually within each. This approach lends itself well to multiprocessor parallelization. However, the tool is intended for offline design optimization so some degree of computational expense is acceptable.

The results of the case study also indicate another rich area for further study: the combination of discrete and continuous actuation in one mechanism. While the distal portions of the arm lend themselves well to digital mechatronic implementation, it may make sense to use continuous actuation to provide the linear base extension and perhaps even base rotation. Continuous actuation in these regions would avoid the complex cascading of actuators and greatly increase the fineness of the workspace distribution. These continuous actuators would be mounted on the base where they are protected and where their bulk does not impede the motion of the manipulator. The consideration of hybrid continuous-discrete actuation could be addressed by a modified version of the optimization approach developed here. Such a hybrid approach would exploit the strengths of both actuation styles.

Chapter 6

Conclusion

6.1 Contributions

This thesis developed system and mechanism designs for down-well tactile exploration manipulators. The primary contribution of this work is a tested and proven, minimal-sensor field system architecture proposal. It also presents hyper-redundant serpentine manipulators has a promising kinematic alternative and develops the design tools necessary to optimize these systems.

In Chapter 1, the motivation for this work is related. Economic pressures are driving the oil industry to demand greater capability from its down-well tools. The ability to locate and geometrically characterize branching junctions would enable significant increases in the amount of oil recovered from existing wells. Due to down-well conditions, tactile sensing is the best method for exploring these junctions. Intelligent autonomous tactile exploration that uses minimal data sets is also an important, challenging, and largely unaddressed fundamental research topic.

The feasibility of such a down-well tactile exploration system is reviewed in Chapter 2. This study produces a proposed field system architecture that attempts to achieve mechanical robustness through the use of a minimal-sensor approach.

Chapter 3 describes the design and construction of an experimental system. The system includes an experimental tank that replicates the essential characteristics of the down-well environment. A purpose-built manipulator based on the proposed field system architecture is developed in order to test this system approach.

This experimental system is tested in Chapter 4. Initial tests reveal problems in the

experimental system and guide several small redesigns. Subsequent tests indicate that the mechanical design of the joint drive trains, especially those including bevel gears, interacts closely with the control methods used to determine system performance. The careful design and tuning of these aspects of the proposed field system architecture must be done together. Preliminary trials of intelligent data-efficient tactile exploration algorithms prove the viability of the field system architecture as well as the concept of geometry characterization with minimal data sets. The geometric characterization of an oil well junction with an impressively small number of tactile data points is demonstrated.

Finally Chapter 5 develops design optimization methods for digital mechatronic hyper-redundant manipulators. This kinematic structure is promising for the oil application due to its inherent ability to work around obstacles and in constrained spaces. While this new hyper-redundant approach is very different from that considered in the field system feasibility and design study, with the use of digital mechatronics the fundamental emphasis on mechanical robustness through minimal-sensor implementations is maintained.

The intelligent, data-efficient characterization of down-well junction geometry is feasible. It has been shown that the best system design approach is to use the minimum number of sensors. The mapping of model junctions using small tactile data sets has been demonstrated experimentally.

6.2 Future Work

Experimental testing needs to continue in a number of areas. An examination of the effects of fluid interactions on the control of the tactile manipulator is needed. Initial trials could use water as a testing fluid before graduating to more viscous fluids. Additionally, the effects of mud cake on both control and the accuracy of the retrieved tactile data should be tested. The further exploration and characterization of the nonlinear joint backlash and elasticity is also an interesting topic. Better characterization of these errors would enable better compensation and reduced tactile sensing error. Most importantly, the experimental system should be used to support the continued development of intelligent, data-efficient tactile search algorithms.

Hyper-redundant, digital mechatronic manipulators have potential for down-well applications and efforts to develop these manipulators should continue. Continued work should

focus on the mechanical implementation and control of these manipulators. The selection of viable actuators and components would enable a design study to produce an initial down-well design. Significant controls work is necessary to fully exploit the potential of such a mechanism for the tactile exploration task.

References

[1] Ahn S. Least Squares Orthogonal Distance Fitting of Curves and Surfaces in Space. Heidelberg: Springer-Verlag, 2004.

[2] Allen P, Michelman P. "Acquisition and interpretation of 3-D sensor data from touch." IEEE Trans. Robotics and Automation. 6(4): 397-404, 1990.

[3] Anderson V, Horn R. "Tensor arm manipulator design." ASME Paper 67-DE-57, 1967.

[4] Beccari G, Caselli S, et al. "Pose-independent recognition of convex objects from sparse tactile data." Proc. IEEE Int. Conf. Robotics and Automation, Albuquerque, NM, USA. pp. 3397-3402, 1997.

[5] Benko P, Kos G, et al. "Constrained fitting in reverse engineering." Computer Aided Geometric Design. 19(3): 173-205, 2002.

[6] Besl P, Jain R. "Segmentation through variable-order surface fitting." IEEE Trans. Pattern Analysis and Machine Intelligence. 10(2): 167-192, 1988.

[7] Bolle R, Vemuri B, et al. "On three-dimensional surface reconstruction methods." IEEE Trans. Pattern Analysis and Machine Intelligence. 13(1): 1-13, 1991.

[8] Box M. "A new method of constrained optimization and a comparison with other methods." The Computer Journal. 8: 42-52, 1965.

[9] Canudas de Wit C, Siciliano B, Bastin G. Theory of Robot Control. Heidelberg: Springer-Verlag, 1996.

[10] Caselli S, Magnanini C, et al. "Efficient exploration and recognition of convex objects based on haptic perception." Proc. IEEE Int. Conf. Robotics and Automation, Minneapolis, MN, USA. pp. 3508-3513, 1996.

[11] Ceccarelli M, Lanni C. "A multi-objective optimum design of general 3R manipulators for prescribed workspace limits." Mechanism and Machine Theory. 39:119-132, 2004.

[12] Chew L. "Guaranteed-quality mesh generation for curved surfaces." Proc. ninth annual Symposium on Computational Geometry. pp. 274-280, 1993.

[13] Chirikjian G. "A binary paradigm for robotic manipulators." Proc. of the IEEE Int. Conf. on Robotics and Automation, San Diego, CA, USA. pp. 3063-3069, 1994.

[14] Chirikjian G, Burdick J. "The kinematics of hyper-redundant robot locomotion." IEEE Trans. Robotics and Automation. 11(6): 781-793, 1995.

[15] Cimino W, Pennock G. "Workspace of a six-revolute decoupled robot manipulator." Proc. of the IEEE Int. Conf. on Robotics and Automation. pp. 1848-1852, 1986.

[16] DeVita L. An MRI Compatible Manipulator for Prostate Cancer Detection and Treatment. Master Thesis. Department of Mechanical Engineering, Massachusetts Intitute of Technology. 2007.

[17] Ebert-Uphoff I, Chirikjian G. "Inverse kinematics of discretely actuated hyper-redundant manipulators using workspace densities." Proc. of the IEEE Int. Conf. on Robotics and Automation, Minneapolis, MN, USA. pp. 139-145, 1996.

[18] Ebert-Uphoff I, Chirikjian G. "Discretely actuated manipulator workspace generation by closed form convolution." ASME J. Mechanical Design. 120: 245-251, 1998.

[19] Goldberg D. Genetic Algorithms in Search, Optimization, and Machine Learning. New York: Addison-Wesley Publishing Company, 1989.

[20] Gosselin C, Angeles J. "A global performance index for the kinematic optimization of robotic manipulators." ASME J. Mechanical Design. 113:220-226, 1991.

[21] Gosselin C, Guillot M. "The synthesis of manipulators with prescribed workspace." ASME J. Mechanical Design. 113:451-455, 1991.

[22] Hirose S. Biologically Inspired Robots: Snake-Like Locomotors and Manipulators. New York: Oxford University Press, 1993.

[23] Hogan N. "Impedance control – an approach to manipulation: I-Theory. II-Implementation. III-Applications." ASME J. Dynamic Systems, Measurement, and Control. 107: 1-24, 1985.

[24] Immega G, Antonelli K. "The KSI tentacle manipulator." Proc. of the IEEE Int. Conf. on Robotics and Automation, Nagoya, Aichi, Japan. pp. 3149-3154, 1996.

[25] Jiang X, Cheng D. "A novel parameter decomposition approach to faithful fitting of quadric surfaces." Lecture Notes in Computer Science. Hiedelberg: Springer-Verlag, 2005.

[26] Johnson S. The NLopt Nonlinear-Optimization Package. `http://ab-initio.mit.edu/nlopt`. Downloaded December 2008.

[27] Keren D, Rivlin E, et al."Recognizing 3D objects using tactile sensing and curve invariants." J. Mathematical Imaging and Vision. 12(1): 5-23, 2000.

[28] Kim JO, Khosla P. "Dexterity measures for design and control of manipulators." Proc. IEEE Int. Workshop on Intelligent Robots and Systems, Osaka, Japan. pp. 758-763, 1991.

[29] Kos G, Martin R, et al. "Methods to recover constant radius rolling ball blends in reverse engineering." Computer Aided Geometric Design. 17(2): 127-160, 2000.

[30] Kyatkin A, Chirikjian G. "Synthesis of binary manipulators using the Fourier transform on the Euclidean group." Int. J. Robotics Research. 18: 601-615, 1999.

[31] Kyatkin A, Chirikjian G. "Computation of robot configuration and workspaces via the Fourier transform on the discrete-motion group." ASME J. Mechanical Design. 121: 9-14, 1999.

[32] Lagarias J, Reeds J, et al. "Convergence properties of the Nelder-Mead simplex method in low dimensions." Siam J. of Optimization. 9(1): 112-147, 1998.

[33] Leonardis A, Gupta A, et al. "Segmentation of range images as the search for geometric parametric models." Int. J. of Computer Vision 14(3): 253-277, 1995.

[34] Lichter M, Sujan V, Dubowsky S. "Computational issues in the planning and kinematics of binary robots." Proc. IEEE Int. Conf. Robotics and Automation, Washington, DC, USA. pp. 341-346, 2002.

[35] Lukacs G, Martin R, et al. "Faithful least-squares fitting of spheres, cylinders, cones, and tori for reliable segmentation." Lecture Notes in Computer Science. Hiedelberg: Springer-Verlag, 1998.

[36] Mazzini F, Kettler D, Guerrero J, Dubowsky S. "The exploration of unknown surfaces using sparse tactile data: with application to oil well mapping." Submitted to Proc. Int. Symposium on Robotics Research, Lucerne, Switzerland. 2009.

[37] Mazzini F. Title Pending. PhD Thesis. Department of Mechanical Engineering, Massachusetts Intitute of Technology. Cambridge, MA, USA. In Preparation.

[38] Michalec G. Precision Gearing: Theory and Practice. New York: John Wiley & Sons, 1966.

[39] Miller J. "Geometric approaches to nonplanar quadric surface intersection curves." ACM Trans. Graphics. 6(4): 274-307, 1987.

[40] Miyahara K, Chirikjian G. "General kinematic synthesis method for a discretely actuated robotic manipulator (D-ARM)." Proc. of the IEEE Int. Conf. on Intelligent Robots and Systems, Beijing, China. pp. 5889-5894, 1996.

[41] Nelder J, Mead R. "A simplex method for function minimization." The Computer Journal. 7: 308-313, 1965.

[42] Petitjean S. "A survey of methods for recovering quadrics in triangle meshes." ACM Computing Surveys 34(2): 211-262, 2002.

[43] Plante JS, Devita L, Dubowsky S. "A road to practical dielectric elastomer actuators based robotics and mechatronics: discrete actuation." Electroactive Polymer Actuators and Devices, Proc. SPIE. 6524, 652406: 1-15, 2007.

[44] Plante JS, Dubowsky S. "The calibration of a parallel manipulator with binary actuation." Advances in Robot Kinematics: Analysis and Design. Heidelberg: Springer-Verlag, 2008.

[45] Plante JS, DeVita L, Tadakuma K, Dubowsky S. "MRI compatible device for robotic assisted interventions in prostate cancer." Biomedical Applications of Electroactive Polymer Actuators. Hoboken, NJ: Wiley, 2009

[46] Powell M. "Direct search algorithms for optimization calculations." Technical Report, Department of Applied Mathematics and Theoretical Physics, University of Cambridge, 2000, Report # DAMTP 1998/NA04.

[47] Powell M. "The NEWUOA software for unconstrained optimization without derivatives." Technical Report, Department of Applied Mathematics and Theoretical Physics, University of Cambridge, 2004, Report # DAMTP 2004/NA05.

[48] Pribadi K, Bay J, et al. "Exploration and dynamic shape estimation by a robotic probe." IEEE Trans. Systems, Man and Cybernetics. 19(4): 840-846, 1989.

[49] Raibert M, Craig J. "Hybrid Position/Force Control of Manipulators." ASME J. Dynamic Systems, Measurement, and Control. 102: 126-133, 1981.

[50] Reeves C, Rowe J. Genetic Algorithms – Principles and Perspectives. Boston: Kluwer Academic Publishers, 2003.

[51] Requicha A, Voelcker H. "Solid modeling: a historical summary and contemporary assessment." IEEE Computer Graphics and Applications. 2(2): 9-24, 1982.

[52] Roberts K. "Robot active touch exploration: constraints and strategies." Proc. IEEE Int. Conf. Robotics and Automation, Cincinnati, OH, USA. pp. 980-985, 1990.

[53] Roth B, Rastegar J, Scheinman V. "On the design of computer controlled manipulators." Proc. CISM-IFTMM Symposium on Theory and Practice of Robots and Manipulators. pp. 93-113. 1973.

[54] Rowan T. Functional Stability Analysis of Numerical Algorithms. PhD thesis. Department of Computer Science, University of Texas at Austin. 1990.

[55] Samuel G. Downhole Drilling Tools. Houston, TX: Gulf Publishing Company, 2007.

[56] Schneiter J. Automated Tactile Sensing for Object Recognition and Localization. PhD Thesis. Department of Mechanical Engineering, Massachusetts Intitute of Technology. Cambridge, MA, USA. 1986.

[57] Schlumberger Limited. Internal Schlumberger Communication.

[58] Sciavicco L, Siciliano B. "An algorithm to compute the reachable workspace for 2R and 3R planar pair mechanical arms." Proc. IEEE Int. Conf. Robotics and Automation, Philadelphia, PA, USA. pp. 628-629, 1988.

[59] Sujan V, Dubowsky S. "Design of a lightweight hyper-redundant deployable binary manipulator." ASME J. Mechanical Design. 126: 29-39, 2004.

[60] Sujan V, Dubowsky S. "Efficient information-based visual robotic mapping in unstructured environments." Int. J. Robotics Research. 24(4): 275-293, 2005.

[61] Suthakorn J, Chirikjian G. "Design and implimentation of a new discretely-actuated manipulator." Experimental Robotics VII, LNCIS 271. Heidelberg: Springer-Verlag, 2001.

[62] Tadakuma K, DeVita L, Dubowsky S. "The experimental study of a precision parallel manipulator with binary actuation: with application to MRI cancer treatment." Proc. IEEE Int. Conf. Robotics and Automation, Pasadena, CA, USA. pp. 2503-2508, 2008.

[63] Thrun S, Burgard W, Fox D. Probabilistic robotics. Boston: MIT Press, 2005.

[64] Vida J, Martin R, et al. "A survey of blending methods that use parametric surfaces." Computer-Aided Design. 26(5): 341-365, 1994.

[65] Vosniakos G, Giannakakis T. "Reverse engineering of simple surfaces of unknown shape with touch probes: scanning and compensation issues." Proc. Institution of Mechanical Engineers, Part B: J.Engineering Manufacture. 217(4): 563-568, 2003.

[66] Wang W, Goldman R, et al. "Enhancing Levin's method for computing quadric-surface intersections." Computer Aided Geometric Design. 20(7): 401-422, 2003.

[67] Wingert A, Lichter M, Dubowsky S. "On the design of large degree-of-freedom digital mechatronic devices based on bistable dielectric elastomer actuators." IEEE/ASME Trans. Mechatronics. 11(4): 448-456, 2006.

Appendix A

Experimental System Design Drawings

A.1 Manipulator Design Data

The experimental manipulator is purpose-built to demonstrate the field system architecture developed in Chapter 2 and to test intelligent tactile exploration algorithms for tactile mapping with sparse data. The essential information describing its components is listed here.

The manipulator contains a number of commercial components, primarily associated with joint drive trains and joint sealing. These components are listed here in tables by associated manipulator joint.

Table A.1: Joint 1 Commercial Components

Identification #	Supplier	Description
23DT2R-218E	Portescap	Brushed DC Motor
HEDS 5500	Portescap	Incremental Encoder, 500 lines
R32-0574	Portescap	Planetary gearhead, 574:1
S10A6Z-032H032	Stock Drive Parts	Spur Gear, 32 teeth
S10A6Z-032H064	Stock Drive Parts	Spur Gear, 64 teeth
7201BEP	SKF	Angular Contact Bearing, 32mm OD, 12mm ID for joint axle
7204BEP	SKF	Angular Contact Bearing, 47mm OD, 20mm ID for joint axle
1ZFZ4	Dayton	Deep Groove Bearing, 0.875 in OD, 0.625 in ID for pinion axle

Table A.2: Joint 2 Commercial Components

Identification #	Supplier	Description
23DT2R-218E	Portescap	Brushed DC Motor
HEDS 5500	Portescap	Incremental Encoder, 500 lines
R32-0574	Portescap	Planetary gearhead, 574:1
SH192-P	Boston Gear	Spiral Bevel Pinion, 13 teeth
SH192-G	Boston Gear	Spiral Bevel Gear, 26 teeth
MBG8-5	PIC Design	Deep Groove Bearing, 19mm OD, 6mm ID, Flange for joint axle
MBG6-5	PIC Design	Deep Groove Bearing, 19mm OD, 6mm ID for joint axle
688hZZ A5	Dynaroll	Deep Groove Bearing, 16mm OD, 8mm in ID for pinion axle

Table A.3: Joint 3 Commercial Components

Identification #	Supplier	Description
22V48-208E	Portescap	Brushed DC Motor
E9-500	Portescap	Incremental Encoder, 500 lines
R22-10-0-190	Portescap	Planetary gearhead, 574:1
GSS481Y-P	Boston Gear	Bevel Pinion, 16 teeth
GSS481Y-G	Boston Gear	Bevel Gear, 32 teeth
E2-6-1	PIC Design	Deep Groove Bearing, 0.5in OD, 0.1875in ID, Flange for joint axle
E6-5	PIC Design	Deep Groove Bearing, 0.5in OD, 0.1875in ID for joint axle
E6-5	PIC Design	Deep Groove Bearing, 0.5in OD, 0.1875in ID for pinion axle

Many of the manipulator's components are custom made. Fully dimensioned design drawings for all custom manipulator parts are included here. These drawings are listed in order by the part number $R\#$ they received during the design and construction of the manipulator. Materials are listed on these drawings. For an exploded-view drawing of the manipulator showing all custom and commercial parts and their relations, see Figure 3-9.

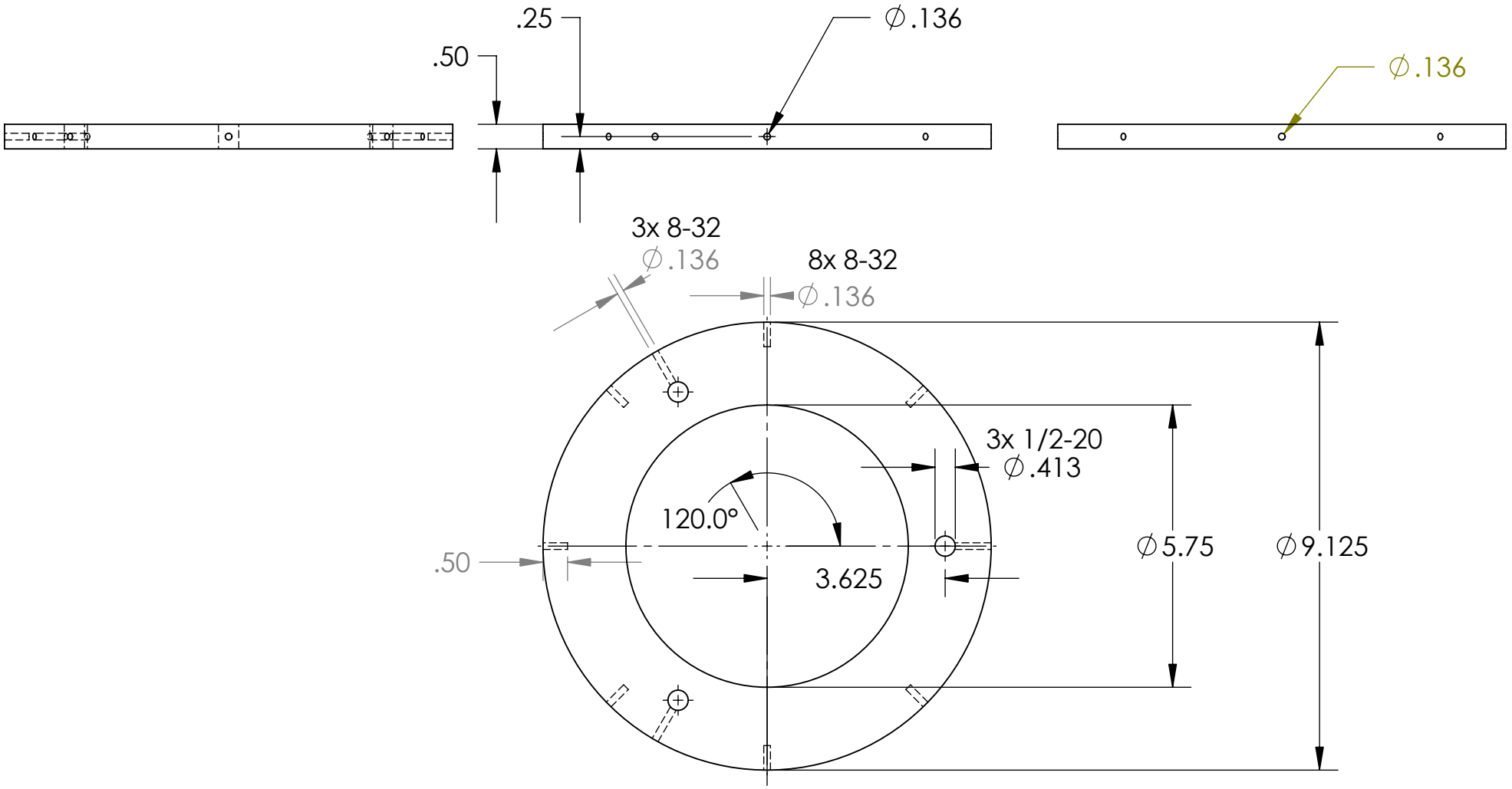

Dan Kettler		
TITLE: Static Base		R1
SIZE A	Material Al 6061	REV 2.5
SCALE: 1:4	Qty: 1	SHEET 1 OF 1

5 4 3 2 1

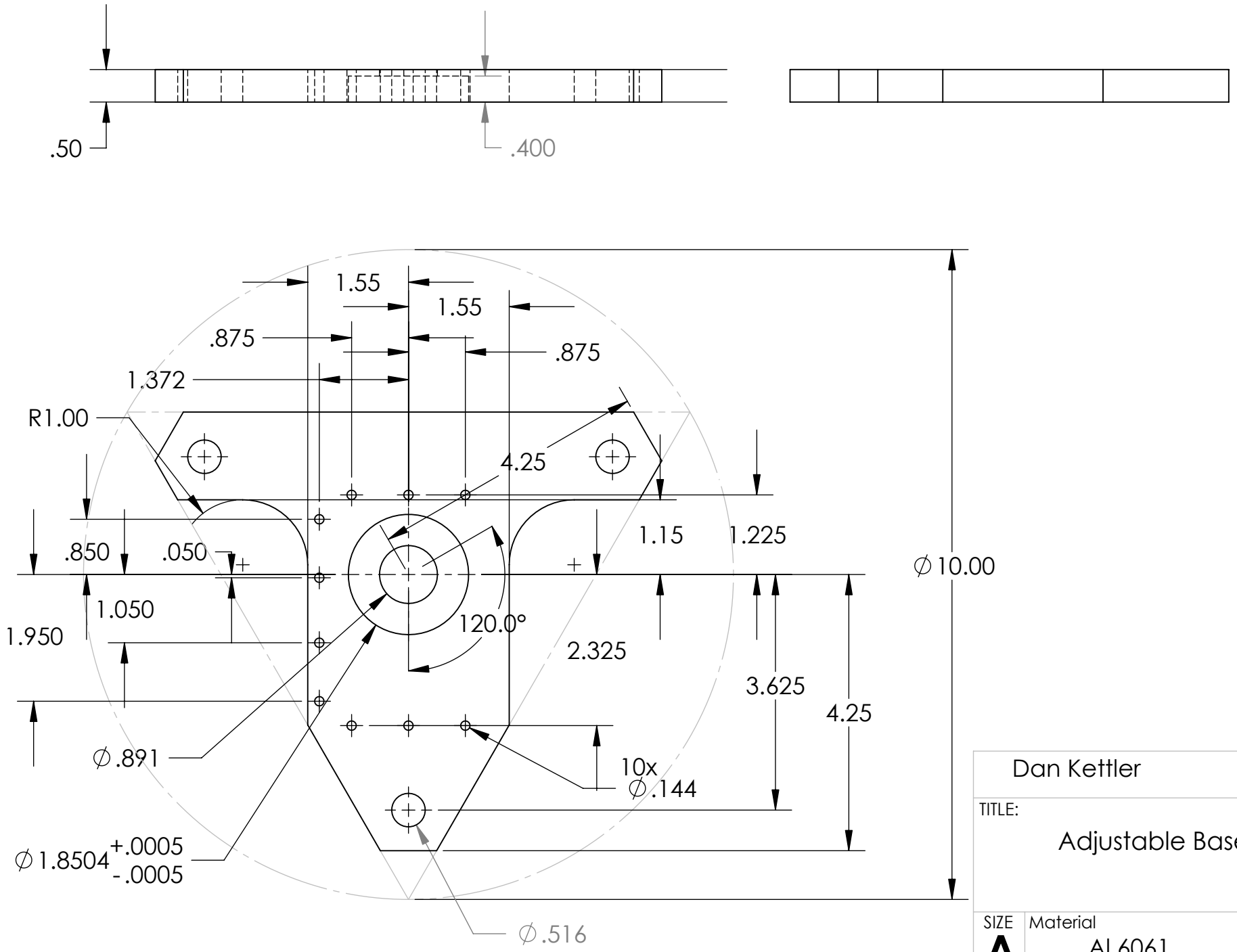

Dan Kettler		
TITLE: Adjustable Base		R2
SIZE A	Material Al 6061	REV 2.4
SCALE: 1:2	Qty: 1	SHEET 1 OF 1

5 4 3 2 1

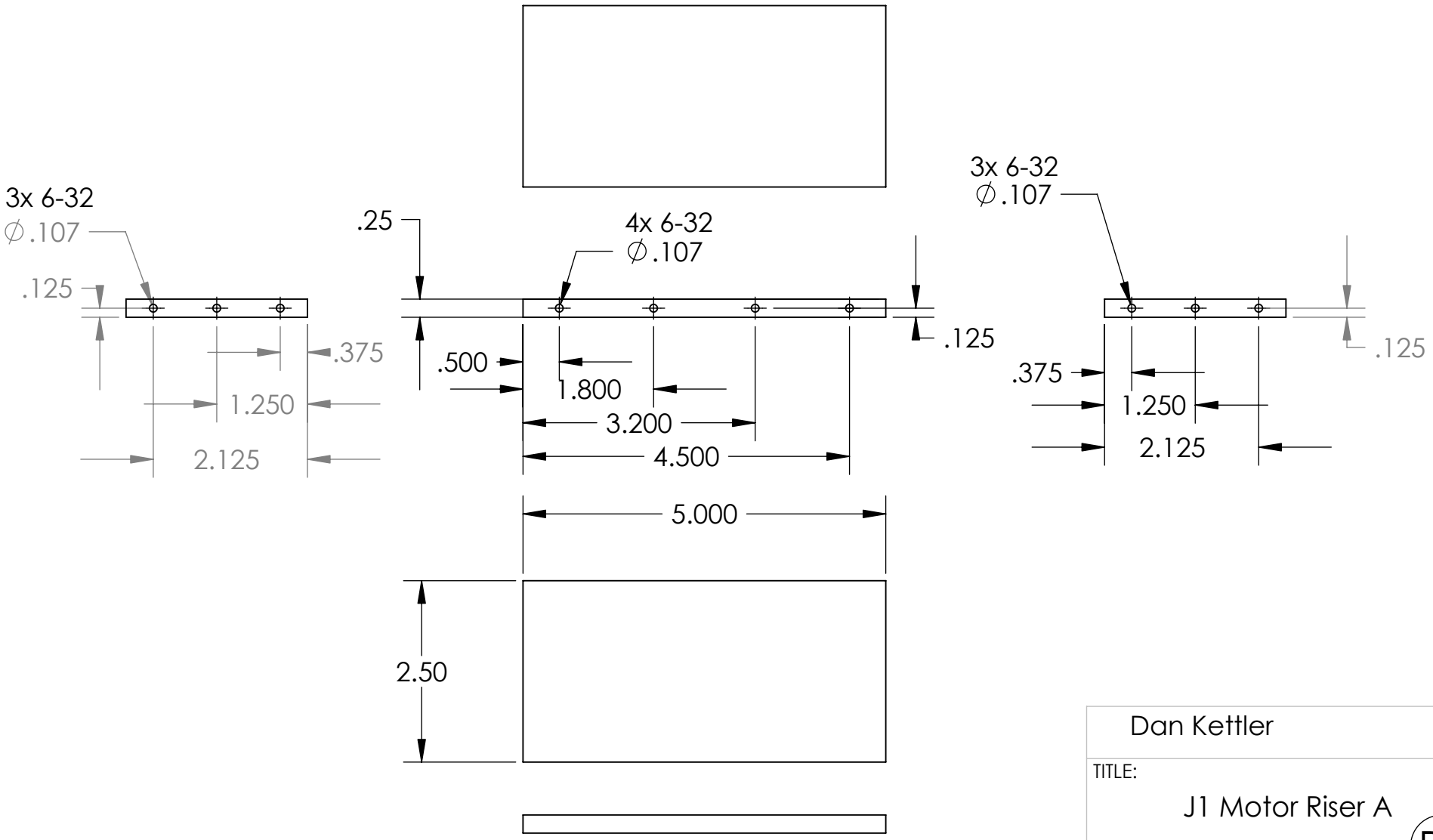

Dan Kettler		
TITLE: J1 Motor Riser A		R3
SIZE A	Material Al 6061	REV 2.4
SCALE: 1:2	Qty: 2	SHEET 1 OF 1

5 4 3 2 1

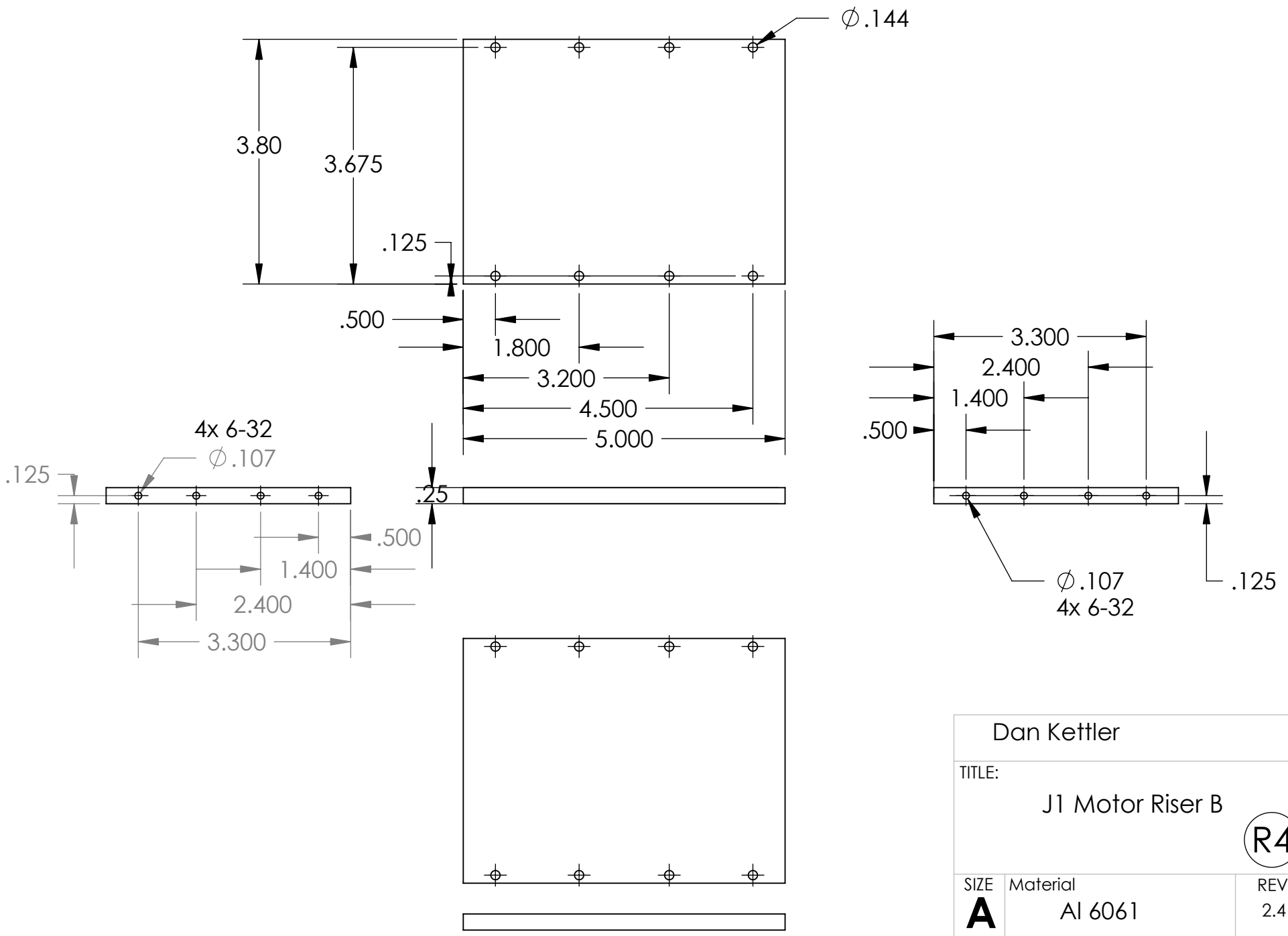

Dan Kettler		
TITLE: J1 Motor Riser B		R4
SIZE A	Material Al 6061	REV 2.4
SCALE: 1:2	Qty: 1	SHEET 1 OF 1

5 4 3 2 1

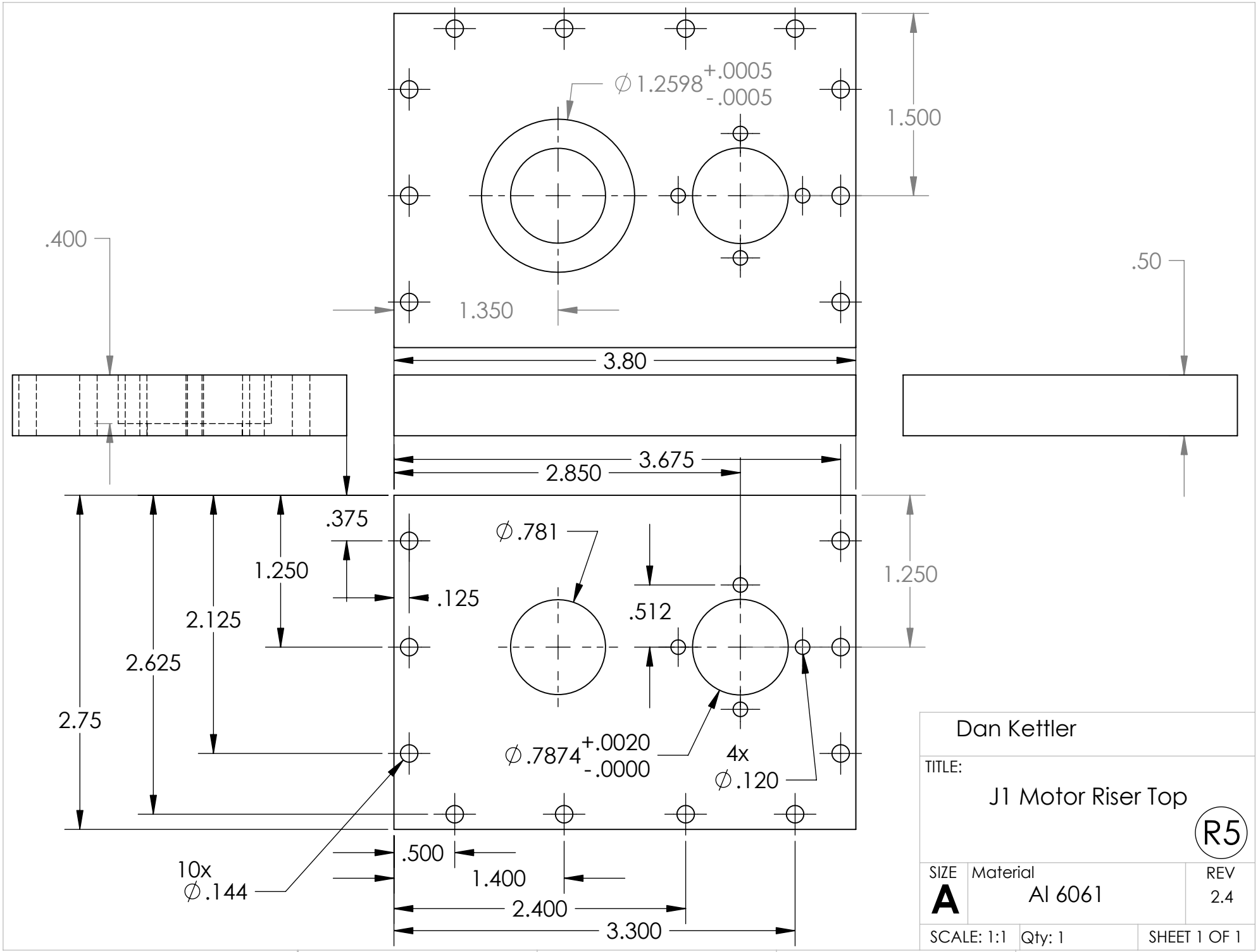

Dan Kettler

TITLE:

J1 Motor Riser Top

R5

SIZE	Material	REV
A	Al 6061	2.4

SCALE: 1:1	Qty: 1	SHEET 1 OF 1

5 4 3 2 1

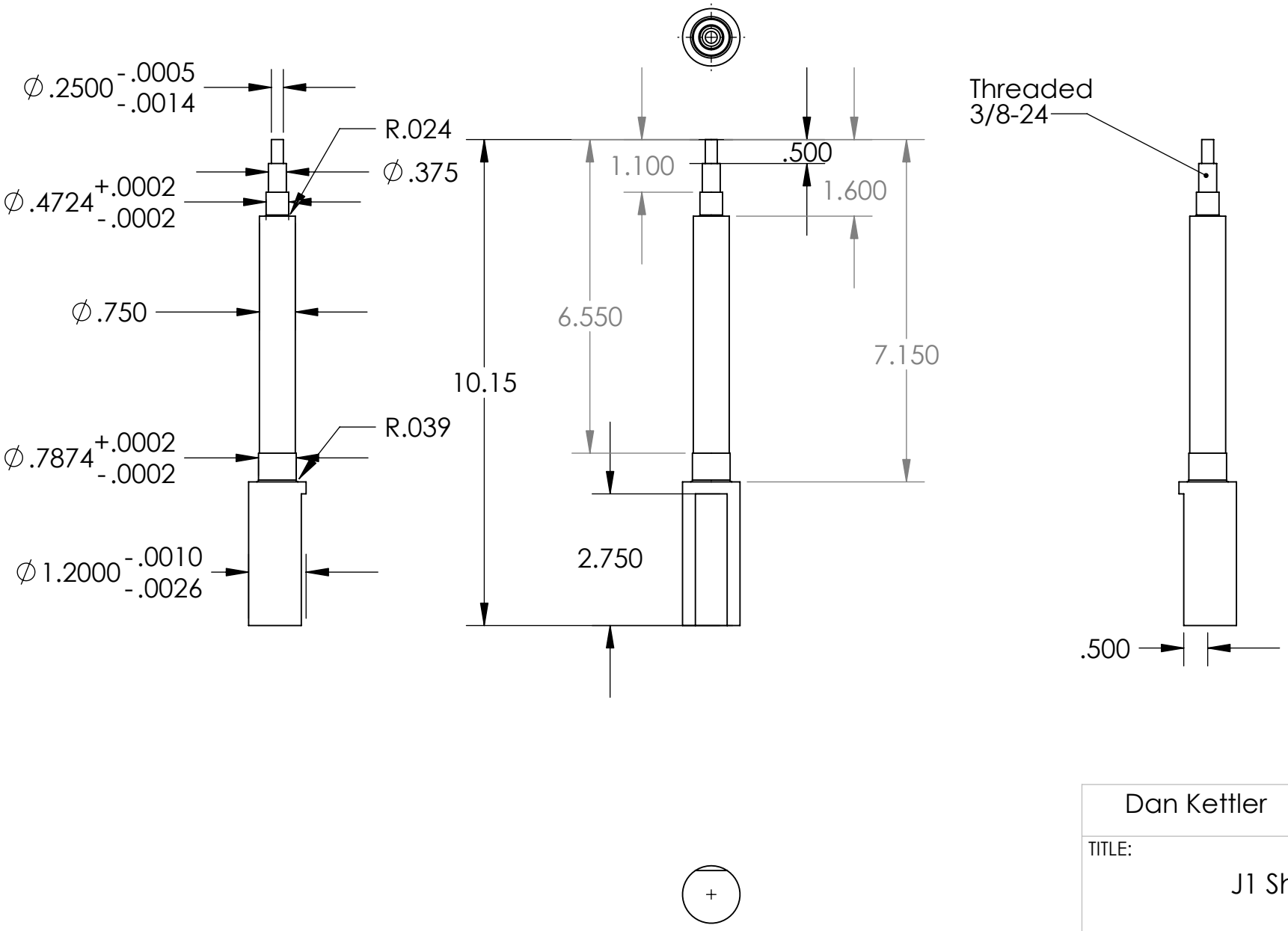

Dan Kettler		
TITLE: J1 Shaft		R6
SIZE A	Material Steel	REV 2.4
SCALE: 1:3	Qty: 1	SHEET 1 OF 1

5 4 3 2 1

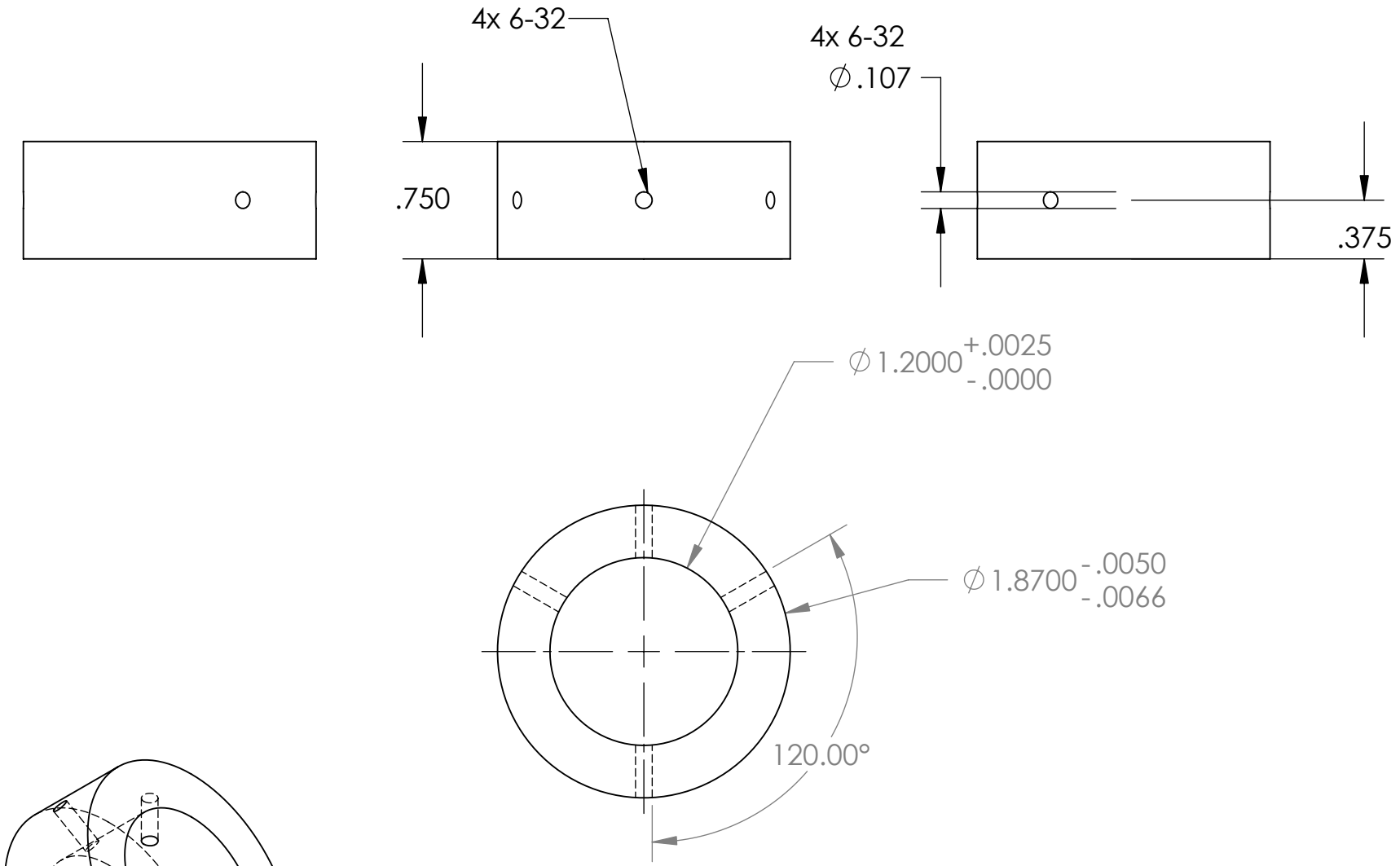

Dan Kettler		
TITLE: J1-Link1 Mounting Boss		R7
SIZE A	Material Al 6061	REV 2.4
SCALE: 1:1	Qty: 2	SHEET 1 OF 1

5 4 3 2 1

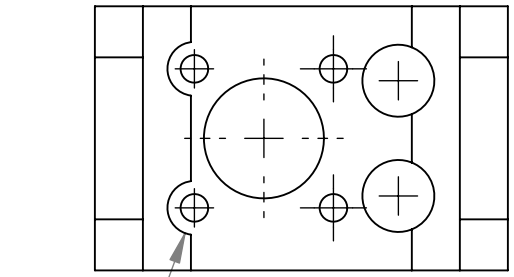

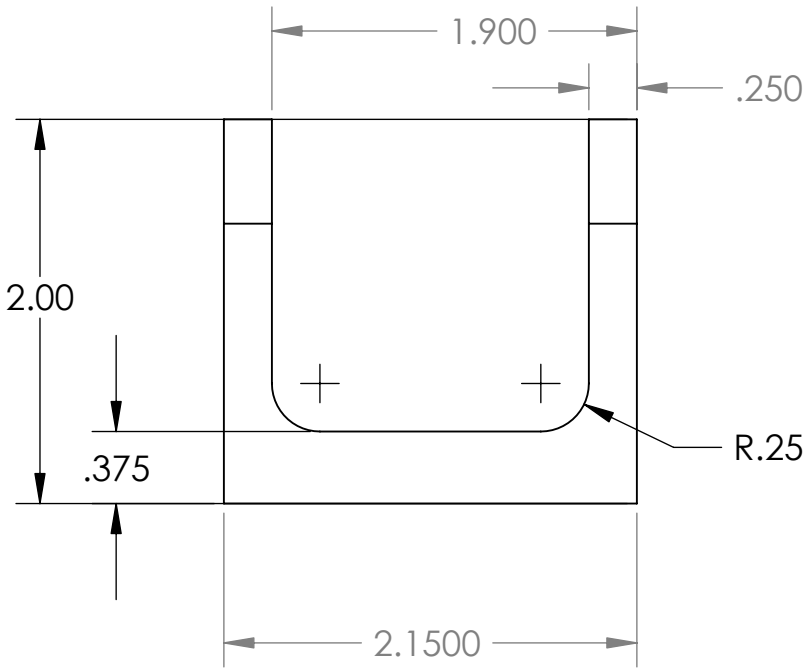

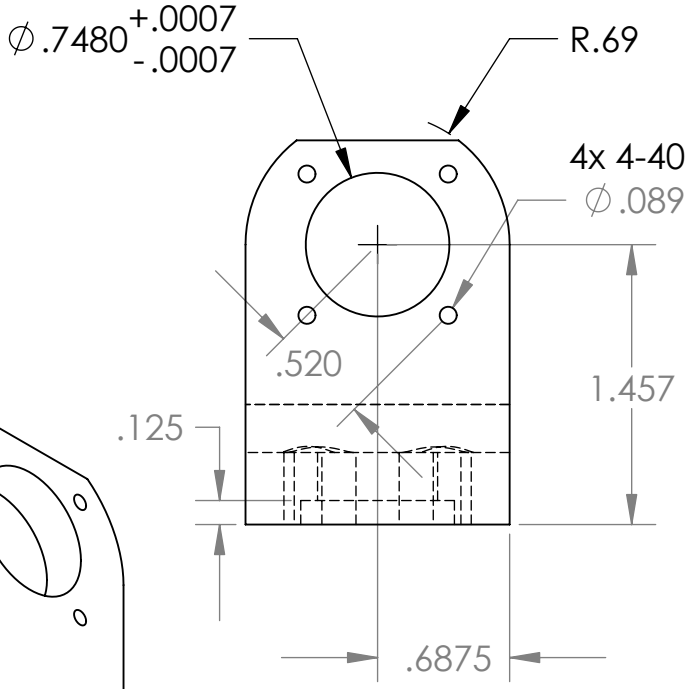

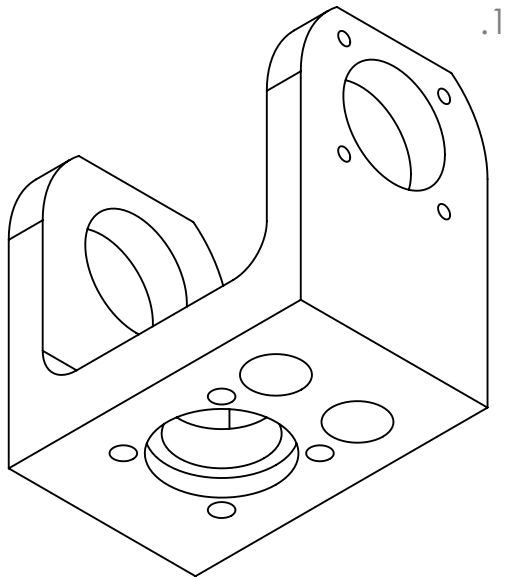

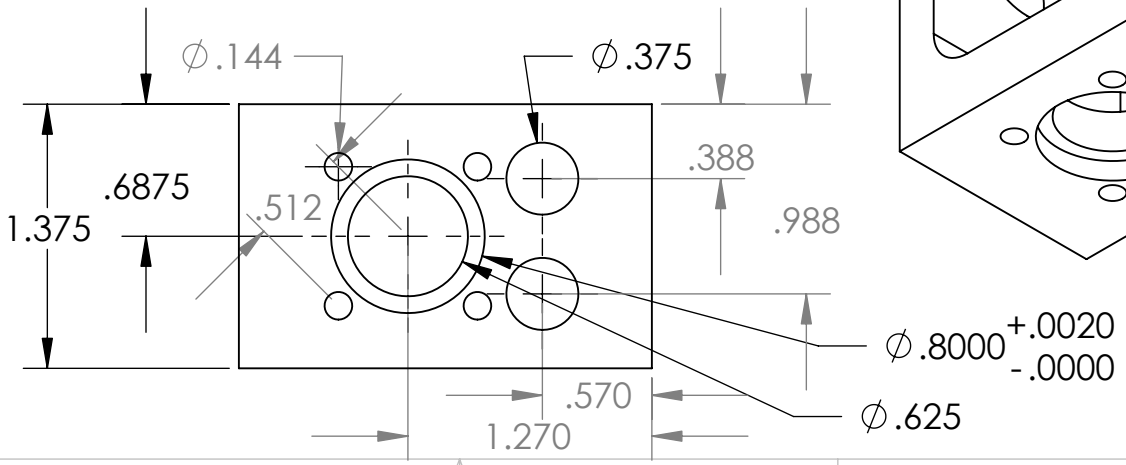

Dan Kettler		
TITLE: J2 Drive Yoke		R8
SIZE A	Material Al 6061	REV 2.4
SCALE: 1:1	Qty: 1	SHEET 1 OF 1

5 4 3 2 1

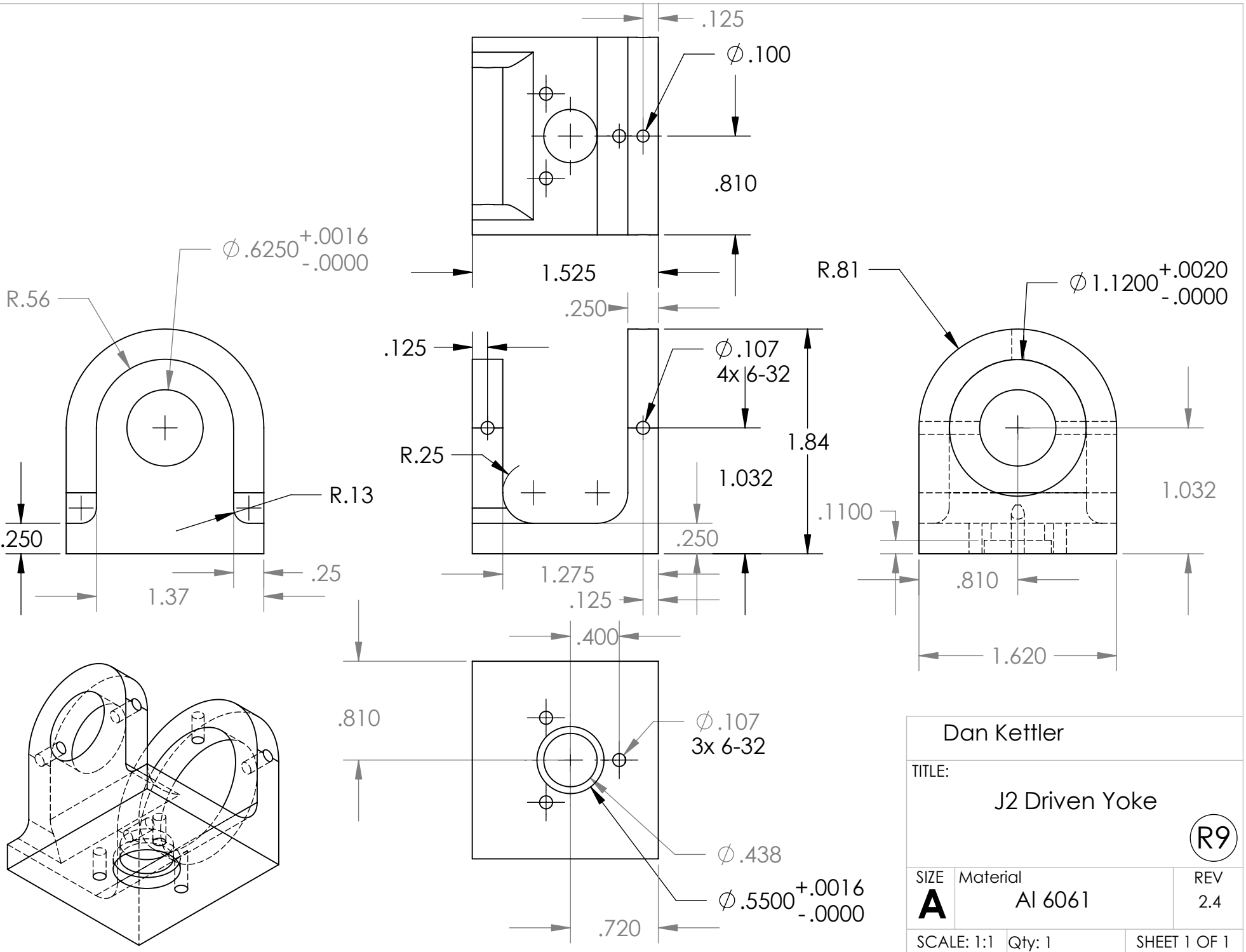

Dan Kettler		
TITLE: J2 Driven Yoke		R9
SIZE A	Material Al 6061	REV 2.4
SCALE: 1:1	Qty: 1	SHEET 1 OF 1

5 4 3 2 1

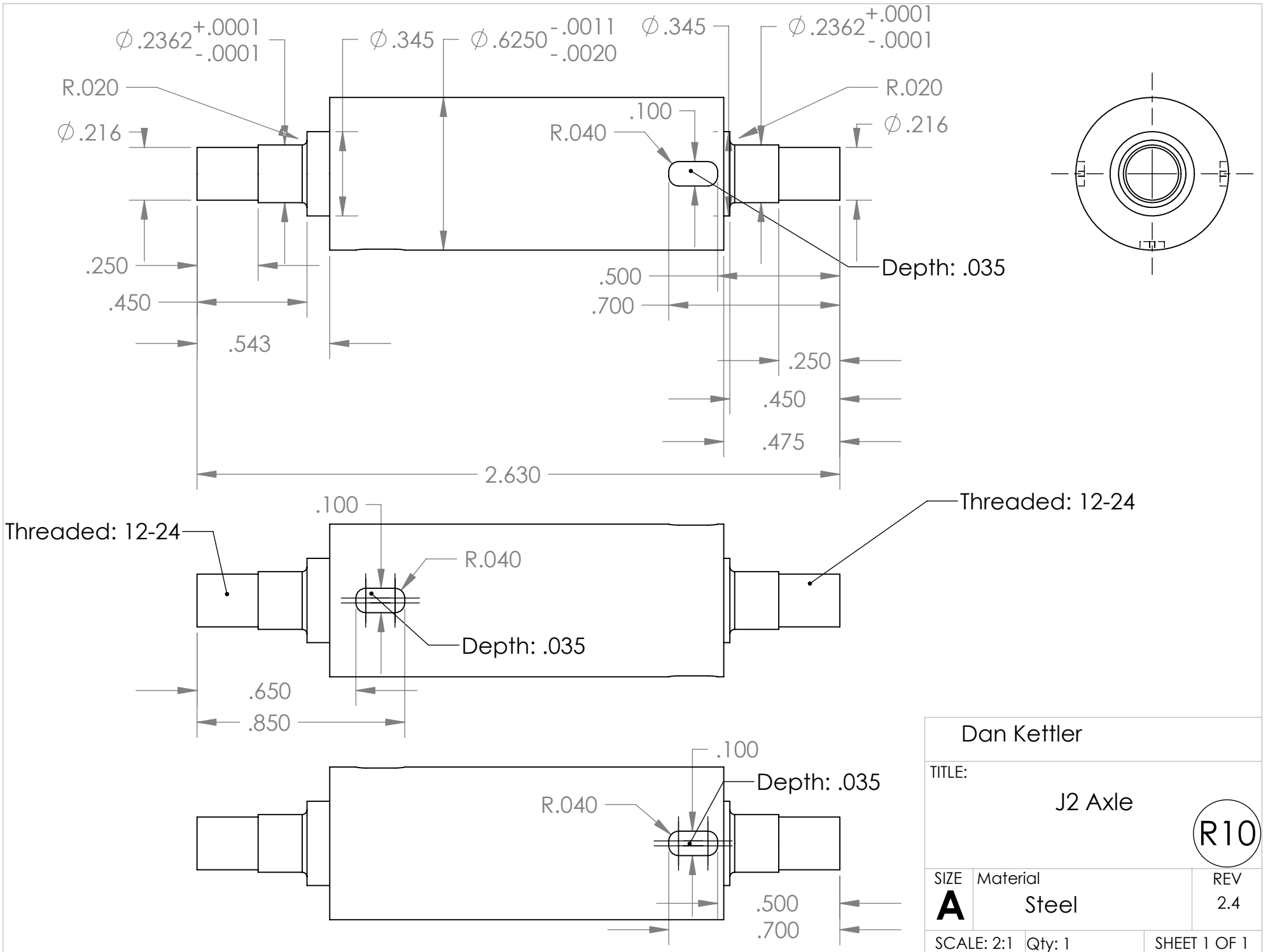
∅.2362 +.0001 -.0001
∅.345
∅.6250 -.0011 -.0020
∅.345
∅.2362 +.0001 -.0001
R.020
R.020
∅.216
∅.216
.100
R.040
Depth: .035
.250
.450
.543
.500
.700
.250
.450
.475
2.630
Threaded: 12-24
Threaded: 12-24
.100
R.040
Depth: .035
.650
.850
.100
Depth: .035
R.040
.500
.700
Dan Kettler
TITLE:
J2 Axle
R10
SIZE
A
Material
Steel
REV
2.4
SCALE: 2:1
Qty: 1
SHEET 1 OF 1
5
4
3
2
1

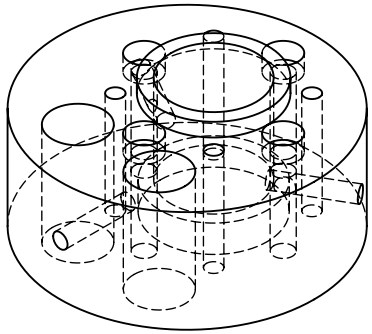

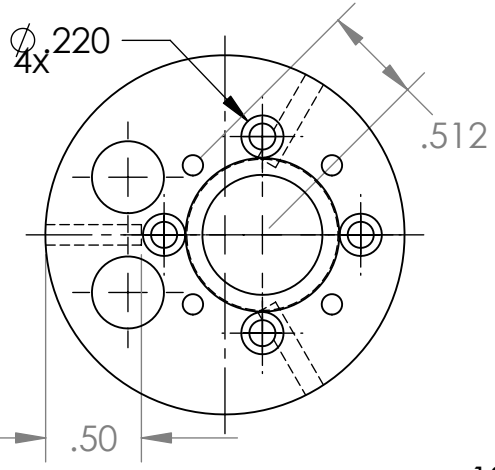

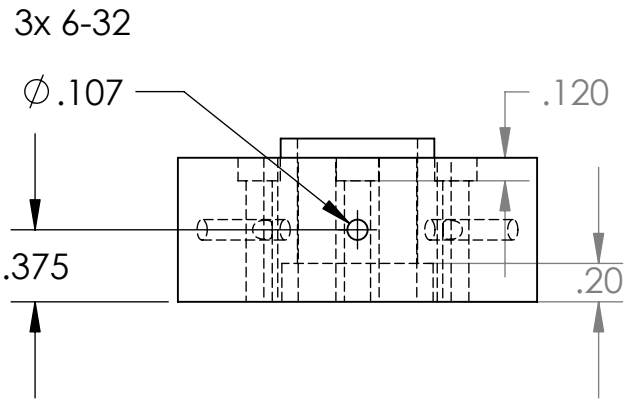

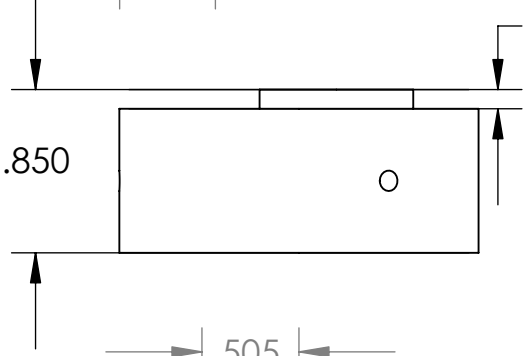

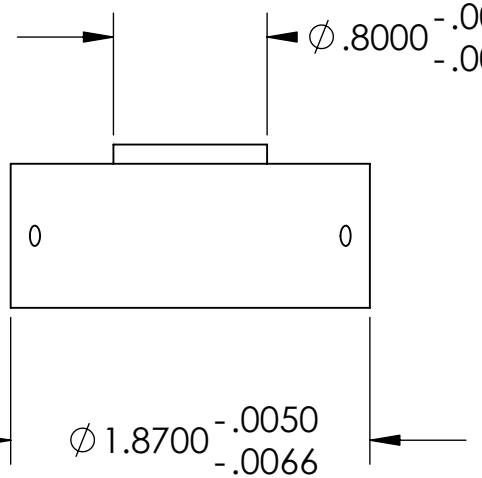

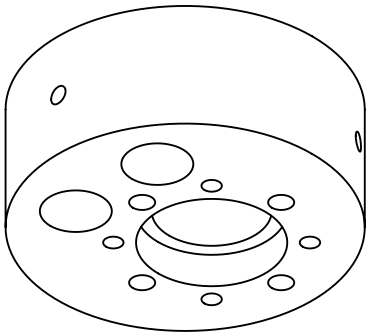

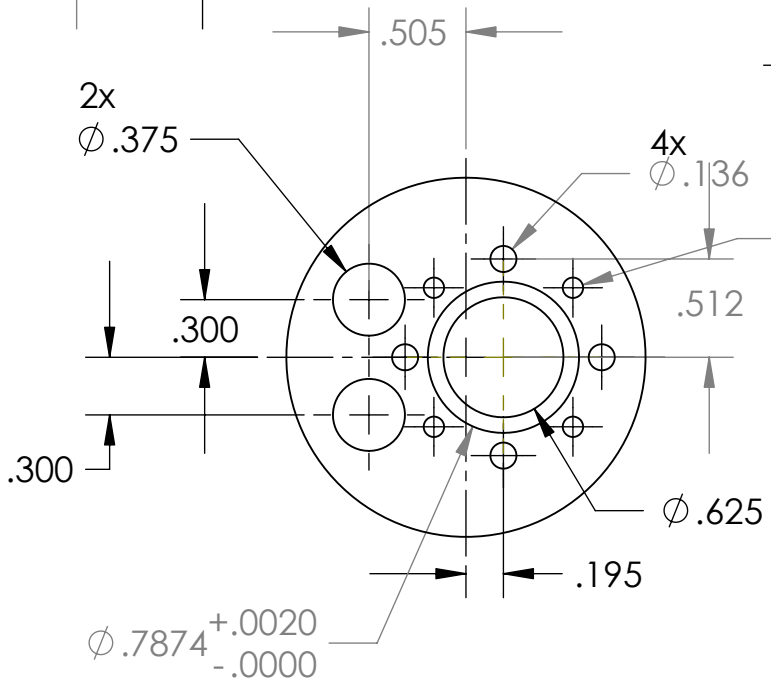

Dan Kettler		
TITLE: J2 Mounting Boss R32-0		R11
SIZE A	Material Al 6061	REV 2.4
SCALE: 1:1	Qty: 1	SHEET 1 OF 1

5 4 3 2 1

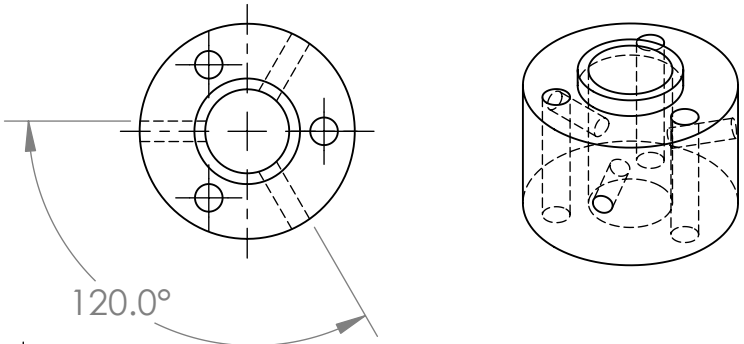

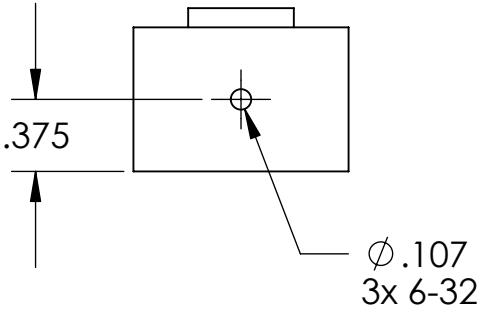

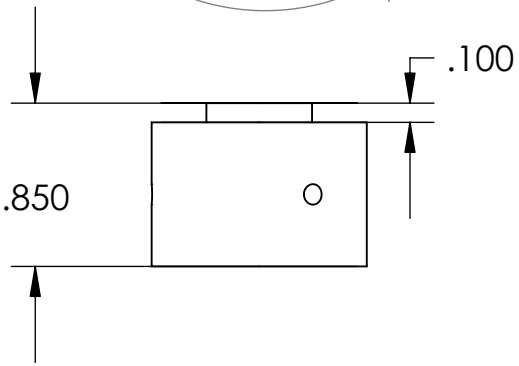

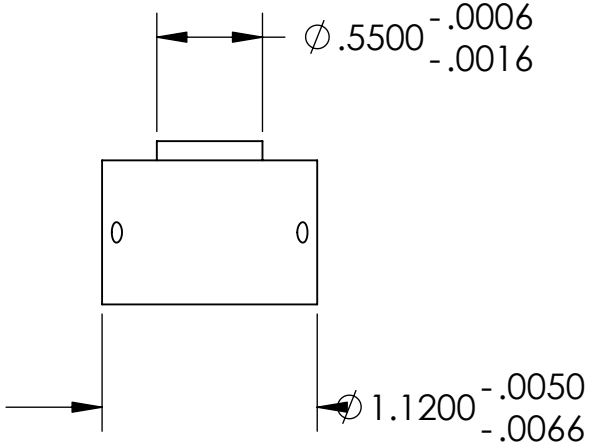

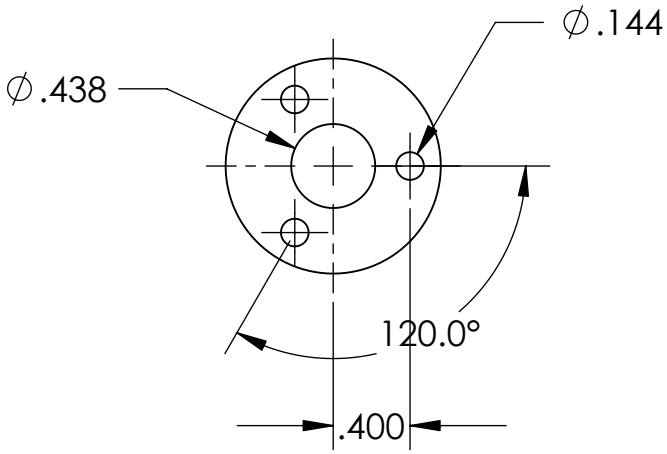

Dan Kettler		
TITLE: J2 Mounting Boss Plain		R12
SIZE A	Material Al 6061	REV 2.4
SCALE: 1:1	Qty: 1	SHEET 1 OF 1

5 4 3 2 1

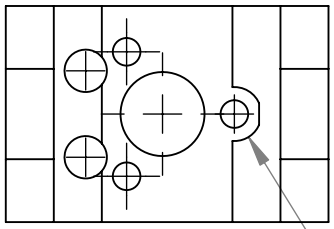

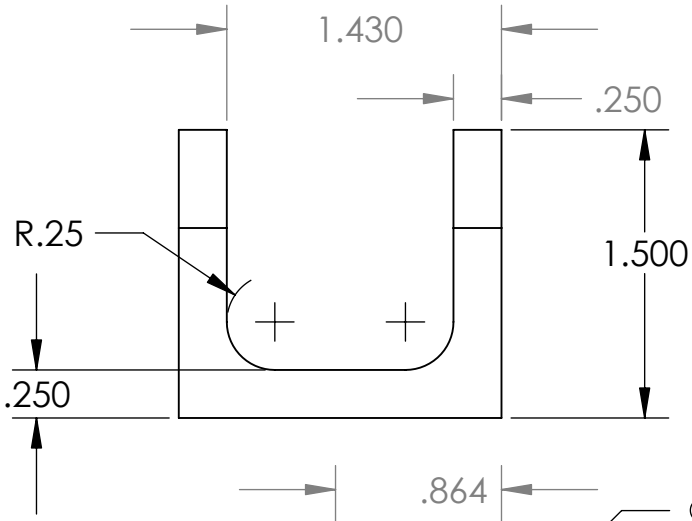

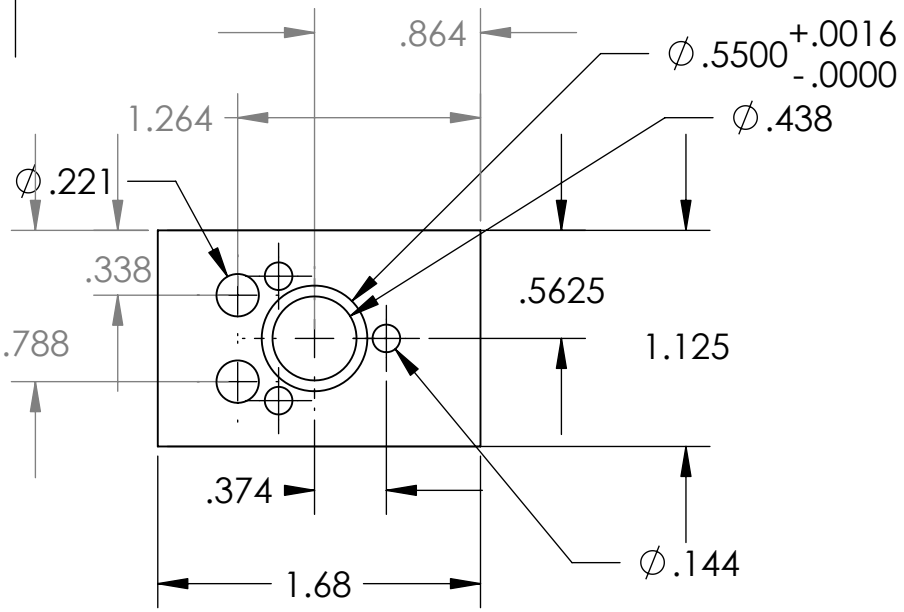

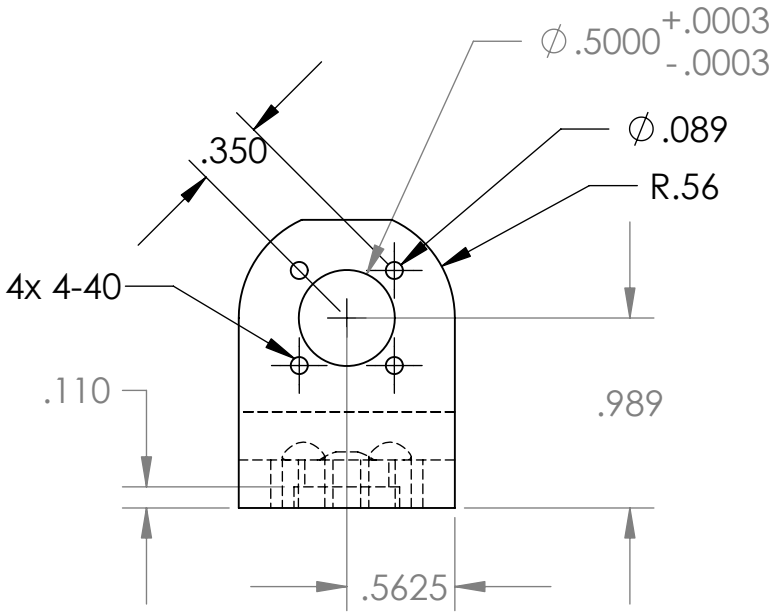

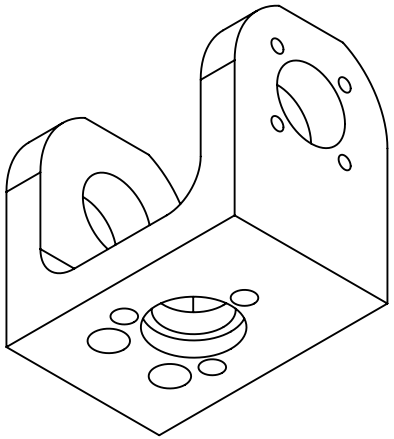

Dan Kettler		
TITLE: J3 Drive Yoke		R13
SIZE A	Material Al 6061	REV 2.4
SCALE: 1:1	Qty: 1	SHEET 1 OF 1

5 4 3 2 1

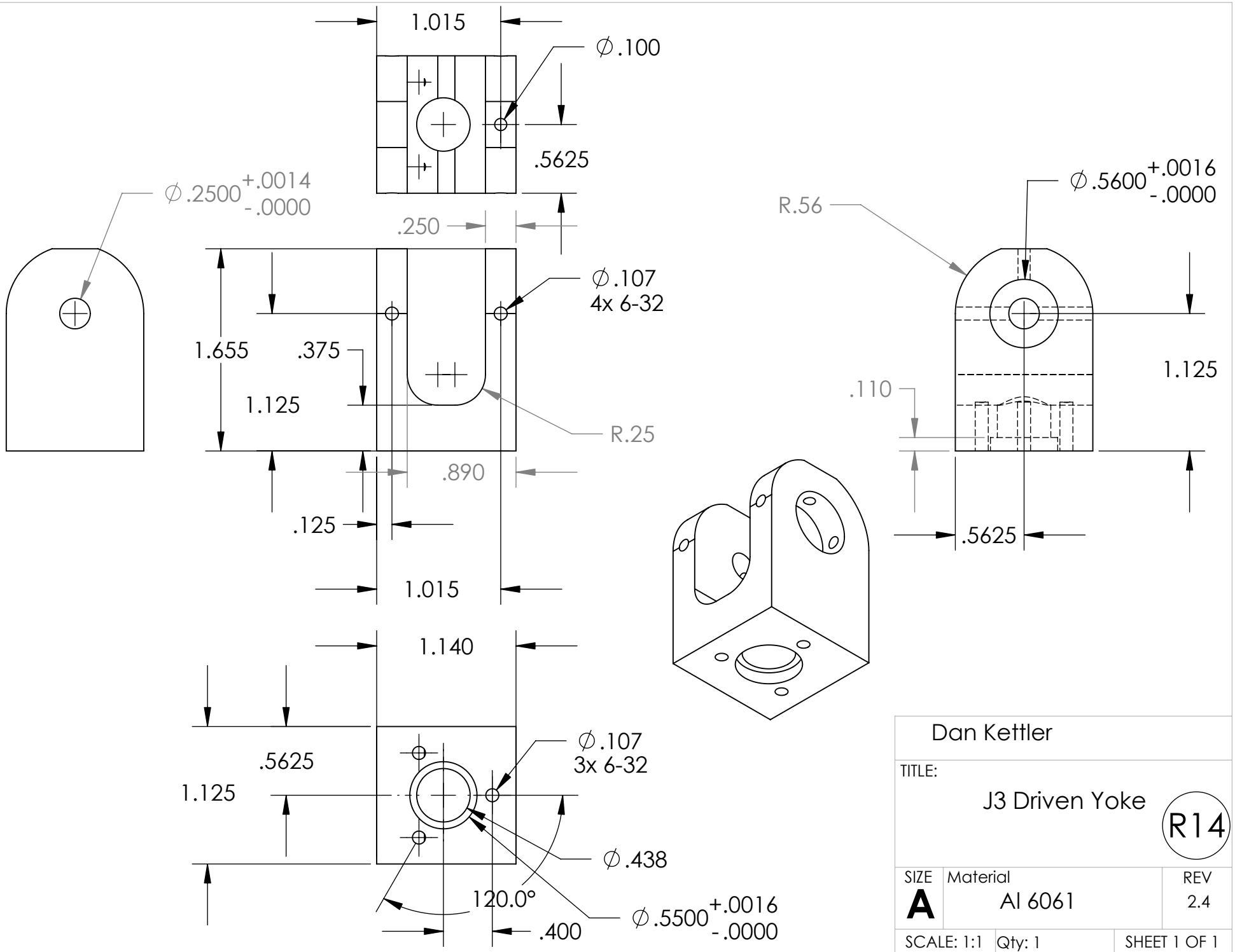

Dan Kettler		
TITLE: J3 Driven Yoke		R14
SIZE A	Material Al 6061	REV 2.4
SCALE: 1:1	Qty: 1	SHEET 1 OF 1

5 4 3 2 1

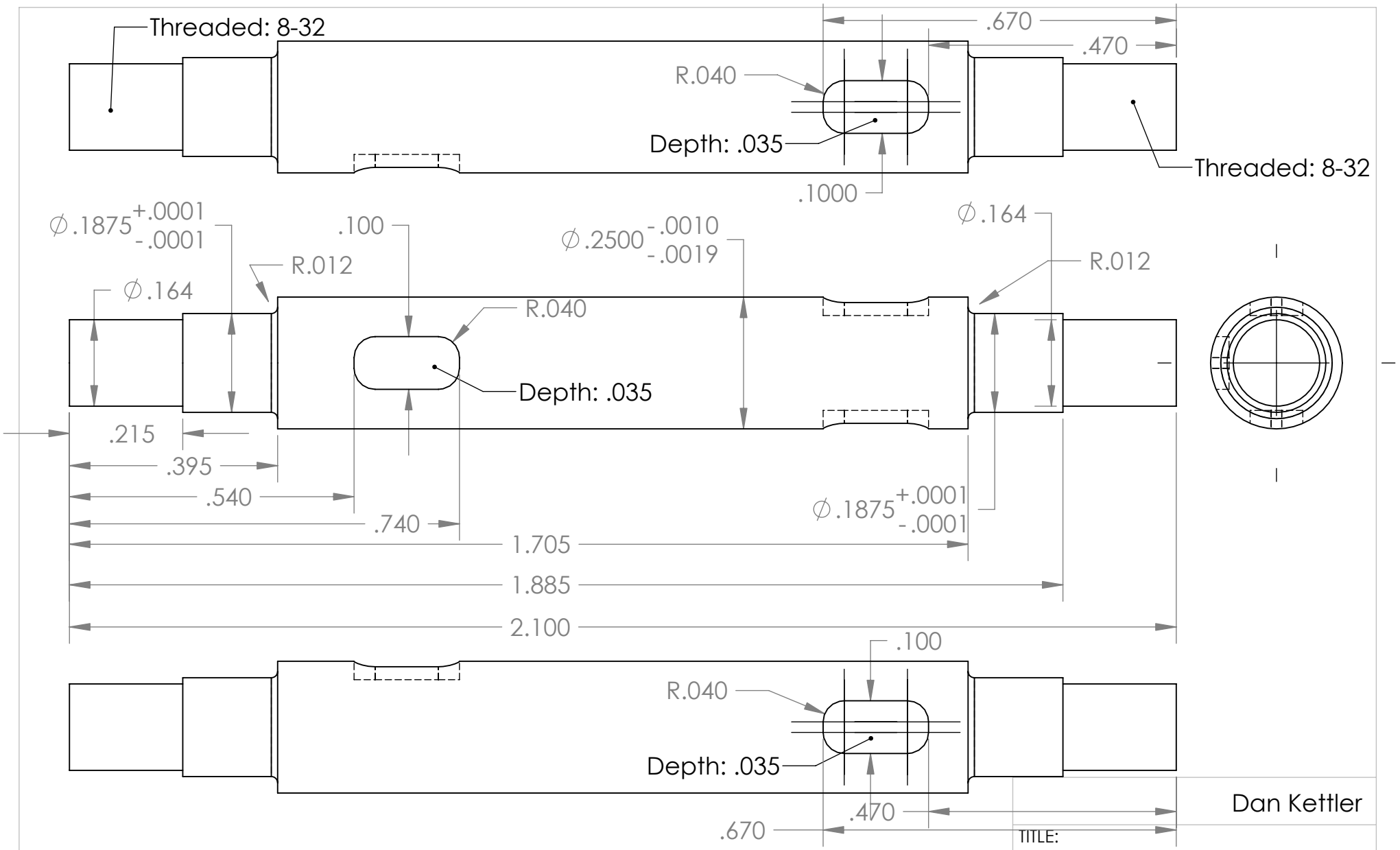

Dan Kettler

TITLE:

J3 Axle

R15

SIZE	Material	REV
A	Steel	2.4

SCALE: 4:1	Qty: 1	SHEET 1 OF 1

5 4 3 2 1

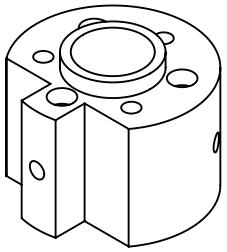

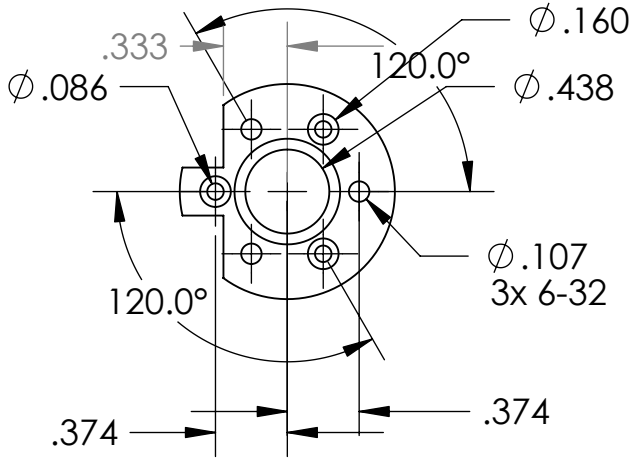

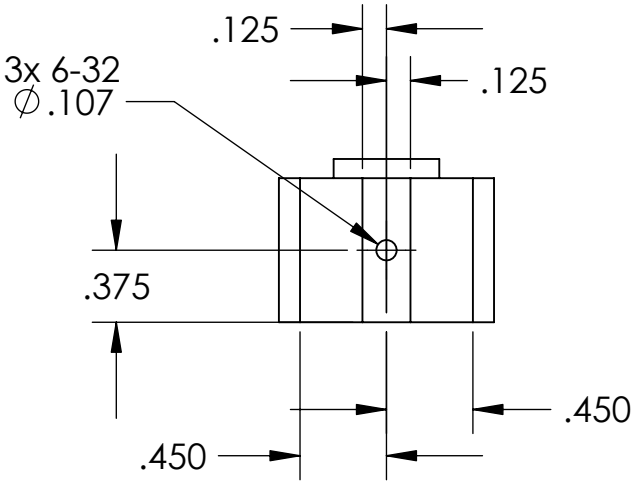

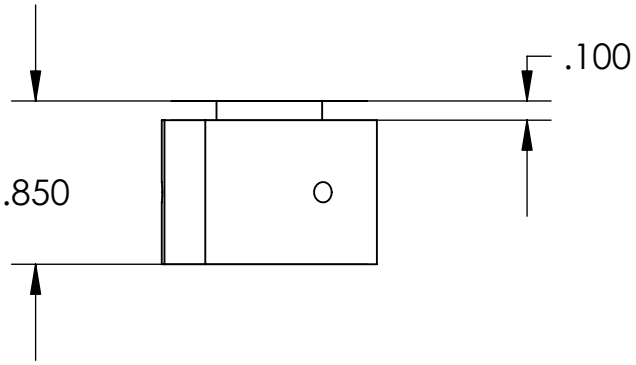

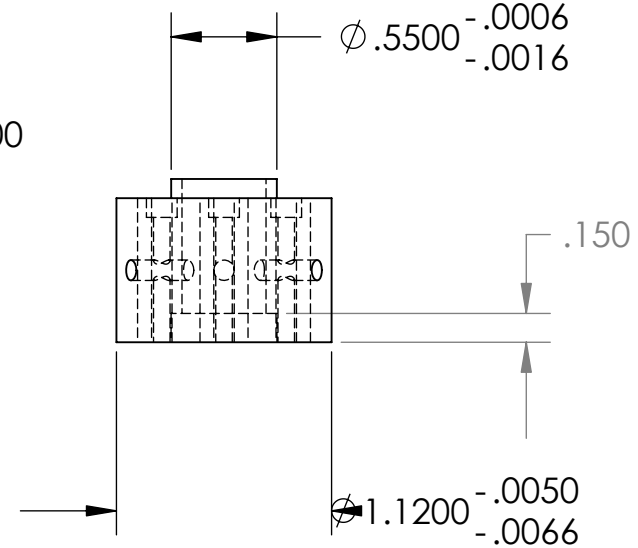

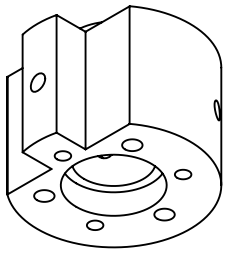

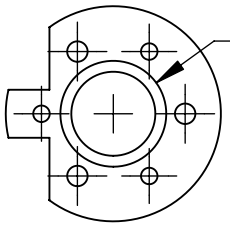

Dan Kettler

TITLE:
J3 Mounting Boss R22

R16

SIZE	Material	REV
A	Al 6061	2.4

SCALE: 1:1	Qty: 1	SHEET 1 OF 1

5 4 3 2 1

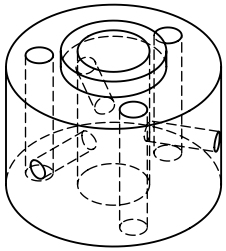

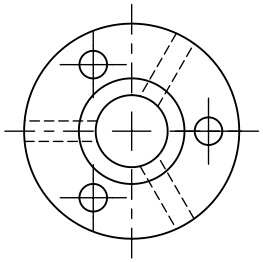

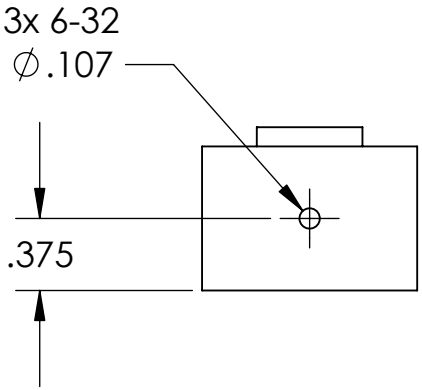

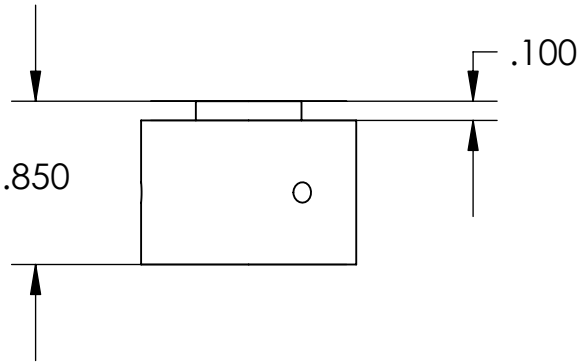

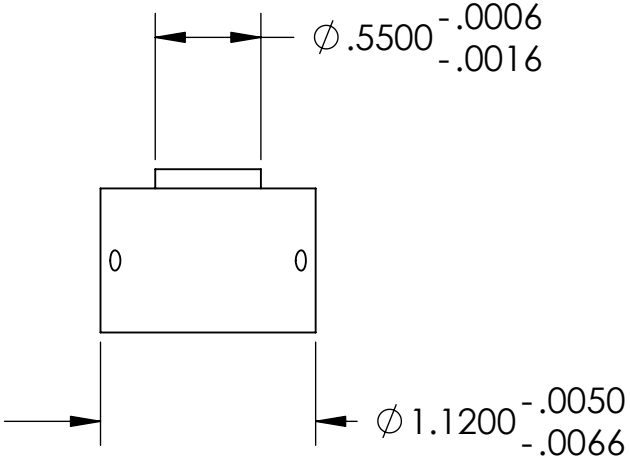

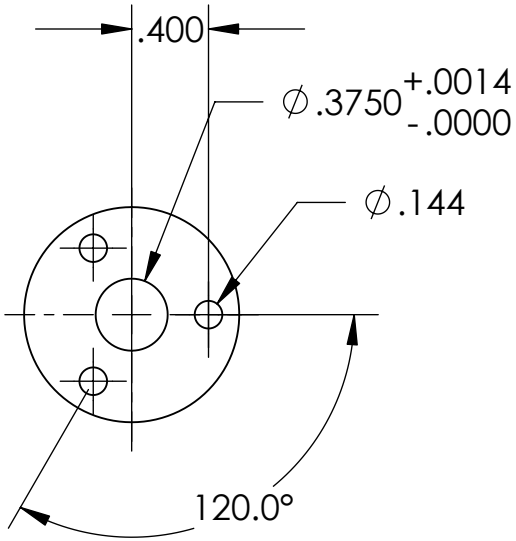

Dan Kettler

TITLE:
J3 Mounting Boss Plain

R17

SIZE	Material	REV
A	Al 6061	2.4

SCALE: 1:1	Qty: 1	SHEET 1 OF 1

5 4 3 2 1

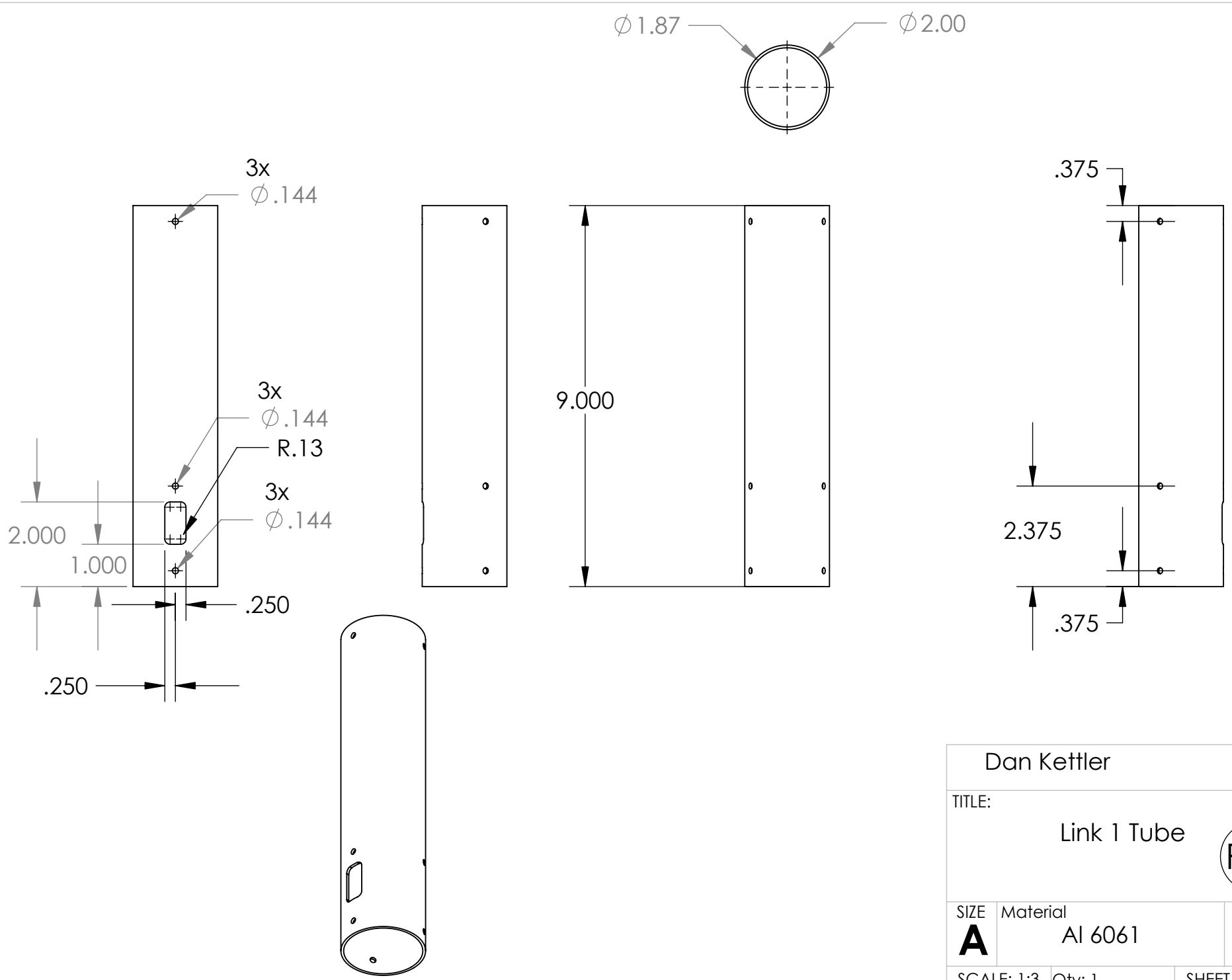

Dan Kettler		
TITLE: Link 1 Tube		R18
SIZE A	Material Al 6061	REV 2.4
SCALE: 1:3	Qty: 1	SHEET 1 OF 1

5 4 3 2 1

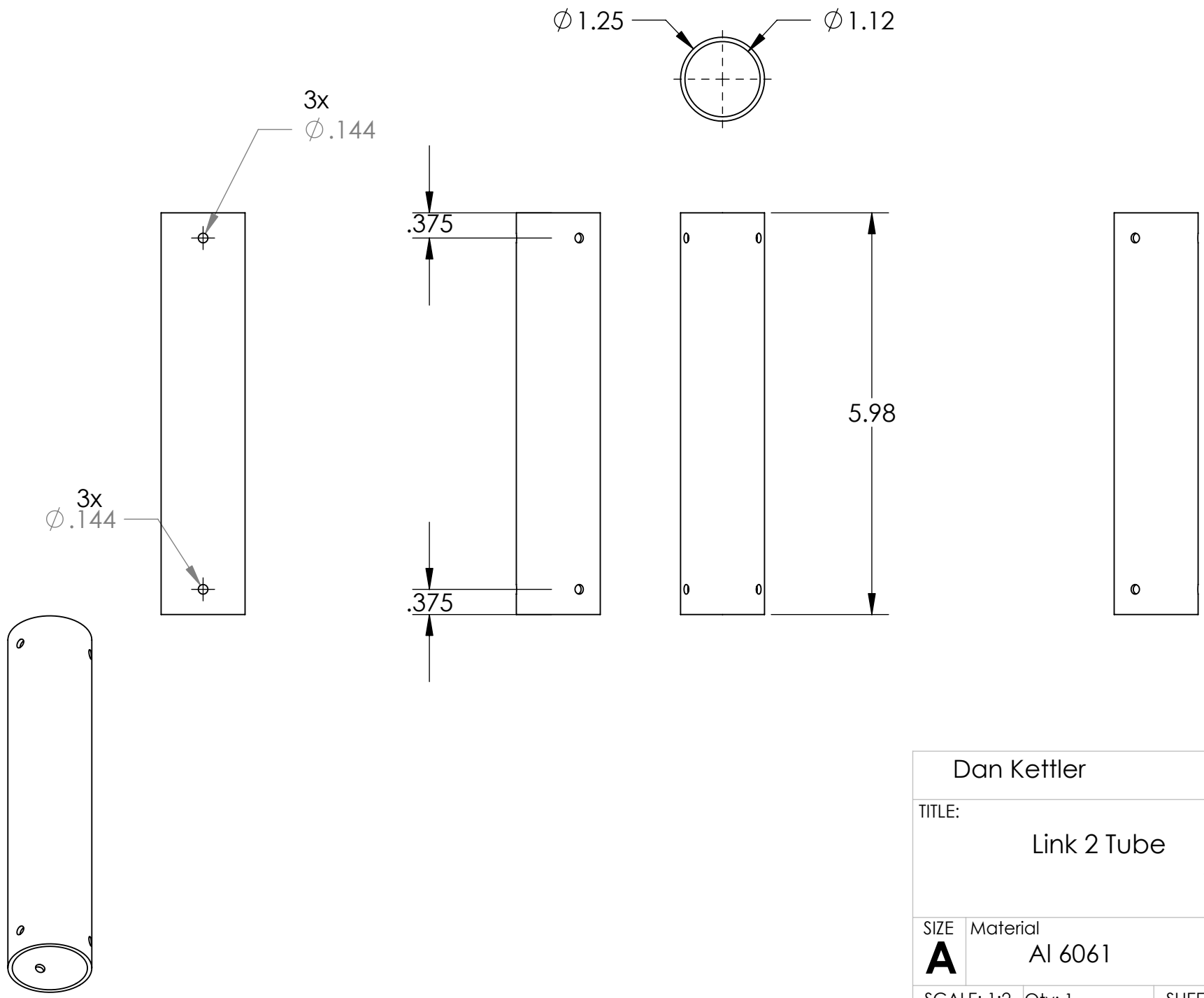

Dan Kettler		
TITLE: Link 2 Tube		R19
SIZE A	Material Al 6061	REV 2.4
SCALE: 1:2	Qty: 1	SHEET 1 OF 1

5 4 3 2 1

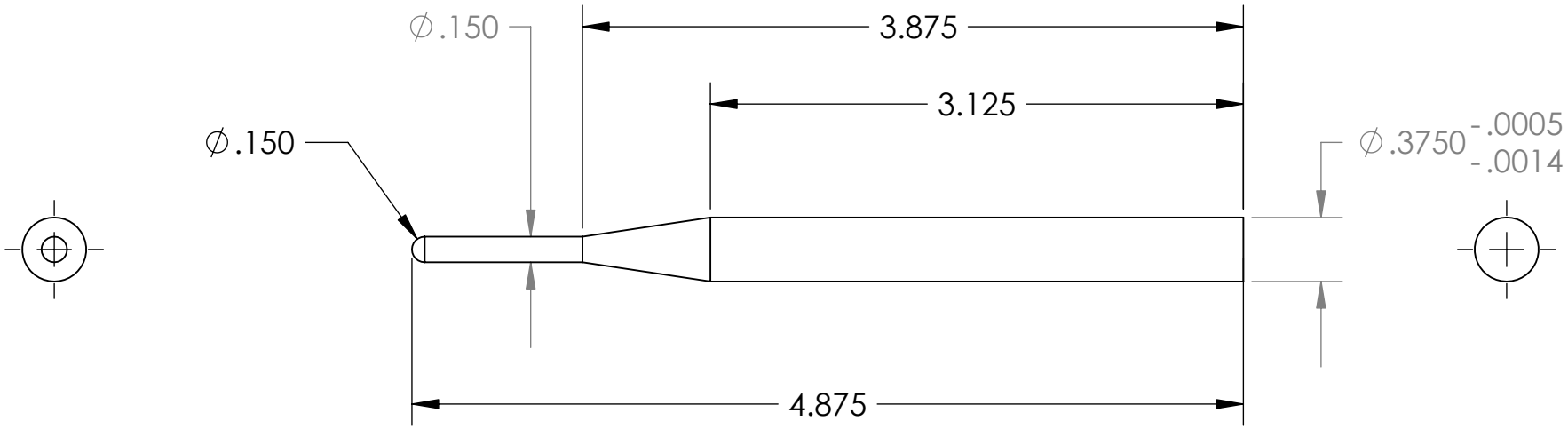

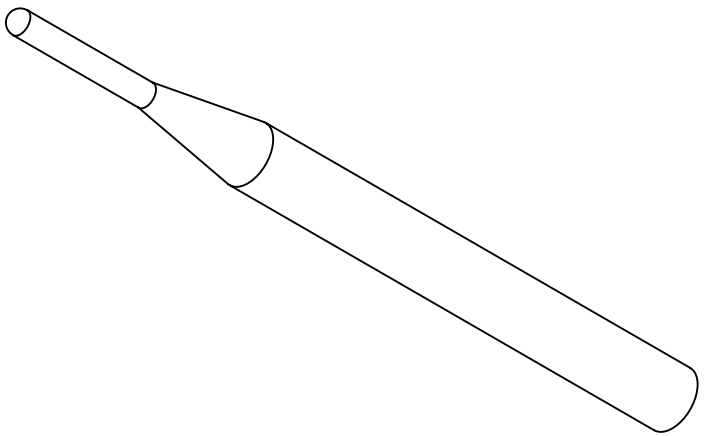

Dan Kettler

TITLE:

Link 3 rod

R20

SIZE	Material	REV
A	SS 316	2.4

SCALE: 1:1	Qty: 1	SHEET 1 OF 1

5 4 3 2 1

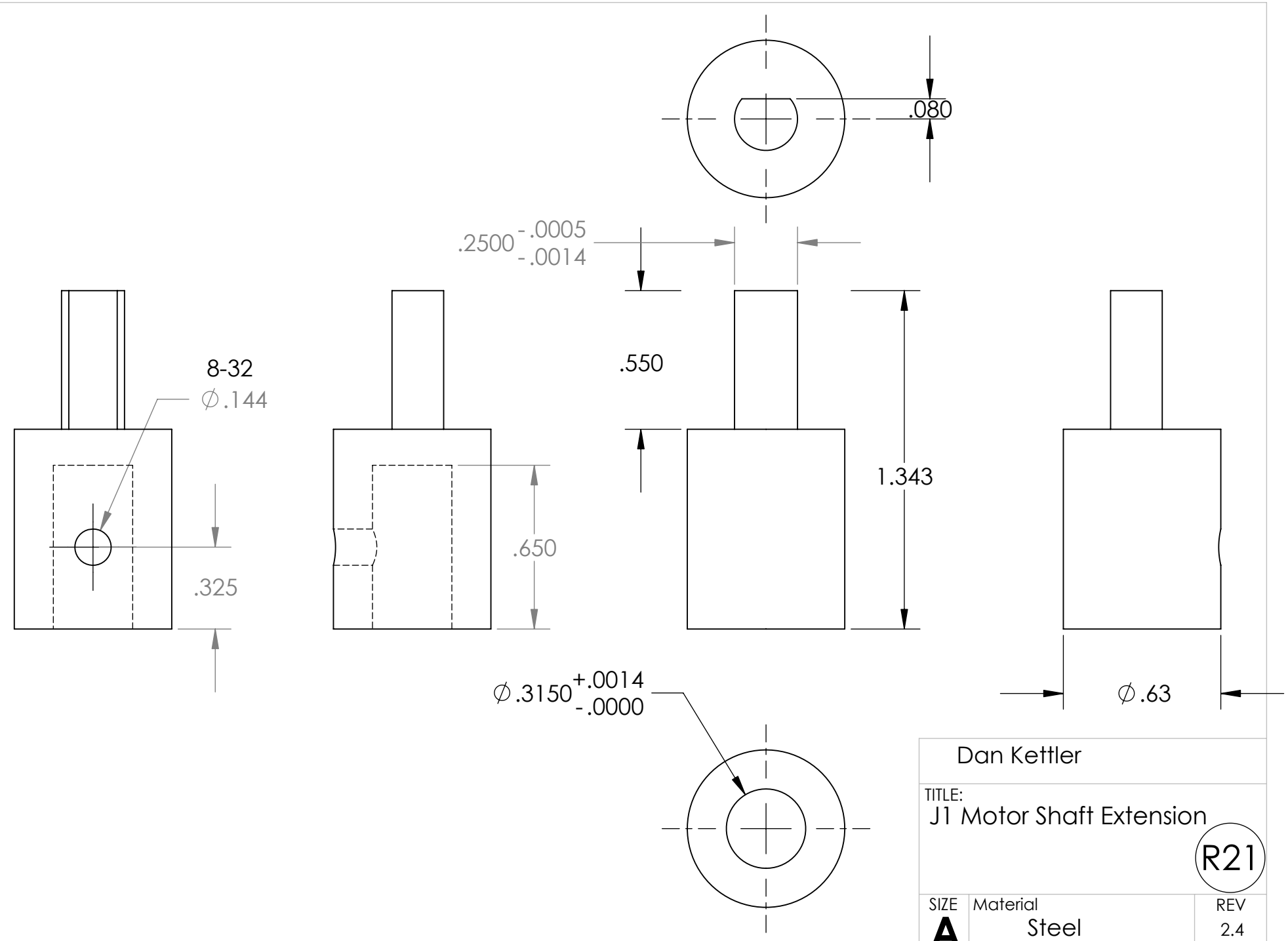

Dan Kettler

TITLE:
J1 Motor Shaft Extension

R21

SIZE	Material	REV
A	Steel	2.4

SCALE: 2:1	Qty: 1	SHEET 1 OF 1

5 4 3 2 1

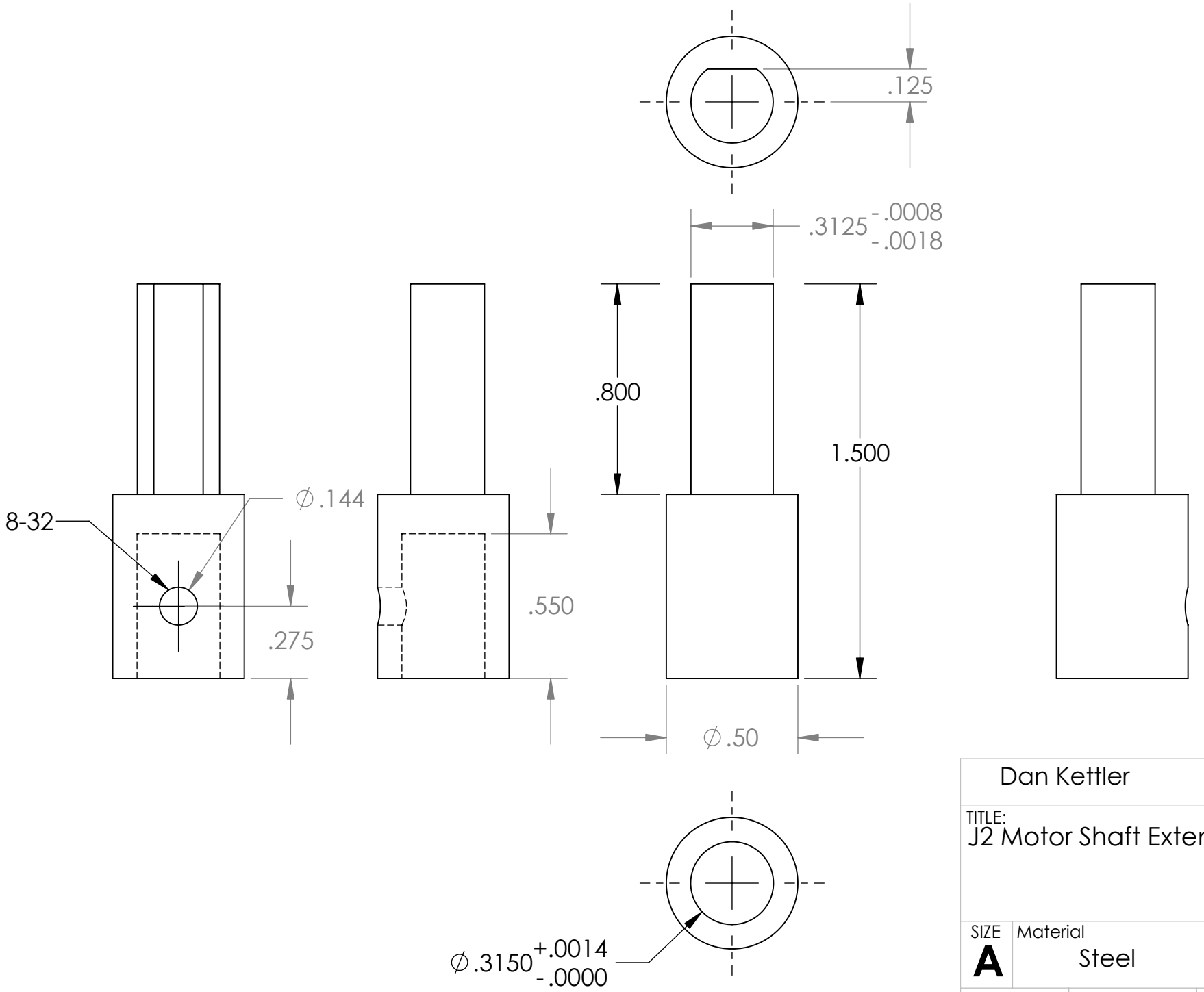

Dan Kettler

TITLE:
J2 Motor Shaft Extension

R22

SIZE	Material	REV
A	Steel	2.4

SCALE: 2:1	Qty: 1	SHEET 1 OF 1

5 4 3 2 1

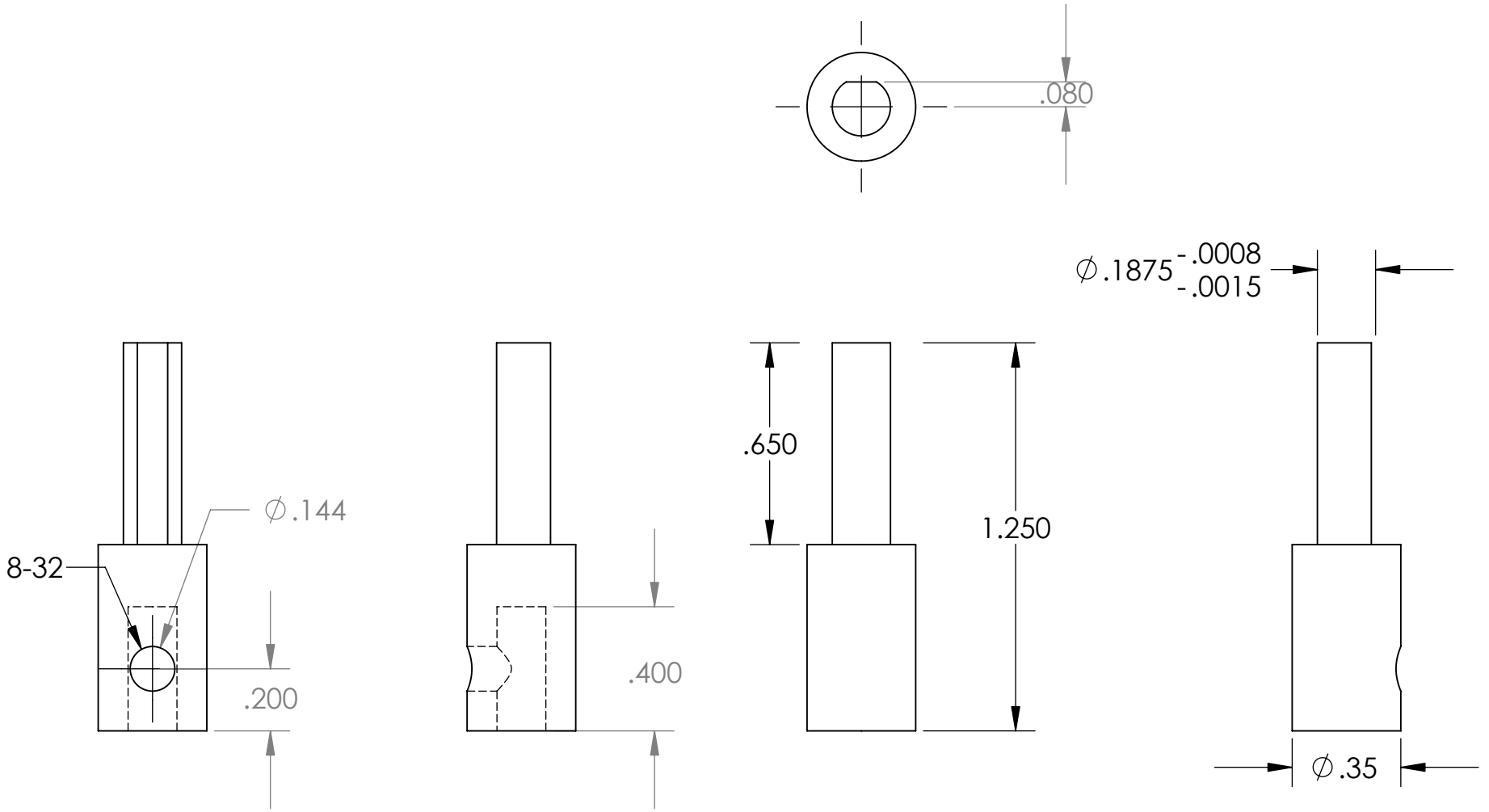

Dan Kettler		
TITLE: J3 Motor Shaft Extension		R23
SIZE A	Material Steel	REV 2.4
SCALE: 2:1	Qty: 1	SHEET 1 OF 1

5 4 3 2 1

A.2 Environment Parts Drawings

The experimental test tank is designed to imitate the form of an oil well junction within lab size constraints. Fully dimensioned design drawings for all major tank components are included here. These drawings are listed in order by the part number *E#* they received during the design and construction of the experimental test tank. Materials are listed on these drawings. For a drawing of the test tank assembly with the major components labeled, see Figure 3-3(b).

In addition to the major components diagrammed here, a number of common plumbing fittings were used in order to create a drain for the tank.

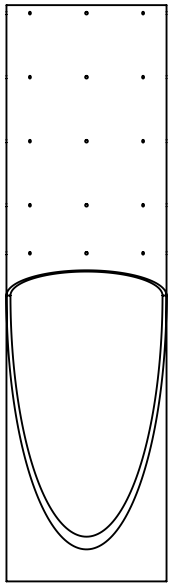

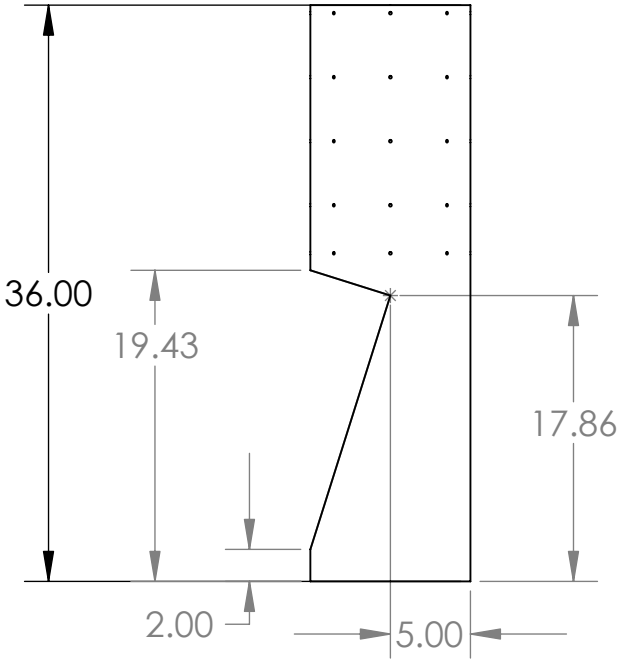

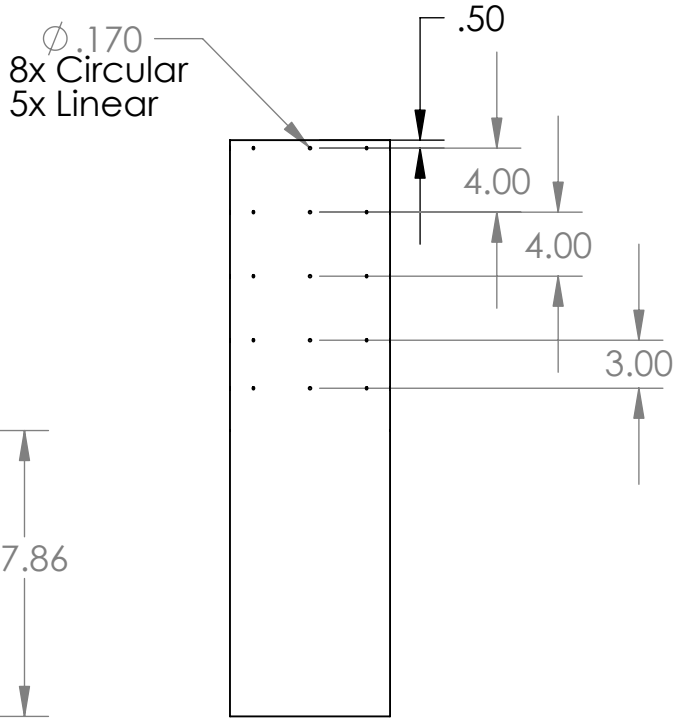

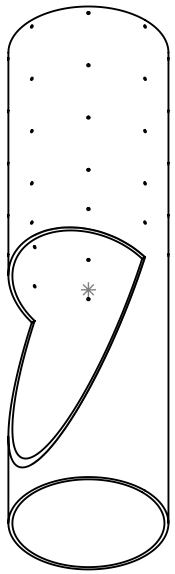

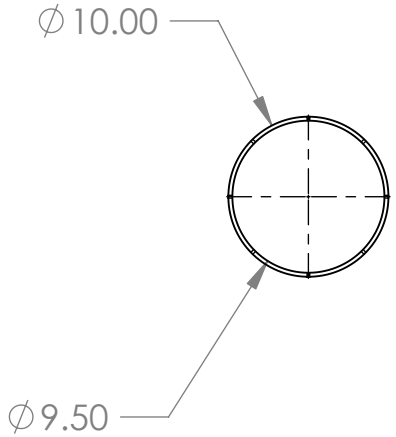

Dan Kettler

TITLE:

Main Tube

E1

SIZE	Material	REV
A	Acrylic	2.4

SCALE: 1:12 | Qty: 1 | SHEET 1 OF 1

5 4 3 2 1

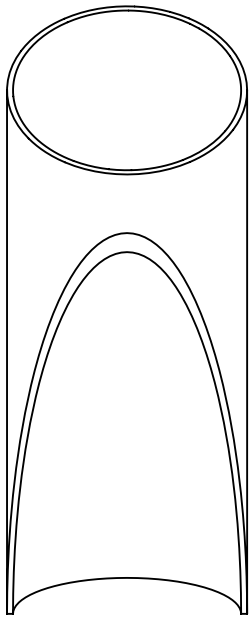

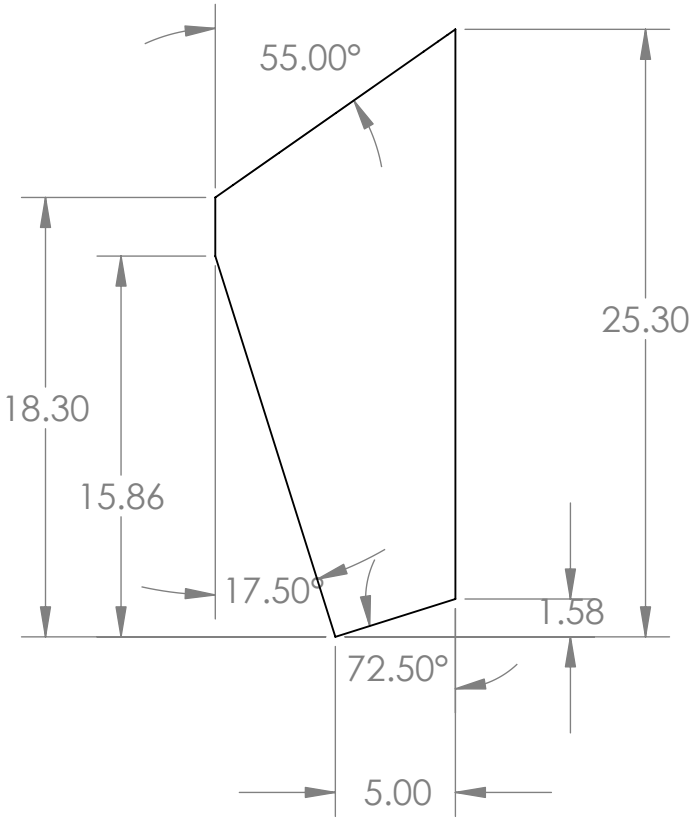

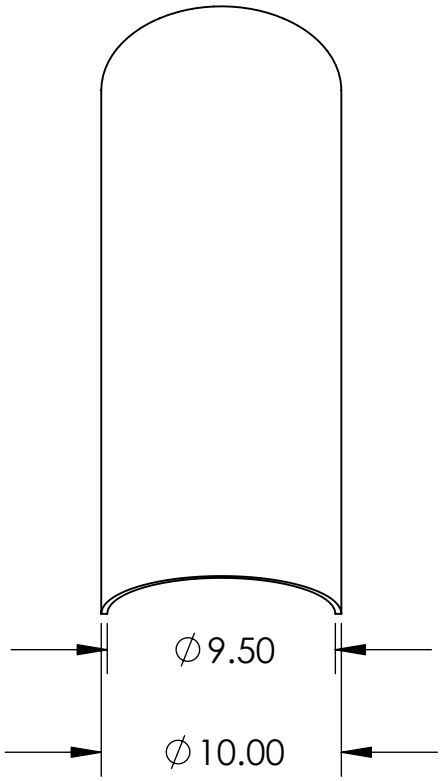

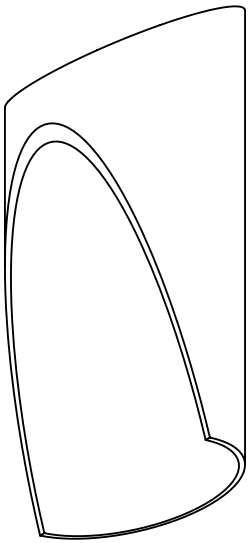

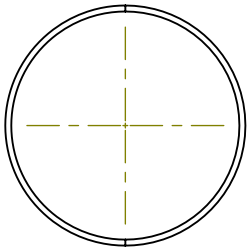

Dan Kettler		
TITLE: Lateral Tube		E2
SIZE A	Material Acrylic	REV 2.4
SCALE: 1:8	Qty: 1	SHEET 1 OF 1

5 4 3 2 1

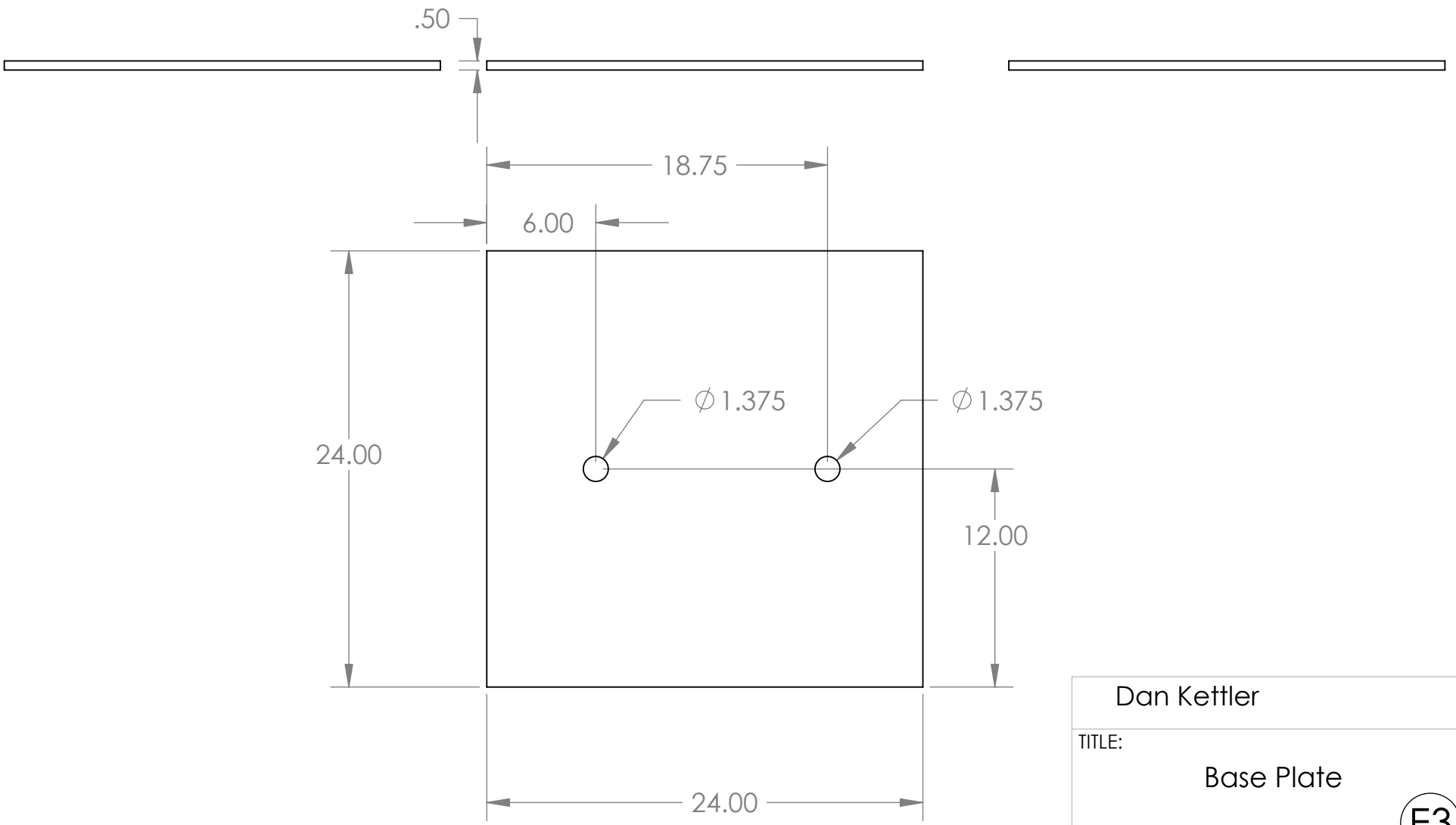

Dan Kettler

TITLE:

Base Plate

E3

SIZE	Material	REV
A	Acrylic	2.4

SCALE: 1:8	Qty: 1	SHEET 1 OF 1

5 4 3 2 1

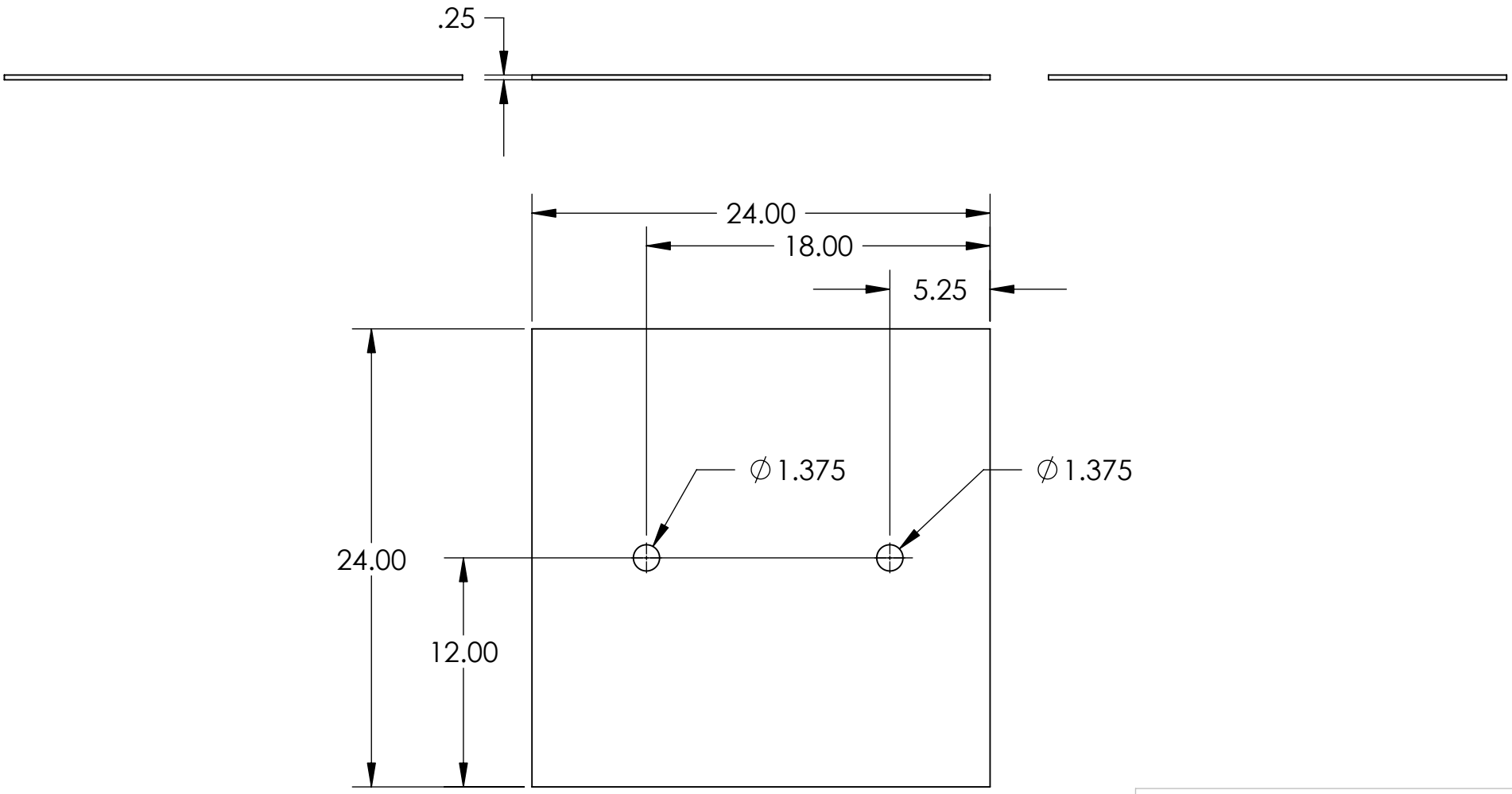

Dan Kettler

TITLE:

Sub Base Plate

E4

SIZE	Material	REV
A	Al 6061	2.4

SCALE: 1:8	Qty: 1	SHEET 1 OF 1

5 4 3 2 1

Appendix B

Serpentine Manipulator Module Kinematics

The kinematics of the serpentine manipulator are represented by decomposing the total manipulator transformation into a series of transformations related to each of the modules in the arm. For each module, the transformation relating location and orientation of the distal base i to the location and orientation of the proximal base $i-1$ must be found. See Figure B-1. This transformation is determined by the parameters and kinematic constraints describing the module. In this design study, the parameters used to define the module are: the radius of the base rings R, the angular locations of the three legs around the circumference of the base rings θ_{1-3}, the contracted leg lengths κ_{1-3}, and the extended leg lengths λ_{1-3}. the kinematic constraints on the module can be described by the joint connections between the module legs and the base rings. At the proximal base ring, the module legs are connected with a revolute joint allowing motion only in a radial plane of the proximal base ring. At the distal base ring the legs are connected with a spherical joint. If the modules are assumed to be axisymmetric ($\theta_1 = 0$, $\theta_2 = 120$, $\theta_3 = 240$, $\kappa_1 = \kappa_2 = \kappa_3$, and $\lambda_1 = \lambda_2 = \lambda_3$) an analytic solution for this transformation matrix exists [59]. However, in the general case of a non-symmetric model with distinct parameter values, a set of six nonlinear constraint equations must be solved in order to find the transformation matrix.

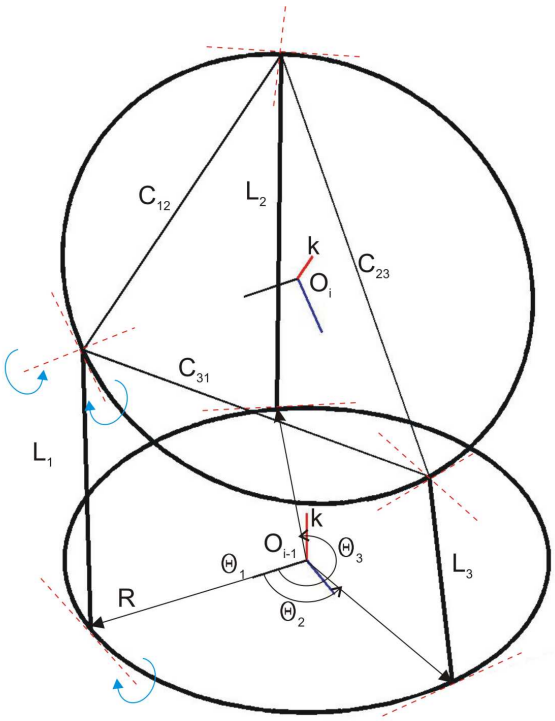

Figure B-1: Diagram showing kinematic module parameters and rotational joint freedom.

B.1 General Constraint Equations

The revolute joint at the proximal base ring constrains each module leg to move within a radial plane of the proximal base ring. The position of the proximal end of each leg is known. The position of the distal end of each leg is constrained to lie within its radial plane and with a distance from the proximal end determined by the leg length. See Figure B-2. Considering these constraints within the radial plane for one leg gives:

$$L^2 = z^2 + (R - s)^2 \tag{B.1}$$

where s is the distance of the distal end of the leg from the central axis of the proximal base ring. The x and y coordinates of the distal end of the leg are then given by:

$$\begin{bmatrix} x \\ y \end{bmatrix} = s\vec{v} = s \begin{bmatrix} \cos\theta \\ \sin\theta \end{bmatrix} \tag{B.2}$$

At the distal base ring, the chord distance C_{ab} between each pair of leg joints is known

because the leg location angles θ_{1-3} are specified. Consequently for one pair of module legs:

$$C_{ab}^2 = (x_a - x_b)^2 + (y_a - y_b)^2 + (z_a - z_b)^2 \qquad \text{or}$$
$$C_{ab}^2 = (s_a\vec{v}_a - s_b\vec{v}_b)^T(s_a\vec{v}_a - s_b\vec{v}_b) + (z_a - z_b)^2 \tag{B.3}$$

Consequently for one module, the six kinematic constraint equations are:

$$L_1^2 = z_1^2 + (R - s_1)^2 \tag{B.4}$$
$$L_2^2 = z_2^2 + (R - s_2)^2$$
$$L_3^2 = z_3^2 + (R - s_3)^2$$
$$C_{12}^2 = (s_1\vec{v}_1 - s_2\vec{v}_2)^T(s_1\vec{v}_1 - s_2\vec{v}_2) + (z_1 - z_2)^2$$
$$C_{23}^2 = (s_2\vec{v}_2 - s_3\vec{v}_3)^T(s_2\vec{v}_2 - s_3\vec{v}_3) + (z_2 - z_3)^2$$
$$C_{31}^2 = (s_3\vec{v}_3 - s_1\vec{v}_1)^T(s_3\vec{v}_3 - s_1\vec{v}_1) + (z_3 - z_1)^2$$

These equations can be solved for the s and z values describing the locations of the distal leg ends. From this information the position and orientation of the origin of the distal base ring may be determined and the transformation matrix from O_{i-1} base ring to O_i ring generated.

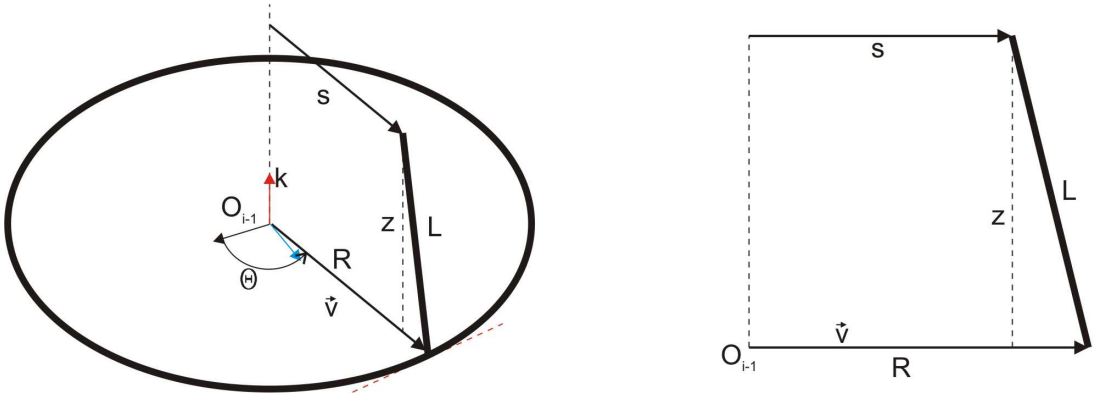

Figure B-2: Diagram of the constrained motion of a leg within its radial plane.